NATIONAL ADVISORY COMMITTEE FOR AERONAUTICS

TECHNICAL NOTE 4109

LOW-SPEED YAWED-ROLLING CHARACTERISTICS AND OTHER ELASTIC PROPERTIES OF A PAIR OF 40-INCH-DIAMETER, 14-PLY-RATING, TYPE VII AIRCRAFT TIRES

By Walter B. Horne and Robert F. Smiley

Langley Aeronautical Laboratory
Langley Field, Va.

NACA

Washington

January 1958

NATIONAL ADVISORY COMMITTEE FOR AERONAUTICS

TECHNICAL NOTE 4109

LOW-SPEED YAWED-ROLLING CHARACTERISTICS AND

OTHER ELASTIC PROPERTIES OF A PAIR OF

40-INCH-DIAMETER, 14-PLY-RATING,

TYPE VII AIRCRAFT TIRES

By Walter B. Horne and Robert F. Smiley

SUMMARY

The low-speed (up to 4 miles per hour) yawed-rolling characteristics of two 40 × 12, 14-ply-rating, type VII aircraft tires under straight-yawed rolling were determined over a range of inflation pressures and yaw angles for two vertical loadings. One load was approximately equal to the rated vertical load and the other load was approximately equal to twice the rated vertical load for these tires. Static tests were also performed to determine the vertical, lateral, torsional, and fore-and-aft elastic characteristics of the tires. The quantities measured or determined included lateral or cornering force, drag force, twisting moment or self-alining torque, pneumatic caster, vertical tire deflection, lateral tire distortion, wheel twist or yaw angle, rolling radius, and relaxation length. Some supplementary tests which included measurements of tire footprint area and the variation of unloaded tire radius and width with inflation pressure were made.

During straight-yawed rolling the normal force generally increased with increasing yaw angle within the test range. The pneumatic caster tended to decrease with increasing yaw angle. The sliding-drag coefficient of friction tended to decrease with increasing bearing pressure.

Measured lateral and torsional spring constants appeared to decrease with increasing amplitude of tire lateral distortion or twist, respectively.

INTRODUCTION

In order to cope with airplane landing and taxiing problems such as landings with yaw, wheel shimmy, and ground handling, designers of

landing gears must have reliable data on many elastic properties of air-
plane tires under such conditions. Until recently, the experimental
data on such tire elastic properties, most of which are summarized and
discussed in reference 1, were limited in both scope and quantity.
Recently, a program was initiated by the National Advisory Committee for
Aeronautics to alleviate this lack of experimental data by determining
experimental values of some essential tire parameters for a range of
tire sizes under static, kinematic (low-speed steady-state), and dynamic
(transient and high-speed) conditions. Some static force-deflection tests
of the program have been completed and the results were reported in ref-
erence 2. The low-speed yawed-rolling and some other elastic character-
istics were reported in reference 3 for two 56-inch-diameter, 24-ply-
rating aircraft tires and in reference 4 for two 26-inch-diameter,
12-ply-rating aircraft tires. The present paper gives results from parts
of the kinematic and static test programs for two 40-inch-diameter,
40 × 12, 14-ply-rating, type VII aircraft tires.

Most of the investigation consisted of towing the tire specimens
along a straight path in a yawed condition. The angle-of-yaw range cov-
ered was from 0° to 24.5° and the inflation-pressure range was from about
74 pounds per square inch to 143 pounds per square inch. The two
vertical-loading conditions investigated were 15,000 and 28,300 pounds
per tire. The 15,000-pound vertical load represented approximately the
rated load for this type of tire as specified by reference 5, whereas
the 28,300-pound vertical load represented approximately twice the rated
load. For each yawed-rolling run, the towing speed was held constant
and did not exceed 4 miles per hour. The quantities measured or deter-
mined included vertical tire deflection, lateral force, drag force, self-
alining torque, pneumatic caster, rolling radius, and relaxation length.
Relaxation-length measurements were also obtained for the case of zero
yaw for a standing and rolling tire.

Drag tests were conducted with the wheels locked to obtain measure-
ments in the fore-and-aft direction of the maximum and sliding coeffi-
cients of friction and the stiffness of the tires for both wet- and dry-
concrete conditions under a vertical load of approximately 9,100 pounds
per tire.

Tests were performed on the standing tires to determine the static
vertical-, lateral-, and torsional-elasticity characteristics. Some
supplementary tests were also performed to measure tire footprint area
and to determine the variation of the free-tire radius and width with
tire inflation pressure.

SYMBOLS

A_g gross footprint area, sq in.

A_n net footprint area, sq in.

b overall tire-ground contact width, in.

d outside diameter of free tire, in.

F_R resultant force, $\sqrt{F_x^2 + F_y^2}$, lb

F_x instantaneous drag or fore-and-aft force (ground force parallel to direction of motion), lb

F_y instantaneous cornering force (ground force perpendicular to direction of motion), lb

F_z vertical load on tire, lb

F_ψ normal force (ground force perpendicular to wheel plane, $F_y \cos \psi + F_x \sin \psi$), lb

$2h$ overall tire-ground contact length, in.

K_x fore-and-aft spring constant, lb/in.

K_α torsional spring constant, lb-in./deg

K_λ lateral or side spring constant, lb/in.

L relaxation length, in.

L_f unyawed-rolling relaxation length, in.

L_s static relaxation length, in.

L_y yawed-rolling relaxation length, in.

M_z twisting moment or self-alining torque, lb-in.

N cornering power (rate of change of cornering force with yaw angle for small yaw angles on a rolling tire, $dF_{y,r,e}/d\psi$ or $dF_{\psi,r,e}/d\psi$ for ψ approaching 0), lb/deg

p tire inflation pressure, lb/sq in.

p_b minimum rated bursting pressure of tire, lb/sq in.

p_o tire inflation pressure at zero vertical load $(F_z = 0)$, lb/sq in.

p_g average gross footprint pressure, F_z/A_g, lb/sq in.

p_n average tire-ground bearing pressure, F_z/A_n, lb/sq in.

q pneumatic caster, $M_{z,r,e}/F_{\psi,r,e}$, in.

r outside radius of free tire, $\dfrac{\text{Tire circumference}}{2\pi}$, in.

r_e rolling radius, $\dfrac{v}{\omega}$, in.

s peripheral distance around tire, in.

v rolling velocity, in./sec

w maximum tire width, in.

x displacement of wheel axle in direction of motion, in. or ft

δ vertical tire deflection due to combined vertical and yaw loads, in.

δ_o vertical tire deflection due to vertical load only, in.

η_λ structural damping coefficient for lateral distortion

λ lateral distortion of tire equator, in.

λ_o lateral distortion of tire equator at center of contact, in.

$\mu_{x,m}$ maximum drag coefficient of friction, $F_{x,n,m}/F_z$

$\mu_{x,s}$ sliding-drag coefficient of friction, $F_{x,n,s}/F_z$

μ_ψ yawed-rolling coefficient of friction, $F_{R,r,e,m}/F_z$

ψ twist or yaw angle, deg

ω wheel angular velocity, radians/sec

Subscripts:

e   equilibrium or steady-state rolling condition

m   maximum

n   nonrolling condition

r   rolling condition

s   sliding condition

Bars over symbols denote the average values of the quantities involved for tires A and B.

APPARATUS

Test Vehicle

The basic test vehicle consisted of the fuselage and wing center section of a cargo airplane, which was towed tail-first by a tractor truck at such an attitude that the original airplane shock struts were nearly vertical. The original yokes and torque links of the landing-gear struts, along with the wheel assemblies, were replaced by steel wheel housings which held the tires and wheels tested. These steel wheel housings were connected together by means of an instrumented truss. Holes located in the wheel housing at angular intervals of 3.5° permitted the wheel frames to be rotated through a yaw-angle range of 0° to 24.5° toe out. A sketch of the basic test vehicle is shown in figure 1. A more detailed description of this test vehicle is given in reference 3 and applies in general to the present investigation.

For most of the tests the weight of the test vehicle was adjusted so that the vertical loading per tire was approximately 9,000 pounds, 15,000 pounds, or 28,000 pounds. The maximum towing force required was approximately 5,000 pounds per tire.

Instrumentation

The test vehicle was equipped with instruments for measuring lateral force, twisting moment (self-alining torque for the yawed-rolling case), drag, vertical tire deflection, horizontal translation, and wheel rotation. Measurements of these quantities were recorded simultaneously on a 14-channel recording oscillograph mounted in the test vehicle. This oscillograph was equipped with a 0.01-second timer. The instrumentation is discussed in detail in reference 3.

Tires

General description.- The tires used in this investigation were a pair of 40-inch-diameter, 40 × 12, 14-ply-rating, type VII, rib-tread tires which were made by the same manufacturer. The specifications for these tires given in table I were obtained either from reference 5 or by direct measurements. Figure 2 shows inflated and deflated half cross sections of the two test tires. These cross sections were obtained from plaster casts taken at the end of the tests when the tires were in a worn condition. There is no appreciable difference between the profiles for the two tires.

Tire wear.- During the course of the present investigation, there was an appreciable progressive change in the cross-sectional shape of the tires due to skidding and working of the tires. Therefore, the chronological order in which the test data were collected may be of some importance in the interpretation of the data. This chronological order is indicated by a test series letter (A, B, C, D, E, or F) which is assigned to all data.

The change in tire-tread pattern due to tire wear during the tests is illustrated in figure 3. At the beginning of the tests the tread pattern of both tires had a rectangular cross section (fig. 3(a)). During test series B the sides of the treads in direct contact with the ground began to wear away, and this wearing away produced the tread shape shown in figure 3(b), which was taken at the end of test series B. During test series E this wear increased to the extent shown in figure 3(c).

Free-tire radius and width.- The hysteresis loops for free-tire radius and width plotted against inflation pressure are shown in figure 4 for tires A and B. The elapsed time from the start is shown for a few of the measurements presented. The variation in tire radius due to hysteresis for a given pressure is seen to be practically negligible (less than 0.2 inch) in the operating pressure range of these tires for this relatively slow rate of change of pressure. The corresponding change in width is about 0.1 inch. Also shown in this figure are several radius

and width measurements which were made after the tires had been left unloaded at constant pressure for at least 24 hours in order to reach an equilibrium condition.

Test Surface

All yawed-rolling and drag tests were conducted by towing the test vehicle along the center of a 9-inch-thick reinforced-concrete taxi strip. This taxi strip had a slight crown so that the tires on the test vehicle were tilted (less than 1°) with respect to the surface. The taxi strip was a boarded concrete surface. Profiles of this concrete surface, indicating its roughness, are shown in both references 3 and 4. The test surface for the unyawed-rolling relaxation-length tests, the static lateral-elasticity tests, and most of the footprint-area measurements was a much smoother, level, reinforced-concrete hangar floor. The test surfaces for all other tests were steel plates.

TEST PROCEDURE AND EXPERIMENTAL RESULTS

The present investigation of tire characteristics is divided into the following parts: yawed-rolling tests, relaxation-length tests, locked-wheel drag tests, static vertical-elasticity tests, static lateral-elasticity tests, static torsional-elasticity tests, and supplementary measurements.

Yawed-Rolling Tests

For each of the yawed-rolling runs, the test vehicle was moved into towing position on the dry, clean, concrete taxi strip and the wheel housings were rotated and locked at the particular yaw angle desired. The tires were adjusted to the test inflation pressure and were then jacked clear of the ground to remove any residual stresses resulting from the previous runs or from the changing of the yaw angles of the wheels. The jacks were removed and the initial vertical tire deflections noted. The vehicle was then towed straight ahead, from this initial essentially unstressed condition, for a distance of approximately 40 feet. Although the speed remained approximately constant throughout any particular run, it varied from run to run within a speed range of approximately 0.7 to 4.0 miles per hour. Figure 5 shows tire B during a run at a yaw angle of 17.5°.

All runs at 0°, 3.5°, 7°, 10.5°, 14°, 17.5°, 21°, and 24.5° were made with both wheels symmetrically yawed with respect to the longitudinal axis of the test vehicle. Although these particular yaw angles

were the only angles easily attainable on the test vehicle, some test runs at 1.75° were made by yawing the wheels unsymmetrically with respect to the longitudinal axis of the test vehicle (that is, one wheel was set at an angle of 0° and the other at 3.5°). When towed ahead with these wheels unsymmetrically yawed, the test vehicle first veers off to the side because of the unsymmetrical forces. After a short distance, however, the vehicle runs smoothly with its longitudinal axis yawed with respect to the direction of motion so that both wheels have the same final intermediate yaw angle of 1.75° with respect to the direction of motion.

From the start of each run the measurements of lateral force, twisting moment or self-alining torque, drag force, vertical tire deflection, wheel rotation, and vehicle translation in the direction of motion were recorded continuously.

Tables II, III, and IV summarize all test data obtained during the final steady-state stage of the yawed-rolling runs and from a few supplementary runs to determine rolling radius at zero yaw. (The run numbers in the tables and figures do not indicate the chronological order in which the runs were made; they are listed only for convenience in referring to the test data.) In tables II, III, and IV, data are presented for three different test series (B, E, and F) which represent different vertical loadings. The variation of normal force $\overline{F}_{\psi,r,e}$, self-alining torque $\overline{M}_{z,r,e}$, and pneumatic caster $\overline{q}$ with yaw angle is shown in figures 6 and 7 for all vertical loads and inflation pressures tested. The rolling radii are plotted in figure 8 as functions of tire inflation pressure and vertical tire deflection.

The buildup of cornering force with horizontal distance rolled during the initial stages of the yawed-rolling runs is illustrated in figure 9 for several inflation pressures and two vertical loadings. Inasmuch as for most runs there was a slight initial residual force or preload in the tires, the original test curves did not always pass exactly through the origin. The test curves shown in figure 9 have been horizontally shifted (if necessary) so that the extrapolation of each curve passes through the origin.

Relaxation-Length Tests

Three types of relaxation length were determined in this investigation, namely, static relaxation length L_s, unyawed-rolling relaxation length L_f, and yawed-rolling relaxation length L_y. The definitions for these relaxation lengths are given in reference 3. The methods used to determine these relaxation lengths are as follows:

Static relaxation length L_s.- The standing tires were given initial lateral deflections by pulling outward, by means of hydraulic rams, plates located underneath the tires. The lateral distortion of the center tire tread relative to the wheel center plane was then measured at several points around each tire circumference between the footprint edge and a point 180° from the center of contact.

Unyawed-rolling relaxation length L_f.- With the wheel housings positioned at 0° yaw, the tires were given initial lateral distortions by pulling outward on plates placed underneath the tires (as for the static relaxation length tests). The test vehicle was then rolled straight ahead for a distance of about 50 feet with the recording oscillograph making a continuous record of lateral force and horizontal translation.

Yawed-rolling relaxation length L_y.- The basic data for the yawed-rolling relaxation lengths were obtained from the initial (force buildup) phase of the yawed-rolling tests. This relaxation length was evaluated for all runs except a few at large yaw angles for which tire skidding appeared to be too significant.

Relaxation-length data.- Samples of the test data used to determine the three types of relaxation length for the tire specimens are shown in figure 10. This figure shows experimental data for three runs, plotted in both linear and semilogarithmic coordinates, together with empirical exponential curves which were obtained by fitting straight lines to these data on the semilogarithmic plots. The corresponding relaxation length for each set of data is, by definition, the denominator of the power of e in the equation of the exponential curve fitted to the data. (For example, the relaxation length for the data in figure 10(c) is 14.1 inches.) The values obtained in this manner from the test runs are listed in table V for the static-relaxation-length tests, in table VI for the unyawed-rolling relaxation-length tests, and in table II for the yawed-rolling relaxation-length tests.

Locked-Wheel Drag Tests

In order to determine tire stiffness and sliding drag in the fore-and-aft direction on dry concrete, the wheels were positioned at 0° yaw and locked to prevent rotation, and the test vehicle was pulled forward by hydraulic rams (see ref. 3) at a speed less than 10 inches per minute (0.009 mile per hour). A continuous record was taken of drag force and horizontal displacement during each run. In addition, several runs were made with the concrete surface wet. For these particular runs, the tires were jacked clear of the concrete surface immediately before a run and the concrete surface below each tire was wetted thoroughly with water by

means of a garden hose. The jacks were then removed and the run was conducted in the same manner as the dry-concrete runs. Throughout each wet-concrete run, a stream of water was directed onto the concrete surface in front of each tire so that the tires would always remain in contact with wet concrete.

During these tests, the weight of the test vehicle remained constant; however, the vertical load on the tires decreased slightly with increasing drag force as a consequence of the moment produced by the drag force. This change in vertical force was taken into account in the computation of friction coefficients. (It was not taken into account in the other tests, since the effect was small for those conditions.)

Most of the experimental data obtained from the locked-wheel drag tests are presented in table VII. Also, typical data are shown in figure 11 for the buildup of fore-and-aft force with horizontal distance pulled for several runs.

Static Vertical-Elasticity Tests

In the static vertical-elasticity tests the vertical loading on each tire was increased by increments from zero loading to a maximum value and was then reduced by increments to zero, the vertical tire deflection was noted for each value of vertical loading, and the unloaded-tire inflation pressure p_0 and loaded-tire inflation pressure p were also measured. This procedure was followed for all test inflation pressures.

The static vertical-elasticity data obtained are presented in figure 12. This figure shows the variation of vertical loading with vertical tire deflection for the two tire specimens at the test inflation pressures.

Static Lateral-Elasticity Tests

In the static lateral-elasticity tests, the test vehicle was oscillated laterally through several cycles, at rates of 0.3 to 1.9 minutes per cycle, by means of double-acting hydraulic rams that were attached to the wheel axles and to the hangar floor. The amplitude of the lateral oscillation was kept approximately constant for successive cycles of each individual run, but was varied between 0.4 inch and 1.6 inches for different runs. The vertical tire deflection and tire inflation were measured prior to each run, and during the run the normal force and lateral tire distortion were recorded continuously on the oscillograph. This procedure was followed for several inflation pressures at both the 14,400-pound (series B) and the 28,300-pound (series E) vertical loadings.

The basic static lateral-elasticity test data are presented in fig-
ures 13 and 14 and table VIII. Figure 13 shows the variation of normal
force with lateral tire distortion for several inflation pressures at
an average vertical loading of 14,400 pounds for each tire (test series B).
Figure 14 shows this variation at an average vertical loading of
28,300 pounds for each tire (test series E). Table VIII contains a list
of all test conditions together with some tire lateral-stiffness and
hysteresis parameters (to be discussed later) derived from the data in
figures 13 and 14.

Static Torsional-Elasticity Tests

In the static torsional-elasticity test, steel turntables were
placed beneath the wheels of the test vehicle. These turntables were
rotated back and forth through several cycles, at rates of 0.5 to
1.9 cycles per minute, by means of double-acting hydraulic rams connected
to each turntable. The amplitude of the torsional oscillation was kept
approximately constant for successive cycles of each individual run, but
was varied between 1.6^o and 7.5^o for different runs.

The vertical tire deflection and tire pressure were measured before
each run. The twisting moment and turntable angular displacement were
recorded continuously on the oscillograph during each run. This pro-
cedure was followed for several inflation pressures at both the
14,400-pound (series B) and the approximately 28,300-pound (series E)
vertical loadings.

The basic static torsional-elasticity test data are shown in fig-
ures 15 and 16. Figure 15 shows the variation of twisting moment with
twist angle for several inflation pressures at a vertical loading of
14,400 pounds for each tire (test series B). Figure 16 shows this vari-
ation at a vertical loading of approximately 28,300 pounds for each tire
(test series E). Table IX contains a list of all test conditions,
together with tire torsional-stiffness parameters obtained from fig-
ures 15 and 16.

Supplementary Measurements

In addition to the tests just described, some tire-contact or
footprint-area measurements were made for the tire specimens at several
inflation pressures and vertical tire deflections. For all runs except
those of test series C these measurements were obtained from the imprint
left on a piece of heavy paper placed between a chalked portion of the
tires and a smooth concrete hangar floor. (For test series C a smooth
steel plate was placed between tire and ground.) Several typical

imprints are shown in figure 17. The data obtained from the tire imprints
are presented in table X.

PRECISION OF DATA

The instruments used in the tests and the methods of reducing the
data are believed to yield results which are, on the average, accurate
within the following limits:

Vertical load on tire, F_z, percent . . . . ± 3

Cornering force, F_y, percent . . . . ± 3

Force perpendicular to wheel plane (normal force) or lateral
  force, F_ψ, percent . . . . ± 3

Drag force, F_x, lb . . . . ± 300

Self-alining torque or twisting moment, M_z, lb-in. . . . . $\pm 3,000$

Tire inflation pressure, p_o or p, lb/sq in. . . . . ± 3

Outside radius of free tire, r, in. . . . . ± 0.02

Rolling radius, r_e, in. . . . . ± 0.2

Horizontal translation in direction of motion, x, percent . . ± 3

Vertical tire deflection, δ_o or δ, in. . . . . ± 0.2

Lateral tire distortion, λ_o or λ, in. . . . . ± 0.02

Yaw angle or twist angle, ψ, deg . . . . ± 0.1

DISCUSSION OF PARAMETERS

Normal Force $F_{\psi, r, e}$

The variation of steady-state normal force with yaw angle, obtained
from the test data in table II, is shown in figure 6 for approximately
the rated vertical loading $\left(\overline{F}_z = 15,000 \text{ pounds, test series B}\right)$, in fig-
ure 7 for approximately twice the rated vertical loading
$\left(\overline{F}_z = 28,300 \text{ pounds, series E}\right)$, and in figure 18 for both vertical
loadings at two inflation pressures. These figures show that the nor-
mal force generally increased with increasing yaw angle within the test
range. For the rated vertical loading (fig. 6), the normal force
appeared to reach a maximum value at yaw angles between 17° and 25°;
for approximately twice the rated loading (fig. 7), the normal force
did not reach its maximum value within the tested yaw-angle range
(up to 24.5^o).

Cornering Force $F_{y,r,e}$

The steady-state cornering force follows substantially the trends that were described for the normal force, as is shown in figure 19 for two typical loading conditions.

Cornering Power N

The variation of cornering power with vertical tire deflection and inflation pressure for the two vertical loadings tested is shown in figures 20(a) and 20(b), respectively. These data, which were derived from the initial slope of the curves for the variation of normal force with yaw angle given in figures 6 and 7, indicate that, for constant vertical tire deflection, the cornering power increases with increasing inflation pressure and that, for constant inflation pressure, the cornering power decreases with increasing vertical tire deflection.

In order to compare the present test results for the 40-inch tires with the results of previous tests on other tires of the same general type (type VII; see ref. 5), cornering-power data from the present tests are compared in figure 21 with data for 56-inch-diameter tires from reference 3, for 26-inch-diameter tires from reference 4, and for 32- and 44-inch-diameter tires from reference 6. These data are presented in the form of a plot of the dimensionless ratio $\dfrac{\overline{N}}{\left(\overline{p} + 0.11\overline{p}_b\right)\overline{w}^2}$ against $\dfrac{\overline{\delta}_o}{\overline{r}}$, where $\overline{p}_b$ is the minimum rated bursting pressure of the tire as taken from reference 5. (The form of these ratios is based on the results of a study of tire characteristics given in ref. 7.) From figure 21 it appears that the indicated cornering-power parameter is approximately the same for the different tires so that the cornering power for any tire of this type (type VII) can be estimated from the solid-line mean curve on the figure, with an error of less than ±20 percent.

Self-Alining Torque $\overline{M}_{z,r,e}$

The variation of self-alining torque with yaw angle is shown in figures 6 and 7 for the two vertical loadings investigated. The self-alining torque generally increased with increasing yaw angle for small yaw angles and decreased with increasing yaw angle at large yaw angles. For constant vertical loading, the data indicate that increasing the inflation pressure tends to reduce the magnitude of the self-alining

torque at large yaw angles. In the case of constant inflation pressure, illustrated in figure 18, increasing the vertical loading increases the self-alining torque.

Maximum Self-Alining Torque $\overline{M}_{z,r,e,m}$

The variation of maximum self-alining torque with inflation pressure is shown in figure 22 for the two test conditions investigated. For constant vertical loading over the range of inflation pressures investigated, increasing the inflation pressure tends to decrease the maximum self-alining torque. For constant inflation pressure, the maximum self-alining torque increases with increasing vertical loading.

Pneumatic Caster $\overline{q} = \overline{M}_{z,r,e} / \overline{F}_{\psi,r,e}$

The variation of pneumatic caster with yaw angle for all test conditions is shown in figures 6 and 7. These figures show that the pneumatic caster is at a maximum at small yaw angles and generally decreases with increasing yaw angle for the test range covered (up to 24.5° yaw). For constant inflation pressure, illustrated in figure 18, the pneumatic caster increases with increasing vertical load.

Drag Force $\overline{F}_{x,r,e}$

The variation of steady-state (rolling condition) drag force with yaw angle for all conditions of the yawed-rolling test is shown in figure 23. These data show that the effect of inflation pressure on drag force for the two vertical loadings investigated is apparently small. In order to show trends more clearly, the ratio of drag force to cornering force $\overline{F}_{x,r,e} / \overline{F}_{y,r,e}$ is plotted against yaw angle for all test conditions in figure 24. If the total horizontal ground force during yawed rolling were normal to the wheel plane, the drag force $\overline{F}_{x,r,e}$ would be equal to the cornering force $\overline{F}_{y,r,e}$ multiplied by the tangent of the yaw angle, or $\overline{F}_{x,r,e} / \overline{F}_{y,r,e} = \tan \psi$. In figure 24, $\tan \psi$ is represented by the solid lines. Since the data do not usually fall along these lines, it appears that some force parallel to the wheel plane exists for most of the yaw-angle range investigated.

Yawed-Rolling Coefficient of Friction $\bar{\mu}_\psi = \overline{F}_{R,r,e,m}/\overline{F}_z$

The variation of yawed-rolling coefficient of friction with average bearing pressure or ground pressure is shown in figure 25 (square symbols), and the data are compared with corresponding data for 26-inch-diameter and 56-inch-diameter type VII tires (from refs. 3 and 4) in figure 26 (see unflagged symbols in fig. 26). From this comparison it appears that the data for the different tires are in fair agreement. (The fact that the coefficients are noticeably smaller for the 26-inch-diameter tires than for the other tires might be explained by consideration of possible experimental errors in the data for the 26-inch-diameter tires.)

Sliding-Drag (Fore-and-Aft) Coefficient of

Friction $\bar{\mu}_{x,s} = \overline{F}_{x,s}/\overline{F}_z$

The variation of sliding-drag coefficient of friction with average bearing pressure for both dry and wet concrete at the one vertical loading tested $\left(\overline{F}_z \approx 9{,}100 \text{ pounds}\right)$ is shown in figure 25. (See circle symbols.) These data are also listed in table VII. The sliding-drag coefficient of friction on dry concrete appears to decrease in magnitude with increasing bearing pressure. The friction coefficients found in the limited number of tests made on wet concrete tended to be slightly smaller than those found on dry concrete. Also shown in figure 25 for comparison purposes are the limited number of coefficient-of-friction values obtained from the yawed-rolling tests. (See square symbols.) A comparison of these data indicates that the sliding-drag coefficients of friction are in fair agreement with the corresponding yawed-rolling coefficients of friction.

Sliding-drag and yawed-rolling coefficients of friction obtained from tests on 56-inch and 26-inch tires (refs. 3 and 4) are compared with present test results in figure 26. The friction coefficients for the different tires are in fairly good agreement and show the same general trend. This general trend for all the data can be described by the empirical equation

$$\bar{\mu}_\psi = \bar{\mu}_{x,s} = 0.93 - 0.0011\bar{p}_n$$

where $\bar{p}_n$ is in pounds per square inch. (See fig. 26.)

Maximum Drag Coefficient of Friction $\bar{\mu}_{x,m} = \bar{F}_{x,m}/\bar{F}_z$

The maximum drag force $\bar{F}_{x,m}$ at incipient slip is sometimes slightly larger than the drag force $\bar{F}_{x,s}$ required for steady sliding of the locked wheels and tires, as is shown in figure 11 for several typical runs. A comparison of maximum and sliding-drag coefficients of friction, presented in figure 27, indicates that the maximum drag coefficient of friction is rarely more than 3 percent greater than the sliding-drag coefficient of friction at the low speeds of these tests (less than 0.009 mile per hour).

Fore-and-Aft Spring Constant $\bar{K}_x$

The variation of fore-and-aft spring constant with tire inflation pressure, obtained from data in table VII for the one vertical loading investigated $\left(\bar{F}_z \approx 9,100 \text{ pounds}\right)$, is shown in figure 28. These data are derived from the initial slope of the curves for the variation of the fore-and-aft (drag) force $\bar{F}_x$ with horizontal displacement $\bar{x}$. Samples of these curves for three test inflation pressures are presented in figure 11. For the one vertical loading tested, figure 28 indicates that the fore-and-aft spring constant increases slightly with increasing inflation pressure in the pressure range investigated.

Lateral Spring Constant $\bar{K}_\lambda$

The variation of lateral spring constant with tire inflation pressure for the two vertical loadings tested is shown in figure 29(a). It may be seen from this figure that the lateral spring constant is approximately the same for both vertical loads tested and increases approximately linearly with increasing inflation pressure.

The effect of amplitude of lateral tire distortion on the spring constant may be seen from figures 14 and 29(b). The data in these figures indicate that the lateral spring constant, for any given inflation pressure and vertical load, decreases slightly with increasing lateral deformation.

Hysteresis Damping Coefficient for Lateral Deformation $\bar{\eta}_\lambda$

The experimental hysteresis damping data obtained from the static lateral-elasticity tests are presented in table VIII and figure 30 in terms of the conventional structural damping coefficient η_λ , which is

defined as the ratio of the maximum half-height of the corresponding
force-deflection hysteresis loop to the maximum total force (that is,
the ratio A/B in the sketch).
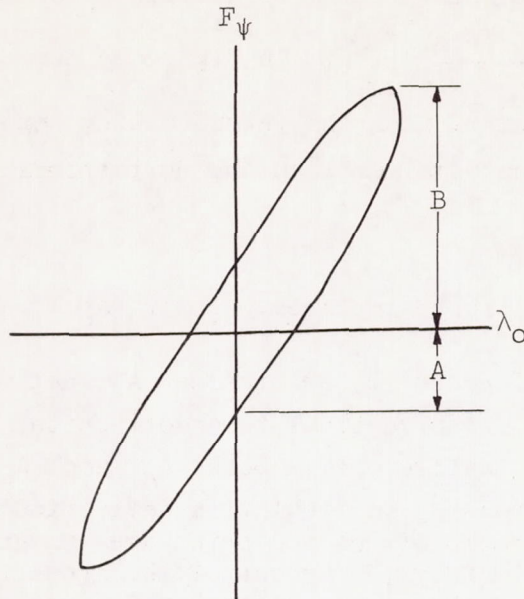
In figure 30 the hysteresis damping coefficient appears to decrease
slightly with increasing inflation pressure for constant vertical load
and to increase with increasing vertical load for constant inflation
pressure.

Torsional Spring Constant K_α

The variation of static torsional spring constant $K_{\alpha,n}$ with tire
inflation pressure for the two vertical loadings tested is shown in
figure 31. The values of static spring constant shown in this figure
(and in table IX) were obtained from the approximately straight-line
portions of the curves in figures 15 and 16. From figure 31 it appears
that the static torsional spring constants for the two tires are in fair
agreement with each other. At constant pressure the static torsional
spring constant increases with increasing vertical load.

The effect of amplitude of tire twist on the spring constant may
be seen from figures 16 and 32. The data in these figures indicate that
the static spring constant decreases appreciably with increasing ampli-
tude of tire twist.

In figure 33 the static torsional spring constants $K_{\alpha,n}$ are compared with the corresponding spring constants $\overline{K}_{\alpha,r}$ obtained from the initial slopes of the self-alining-torque curves of figures 6 and 7 $\left(\text{that is,} \quad \overline{K}_{\alpha,r} = \left(\dfrac{d\overline{M}_{z,r,e}}{d\overline{\psi}} \right)_{\overline{\psi} \to 0} \right).$ In figure 33 the torsional spring constants $K_{\alpha,r}$ obtained from the yawed-rolling tests appear to be about the same as or somewhat smaller than the corresponding static spring constants $K_{\alpha,n}$.

Footprint Area A_g or A_n

The variation of gross footprint area A_g, net footprint area A_n, and the ratio A_n/A_g with vertical tire deflection, obtained from data in table X, is shown in figure 34. Both A_g and A_n appear to increase nonlinearly with increasing vertical tire deflection for the deflection range covered. The ratio of net footprint area to gross footprint area appears to be approximately 75 percent of the gross footprint area. This ratio will, of course, change for tires having tread designs different from the ones tested.

Footprint Length $2h$ and Width b

The variation of footprint length $2h$ and width b with vertical tire deflection, obtained from data in table X, is shown in figure 35. Also shown in this figure as solid lines are the lengths of chords of circles having diameters equal to the free diameter d and maximum width w, respectively, of the tire at its rated inflation pressure and located at a distance $r - \delta_0$ from the center of the circles. A comparison of these quantities indicates that the experimental values of footprint width are approximately equal to the corresponding chord lengths, whereas experimental values of footprint length are usually smaller than the corresponding chord lengths for the vertical-tire-deflection range investigated.

Average Bearing Pressure $\overline{p}_n = \overline{F}_z / \overline{A}_n$ and Average

Gross Footprint Pressure $\overline{p}_g = \overline{F}_z / \overline{A}_g$

The variation of average bearing pressure and average gross footprint pressure with tire inflation pressure is given in figure 36. The

data shown in this figure are derived from mean values of the curves given in figure 12 for the variation of vertical load with vertical tire deflection and from the faired curves given in figure 34 for the variation of footprint area with vertical tire deflection.

The solid line in figure 36 represents $\bar{p}_n = \bar{p}_g = \bar{p}$. Comparison of this line with the data for the average bearing pressure $\bar{p}_n$ indicates that the average bearing pressure is appreciably greater than the inflation pressure and that it increases with increasing vertical deflection. The average gross footprint pressure p_g, however, is not greatly different from the inflation pressure for the inflation-pressure range covered.

Relaxation Length L

The variation of the three types of relaxation length with inflation pressure at two vertical loadings is shown in figure 37. For a given vertical loading the static relaxation length usually appears to be the largest of the three types of relaxation length and the yawed-rolling relaxation length appears to be the smallest. All three types of relaxation length appear to decrease with increasing vertical load and are relatively independent of inflation pressure.

Rolling Radius r_e

The variation of rolling radius with inflation pressure for the three vertical loadings investigated is shown in figure 8(a). The data presented in this figure were obtained from table III and are for essentially unyawed conditions. In order to show more clearly the trends of these data, the effect of inflation pressure has been isolated in figure 8(b), where rolling radius is plotted against vertical tire deflection for several constant inflation pressures. Figure 8(b) shows that, for constant inflation pressure, the rolling radius decreases with increasing vertical tire deflection and, for constant vertical tire deflection, the rolling radius increases slightly with increasing inflation pressure. Similar variations were observed in references 3 and 4 for 56-inch-diameter and 26-inch-diameter tires.

CONCLUSIONS

Tow tests were made primarily to determine the low-speed yawed-rolling characteristics of two 40 × 12, 14-ply-rating, type VII aircraft tires at two vertical loadings which were approximately equal to the

rated vertical loading and twice the rated vertical loading for these
tires. The results of these tests indicated the following primary
conclusions:

1. The normal force generally increased with increasing angle of
yaw within the test range ($0°$ to $24.5°$).

2. The cornering power, under constant inflation pressure, decreased
with increasing vertical tire deflection for the two vertical loadings
investigated. For the case of constant vertical tire deflection,
increasing the vertical loading increased the cornering power.

3. The self-alining torque generally increased with increasing angle
of yaw for small angles of yaw and decreased with increasing angle of yaw
at large angles of yaw.

4. The pneumatic caster generally decreased with increasing angle
of yaw for the test range covered.

5. The sliding-drag coefficient of friction decreased with increasing
bearing pressure; and at comparable bearing pressures, both the sliding-
drag and yawed-rolling coefficients of friction followed approximately
the same trends and magnitudes that were reported for 56-inch-diameter
and 26-inch-diameter tires in NACA Technical Notes 3235 and 3604.

6. The static torsional spring constant, for a given vertical load
and inflation pressure, decreased appreciably with increasing amplitude
of tire twist.

Langley Aeronautical Laboratory,
    National Advisory Committee for Aeronautics,
        Langley Field, Va., July 24, 1957.

REFERENCES

1. Hadekel, R.: The Mechanical Characteristics of Pneumatic Tyres. S & T Memo. No. 5/50, British Ministry of Supply, TPA 3/TIB, Mar. 1950.

2. Horne, Walter B.: Static Force-Deflection Characteristics of Six Aircraft Tires Under Combined Loading. NACA TN 2926, 1953.

3. Horne, Walter B., Stephenson, Bertrand H., and Smiley, Robert F.: Low-Speed Yawed-Rolling and Some Other Elastic Characteristics of Two 56-Inch-Diameter, 24-Ply-Rating Aircraft Tires. NACA TN 3235, 1954.

4. Horne, Walter B., Smiley, Robert F., and Stephenson, Bertrand H.: Low-Speed Yawed-Rolling Characteristics and Other Elastic Properties of a Pair of 26-Inch-Diameter, 12-Ply-Rating, Type VII Aircraft Tires. NACA TN 3604, 1956.

5. Anon: Military Specification - Casings; Aircraft Pneumatic Tire. Military Specification, MIL-C-5041, Sept. 16, 1949; Amendment-2, Feb. 8, 1951.

6. Evans, R. D.: Cornering Power of Airplane Tires. The Goodyear Tire & Rubber Co., Oct. 17, 1946.

7. Smiley, Robert F., and Horne, Walter B.: Mechanical Properties of Pneumatic Tires with Special Reference to Modern Aircraft Tires. NACA TN 4110, 1957.

TABLE I.- TIRE SPECIFICATIONS

Specifications	Military specification (ref. 5)	End of test, tires in worn condition	
		Tire A	Tire B
Tire:			
Type[a]	VII	-----	-----
Ply rating	14	-----	-----
Static load, lb	14,500	-----	-----
Inflation pressure, lb/sq in.	95	-----	-----
Burst pressure, lb/sq in.	380 (min.)	-----	-----
Moment of static unbalance, oz-in.	40 (max.)	-----	-----
Diameter, deflated, in.	------------	38.00	39.10
Diameter, inflated, in.	38.55 (min.) / 39.70 (max.)	39.16	39.30
Maximum width, deflated, in.	------------	11.80	11.80
Maximum width, inflated, in.	11.70 (min.) / 12.35 (max.)	12.12	12.12
Bead width, in.	2.38 (max.)	1.60	1.67
Minimum wall thickness, in.	------------	0.50	0.52
Wall thickness at tread center line (including tread), in.	------------	0.83	0.80
Depth of tread (at tread center line), in.	0.29 (min.)	0.34	0.34
Casing weight, lb	95 (max.)	85	85
Tread pattern	Rib	Rib	Rib
Inner tube:			
Thickness, in.		0.1	0.1
Weight, lb		14	13
Wheel:			
Rim diameter, in.		21.00	21.00
Weight, lb		76	77

[a]Type VII is an extra-high-pressure tire.

TABLE II.- YAW TEST DATA

(a) Series B; $\overline{F}_Z$ = 15,000 pounds

Run	$\bar{p}_o,$ $\dfrac{\text{lb}}{\text{sq in.}}$	$\bar{p},$ $\dfrac{\text{lb}}{\text{sq in.}}$	$\bar{\delta}_o,$ in.	$\bar{\delta},$ in.	$\bar{\psi},$ deg	$\overline{F}_{y,r,e},$ lb	$\overline{F}_{x,r,e},$ lb	$\overline{F}_{\psi,r,e},$ lb	$\overline{M}_{z,r,e},$ lb-in.	$\bar{q},$ in.	$\overline{L}_y,$ in.
1	74	79	3.4	3.5	1.75	1,240	200	1,240	12,100	9.72	(a)
2	74	77	3.4	3.6	3.5	2,440	300	2,450	20,100	8.20	11.5
3	74	78	3.5	3.7	7.0	4,590	1,000	4,670	21,300	4.57	12.8
4	74	78	3.4	3.7	7.0	4,520	900	4,590	23,700	5.17	14.1
5	74	78	3.5	3.9	10.5	6,410	1,600	6,590	25,600	3.88	(b)
6	74	78	3.5	4.3	14.0	8,110	2,300	8,440	23,700	2.81	(b)
7	74	77	3.5	4.6	17.5	9,370	3,200	9,900	21,600	2.18	(b)
8	74	78	3.5	4.6	21.0	9,900	3,800	10,600	12,600	1.19	(b)
9	75	80	3.5	4.8	24.5	10,400	4,100	11,160	14,000	1.25	(b)
10	93	97	2.9	2.9	1.75	1,500	200	1,510	10,100	6.66	(a)
11	93	97	3.0	3.1	3.5	2,970	200	2,980	17,900	6.00	12.7
12	92	98	3.0	3.1	7.0	5,840	1,000	5,920	25,400	4.29	12.2
13	93	97	3.0	3.2	7.0	5,580	700	5,620	24,200	4.31	12.4
14	93	97	2.9	3.4	10.5	7,940	1,700	8,110	20,900	2.57	(b)
15	93	96	3.0	3.4	14.0	9,480	2,300	9,760	16,600	1.70	(b)
16	93	97	3.0	3.7	17.5	10,760	3,400	11,290	15,700	1.39	(b)
17	95	98	3.0	3.7	17.5	10,120	3,100	10,600	19,000	1.79	(b)
18	93	97	3.0	3.8	21.0	10,620	3,900	11,310	7,500	.67	(b)
19	95	98	3.1	3.9	24.5	10,510	4,400	11,380	10,500	.93	(b)
20	113	116	2.6	2.6	1.75	1,850	100	1,850	12,900	6.96	(a)
21	113	116	2.6	2.7	3.5	3,470	200	3,480	18,900	5.44	13.1
22	113	116	2.6	3.0	7.0	6,260	900	6,320	23,700	3.74	(a)
23	113	115	2.6	2.9	10.5	8,610	1,800	8,790	19,800	2.25	(b)
24	113	115	2.7	3.2	14.0	10,310	2,500	10,600	15,500	1.47	(b)
25	113	119	2.6	3.1	17.5	10,810	3,000	11,210	14,100	1.26	(b)
26	113	116	2.7	3.2	17.5	10,440	3,100	10,880	12,900	1.18	(b)
27	113	118	2.7	3.2	21.0	10,250	3,600	10,870	5,300	.49	(b)
28	133	134	2.3	2.4	1.75	2,020	100	2,020	10,000	4.95	13.2
29	133	135	2.4	2.4	3.5	4,070	200	4,080	19,200	4.70	14.2
30	133	135	2.4	2.6	7.0	7,100	1,100	7,180	21,700	3.02	(a)
31	133	134	2.4	2.6	7.0	7,150	1,100	7,230	15,700	2.17	13.9
32	132	135	2.4	2.7	10.5	9,550	1,900	9,730	17,600	1.81	(b)
33	132	134	2.4	2.6	14.0	10,540	2,400	10,810	11,800	1.09	(b)
34	130	132	2.4	2.8	17.5	(a)	3,100	(a)	(a)	(a)	(b)
35	133	134	2.4	2.6	17.5	11,090	3,300	11,560	13,800	1.19	(b)
36	132	134	2.4	2.7	21.0	10,470	3,600	11,080	5,800	.53	(b)

[a]Value could not be accurately determined.

[b]Value not determined.

TABLE II.- YAW-TEST DATA - Concluded

(b) Series E; $\overline{F}_z = 28,300$ pounds

Run	$\bar{p}_o$, lb/sq in.	$\bar{p}$, lb/sq in.	$\bar{\delta}_o$, in.	$\bar{\delta}$, in.	$\bar{\psi}$, deg	$\overline{F}_{y,r,e}$, lb	$\overline{F}_{x,r,e}$, lb	$\overline{F}_{\psi,r,e}$, lb	$\overline{M}_{z,r,e}$, lb-in.	$\bar{q}$, in.	$\overline{L}_y$, in.
37	95	104	5.2	5.3	1.75	1,100	700	1,120	11,600	10.36	(a)
38	95	105	5.1	5.3	1.75	1,020	300	1,030	12,900	15.52	(a)
39	95	105	5.2	5.2	3.5	1,860	800	1,910	22,700	11.88	8.9
40	95	105	5.1	5.3	3.5	1,860	700	1,900	19,800	10.42	(a)
41	95	105	5.2	5.3	7.0	3,200	1,100	3,310	43,300	13.08	7.8
42	95	105	5.1	5.4	7.0	3,400	1,400	3,550	41,600	11.72	(a)
43	95	105	5.2	5.7	10.5	5,020	2,500	5,390	55,000	10.20	8.6
44	95	105	5.2	5.7	10.5	4,960	2,200	5,280	58,100	11.00	8.2
45	95	105	5.1	5.9	14.0	6,880	3,600	7,550	52,200	6.91	10.1
46	95	105	5.3	6.5	17.5	8,590	4,700	9,610	54,200	5.64	(b)
47	115	125	4.5	4.5	1.75	1,340	100	1,340	12,200	9.10	11.8
48	115	124	4.5	4.6	3.5	2,490	800	2,530	23,800	9.41	10.4
49	115	122	4.5	4.7	7.0	4,910	1,300	5,030	49,900	9.92	8.6
50	115	125	4.5	4.7	7.0	4,760	1,500	4,910	43,000	8.76	10.5
51	115	124	4.5	5.0	10.5	7,040	2,400	7,360	48,100	6.54	(a)
52	115	124	4.6	5.4	14.0	8,880	3,700	9,510	45,900	4.83	(a)
53	115	125	4.5	5.3	14.0	9,680	3,600	10,260	52,700	5.14	10.1
54	115	125	4.5	5.5	17.5	11,530	4,800	12,440	52,200	4.20	(b)
55	115	124	4.6	5.7	17.5	10,850	4,900	11,820	45,900	3.88	(b)
56	135	142	4.0	4.2	1.75	1,470	100	1,470	12,100	8.23	(a)
57	135	143	4.0	4.0	1.75	1,430	100	1,430	9,400	6.57	7.5
58	135	142	4.1	4.1	3.5	2,910	400	2,930	24,700	8.43	11.6
59	135	143	4.0	4.1	7.0	5,790	1,400	5,920	49,500	8.36	13.1
60	135	141	4.0	4.2	7.0	5,730	1,500	5,870	44,000	7.50	9.5
61	135	143	4.0	4.4	10.5	8,770	2,300	9,040	45,500	5.03	12.1
62	135	143	4.0	4.8	14.0	11,530	3,700	12,080	42,100	3.49	12.4
63	135	142	4.0	5.0	17.5	13,900	5,000	14,760	35,900	2.43	(b)

[a]Value could not be accurately determined.

[b]Value not determined.

TABLE III.- ROLLING-RADIUS DATA FOR SMALL YAW ANGLES

Run	Test series	ψ, deg	Tire A						Tire B					
			p_0, $\frac{lb}{sq\ in.}$	p, $\frac{lb}{sq\ in.}$	F_z, lb	δ_0, in.	r_e, in.	r, in.	p_0, $\frac{lb}{sq\ in.}$	p, $\frac{lb}{sq\ in.}$	F_z, lb	δ_0, in.	r_e, in.	r, in.
64	B	0	74	77	14,900	3.4	17.8	(a)	74	77	15,000	3.5	17.8	(a)
65	B	0	93	96	14,900	3.0	18.0	(a)	93	96	15,000	2.9	18.1	(a)
66	B	0	113	115	14,900	2.6	18.3	(a)	113	115	15,000	2.6	18.4	(a)
67	B	0	133	134	14,900	2.4	18.5	(a)	133	135	15,000	2.4	18.5	(a)
68	E	0	95	105	28,400	5.1	17.6	(a)	95	105	28,200	5.1	17.6	(a)
69	E	1.75	95	104	28,400	5.2	17.6	(a)	95	104	28,200	5.2	17.6	(a)
70	E	0	115	124	28,400	4.5	17.9	(a)	115	124	28,200	4.5	17.9	(a)
71	E	1.75	115	124	28,400	4.5	17.9	(a)	115	125	28,200	4.5	17.9	(a)
72	E	0	135	143	28,400	4.0	18.1	(a)	135	143	28,200	4.0	18.1	(a)
73	E	1.75	135	142	28,400	4.0	18.1	(a)	135	142	28,200	4.0	18.1	(a)
74	E	1.75	135	142	28,400	4.0	18.0	(a)	135	143	28,200	4.0	18.1	(a)
75	F	0	75	77	(b)	2.4	18.2	19.61	75	78	(b)	2.4	18.2	19.60
76	F	0	95	97	(b)	2.1	18.5	19.65	95	97	(b)	2.1	18.5	19.64
77	F	0	125	126	(b)	1.7	18.8	19.70	112	114	(b)	1.8	18.7	19.66

[a]Value not measured.

[b]Between 9,000 and 10,000 pounds.

TABLE IV.- PARAMETERS EVALUATED FROM YAW-TEST DATA[a]

Runs	Test series	$\bar{p}_0$, $\frac{lb}{sq\ in.}$	$\bar{p}$, $\frac{lb}{sq\ in.}$	$\bar{\delta}_0$, in.	$\bar{F}_z$, lb	$\bar{N}$, lb/deg	$\bar{K}_{\alpha,r}$, $\frac{lb\text{-}in.}{deg}$	$\bar{M}_{z,r,e,m}$, lb-in.	$\bar{F}_{\psi,r,e,m}$, lb	$\bar{\mu}_\psi$
1 to 9	B	74	78	3.5	15,000	680	(b)	25,000	(b)	(b)
10 to 19	B	93	97	3.0	15,000	860	(b)	24,000	11,400	0.76
20 to 27	B	113	116	2.6	15,000	970	(b)	23,000	11,100	.74
28 to 36	B	133	134	2.4	15,000	1,140	(b)	22,000	11,300	.75
37 to 46	E	95	105	5.2	28,300	515	6,100	56,000	(b)	(b)
47 to 55	E	115	124	4.5	28,300	715	6,700	51,000	(b)	(b)
56 to 63	E	135	142	4.0	28,300	850	7,000	49,000	(b)	(b)

[a]Only approximate values of pressure and vertical deflection are listed in this table. All listed maximum values of force and moment were established with the aid of the faired curves in figures 6 and 7.

[b]Value could not be accurately determined.

TABLE V.- STATIC RELAXATION-LENGTH DATA

Run	Test series	Tire A					Tire B				
		p_o, $\dfrac{lb}{sq\ in.}$	p, $\dfrac{lb}{sq\ in.}$	F_z, lb	δ_o, in.	L_s, in.	p_o, $\dfrac{lb}{sq\ in.}$	p, $\dfrac{lb}{sq\ in.}$	F_z, lb	δ_o, in.	L_s, in.
78	B	74	78	14,400	3.9	18.3	74	78	14,400	3.8	(a)
79	B	93	97	14,400	3.2	15.5	93	97	14,400	3.5	(a)
80	B	93	100	14,400	3.3	15.7	93	95	14,400	3.3	16.5
81	B	113	116	14,400	2.5	16.6	113	119	14,400	2.6	16.1
82	B	133	(b)	14,400	2.5	13.4	133	(a)	14,400	2.6	14.3
83	E	96	105	28,400	5.0	12.6	96	104	28,200	5.0	11.8
84	E	95	105	28,400	4.9	12.6	95	104	28,200	5.0	11.2
85	E	115	125	28,400	4.4	15.5	115	124	28,200	4.3	14.7
86	E	134	140	28,400	3.9	13.3	135	140	28,200	3.9	13.3

[a]Value could not be accurately determined.

[b]Value not measured.

TABLE VI.- UNYAWED-ROLLING RELAXATION-LENGTH DATA

Run	Test series	$\bar{p}_o$, $\dfrac{lb}{sq\ in.}$	$\bar{p}$, $\dfrac{lb}{sq\ in.}$	$\bar{F}_z$, lb	$\bar{\delta}_o$, in.	$\bar{L}_f$, in.
87	B	(a)	75	14,400	3.3	14.4
88	B	(a)	75	14,400	3.4	14.7
89	B	(a)	95	14,400	3.0	15.0
90	B	(a)	115	14,400	2.7	15.4
91	B	(a)	135	14,400	2.4	16.3
92	B	(a)	135	14,400	2.3	15.0
93	E	135	142	28,300	4.1	9.0

[a]Value not measured.

TABLE VII.- LOCKED-WHEEL DRAG-TEST DATA

[Test series D: $\bar{F}_Z$ = 9,390 pounds for $\bar{F}_X$ = 0; $\bar{F}_Z \approx$ 9,100 pounds for all values of $\bar{F}_X$ in this table]

Run	$\bar{p}_O$, $\frac{lb}{sq\ in.}$	$\bar{p}$, $\frac{lb}{sq\ in.}$	$\bar{\delta}_O$, in.	$\bar{F}_{X,n,m}$, lb	$\bar{F}_{X,n,s}$, lb	$\bar{\mu}_{X,m}$	$\bar{\mu}_{X,s}$	$\bar{K}_X$, $\frac{lb}{in.}$	Remarks
94	35	38	3.7	7,530	7,530	0.83	0.83	2,700	Dry concrete
95	45	47	3.2	7,680	7,680	.84	.84	2,800	}Dry concrete
96	45	48	3.3	6,880	(a)	.76	(a)	2,800	
97	45	48	3.1	7,190	(a)	.79	(a)	2,700	Wet concrete
98	60	63	2.7	7,000	(a)	.77	(a)	3,100	}Dry concrete
99	63	64	2.7	7,400	7,370	.81	.81	3,100	
100	60	62	2.6	7,160	(a)	.79	(a)	3,000	Wet concrete
101	75	76	2.3	7,330	7,250	.81	.80	3,400	}Dry concrete
102	75	76	2.4	6,800	6,800	.75	.75	3,200	
103	82	84	2.3	6,770	6,700	.74	.74	3,400	Dry concrete
104	81	82	2.3	6,630	6,550	.73	.72	3,400	}Wet concrete
105	81	83	2.2	6,840	6,810	.75	.75	3,800	
106	92	93	2.1	7,090	6,900	.78	.76	3,600	Dry concrete
107	97	98	2.1	6,670	6,670	.73	.73	3,400	Dry concrete
108	97	98	2.0	6,320	6,290	.69	.69	3,400	}Wet concrete
109	97	98	2.0	6,710	6,620	.74	.73	3,400	
110	101	102	2.0	7,100	6,920	.78	.76	3,700	Dry concrete
111	110	111	1.9	6,740	6,550	.74	.72	3,500	Dry concrete
112	120	121	1.9	7,000	(a)	.77	(a)	(a)	}Dry concrete
113	120	121	1.9	7,340	(a)	.81	(a)	3,600	
114	124	125	1.8	6,550	6,550	.72	.72	3,600	}Dry concrete
115	124	124	1.8	6,570	6,390	.72	.70	4,100	
116	124	124	1.8	6,530	6,220	.72	.68	3,600	}Wet concrete
117	127	128	1.8	6,620	6,310	.73	.69	3,600	
118	134	135	1.7	7,010	6,500	.77	.71	3,700	Dry concrete

[a]Value could not be accurately determined.

TABLE VIII.- STATIC LATERAL-ELASTICITY TEST DATA

Run	Test series	$\bar{F}_z$, lb	$\bar{p}_o$, $\dfrac{lb}{sq\ in.}$	$\bar{p}$, $\dfrac{lb}{sq\ in.}$	δ_o, in.	$\bar{K}_\lambda$, lb/in.	$\bar{\eta}_\lambda$	$\bar{\lambda}_{o,max}$, in.	Minutes per cycle
119	B	14,400	75	(a)	3.3	1,850	0.10	1.5	0.7
120	B	14,400	75	(a)	3.3	1,820	.09	1.6	.4
121	B	14,400	95	(a)	2.8	2,360	.10	1.3	.4
122	B	14,400	115	(a)	2.6	2,640	.07	1.2	.4
123	B	14,400	135	(a)	2.3	2,840	.08	1.1	.4
124	B	14,400	135	(a)	2.3	3,280	(b)	1.1	.3
125	E	28,300	95	105	5.0	2,340	.14	.7	1.3
126	E	28,300	95	105	5.0	2,200	.13	1.6	1.7
127	E	28,300	115	124	4.3	2,750	.12	.7	1.3
128	E	28,300	115	124	4.4	2,500	.09	1.4	1.9
129	E	28,300	135	142	3.8	3,530	.11	.4	1.1
130	E	28,300	135	142	3.8	3,530	.11	.5	1.2
131	E	28,300	135	142	3.8	3,670	.07	.7	1.4
132	E	28,300	135	142	3.8	3,160	.08	.9	1.4
133	E	28,300	135	142	3.8	3,170	(b)	1.0	1.3
134	E	28,300	135	142	3.8	2,970	.10	1.1	1.1

^{a}Value not determined.
^{b}Value could not be accurately determined.

TABLE IX.- STATIC TORSIONAL-ELASTICITY TEST DATA

Run	Test series	Minutes per cycle	Tire A						Tire B					
			F_z, lb	p_o, $\dfrac{lb}{sq\ in.}$	p, $\dfrac{lb}{sq\ in.}$	δ_o, in.	ψ_{max}, deg	$K_{\alpha,n}$, $\dfrac{lb\text{-}in.}{deg}$	F_z, lb	p_o, $\dfrac{lb}{sq\ in.}$	p, $\dfrac{lb}{sq\ in.}$	δ_o, in.	ψ_{max}, deg	$K_{\alpha,n}$, $\dfrac{lb\text{-}in.}{deg}$
135	B	0.7	14,400	(a)	^{b}75	3.2	3.7	5,750	14,400	(a)	^{b}75	3.3	4.1	4,850
136	B	.6	14,400	(a)	^{b}75	3.2	4.8	4,620	14,400	(a)	^{b}75	3.3	4.6	4,970
137	B	.5	14,400	(a)	^{b}95	2.8	4.4	4,150	14,400	(a)	^{b}95	2.8	4.1	4,310
138	B	.6	14,400	(a)	^{b}115	2.5	4.9	3,730	14,400	(a)	^{b}115	2.5	4.2	4,030
139	B	1.2	14,400	(a)	^{b}134	2.2	4.2	3,550	14,400	(a)	^{b}132	2.3	3.9	3,860
140	B	.5	14,400	(a)	^{b}135	2.3	4.4	3,600	14,400	(a)	^{b}137	(a)	4.3	3,600
141	E	.6	28,400	95	105	5.1	1.8	9,520	28,200	95	105	5.1	1.8	9,350
142	E	.7	28,400	95	104	5.1	3.2	7,740	28,200	95	104	5.1	3.2	7,810
143	E	1.2	28,400	95	105	4.9	5.1	6,950	28,200	95	105	4.9	5.2	7,400
144	E	1.2	28,400	95	105	5.0	7.4	6,450	28,200	95	105	4.9	7.0	6,860
145	E	.7	28,400	115	125	4.3	1.8	8,700	28,200	115	124	4.4	1.8	9,160
146	E	1.0	28,400	115	125	4.2	3.5	7,350	28,200	113	123	4.3	3.4	7,280
147	E	1.6	28,400	115	124	4.3	5.4	6,740	28,200	115	123	4.3	5.6	7,100
148	E	1.9	28,400	115	125	4.3	7.5	6,900	28,200	115	125	4.3	7.1	6,970
149	E	1.7	28,400	115	125	4.3	7.5	6,500	28,200	115	125	4.3	7.1	6,500
150	E	.8	28,400	135	142	3.9	1.6	9,000	28,200	135	142	3.9	1.7	9,330
151	E	1.1	28,400	135	142	3.9	3.6	7,240	28,200	135	142	4.0	3.6	7,240
152	E	1.1	28,400	135	142	3.9	5.1	6,450	28,200	135	141	3.9	5.1	6,500
153	E	1.5	28,400	135	142	3.8	7.1	6,080	28,200	134	140	3.8	7.1	6,160

^{a}Value not determined.
^{b}May be as much as 10 lb/sq in. too low.

TABLE X.- TIRE FOOTPRINT DATA

(a) Tire A

Run	Test series	p_o, $\frac{\text{lb}}{\text{sq in.}}$	p, $\frac{\text{lb}}{\text{sq in.}}$	F_z, lb	δ_o, in.	A_g, in.^{2}	A_n, in.^{2}	b, in.	$2h$, in.	Remarks
154	A	37	(a)	(b)	3.20	172	130	10.3	17.9	(c)
155	A	37	(a)	(b)	3.22	177	133	10.6	18.0	(c)
156	A	57	(a)	(b)	2.59	128	100	10.0	15.6	(c)
157	A	77	(a)	(b)	2.03	105	82	9.4	14.1	(c)
158	A	97	(a)	(b)	1.90	90	68	8.5	13.5	(c)
159	A	(a)	37	(b)	3.28	180	139	10.7	18.3	(d)
160	A	34	38	(b)	3.08	172	130	10.6	17.9	(d)
161	A	54	58	(b)	2.34	129	98	10.0	15.6	(d)
162	A	59	63	(b)	2.48	139	106	10.5	15.7	(d)
163	A	74	75	(b)	2.05	115	88	9.5	15.1	(d)
164	A	83	84	(b)	2.11	108	84	9.4	14.5	(d)
165	A	93	97	(b)	1.87	88	68	8.4	13.4	(d)
166	A	98	99	(b)	1.98	92	72	8.6	13.8	(d)
167	A	108	113	(b)	1.69	80	61	7.8	13.2	(d)
168	A	129	131	(b)	1.45	72	55	7.3	12.6	(d)
169	B	75	80	14,900	3.31	168	128	10.7	18.0	
170	B	96	98	14,900	2.83	148	112	10.4	16.6	
171	B	115	119	14,900	2.46	131	98	10.1	15.8	
172	B	134	135	14,900	2.30	120	92	9.8	15.3	
173	C	95	(a)	27,670	5.07	234	(e)	12.0	21.6	⎫ r = 19.64 in.;
174	C	95	(a)	21,050	3.97	186	(e)	11.3	18.9	⎬ w = 12.20 in.
175	C	95	(a)	14,830	3.02	139	(e)	10.4	16.1	
176	C	95	(a)	9,290	2.07	91	(e)	8.5	13.3	
177	C	95	(a)	3,520	1.00	37	(e)	5.0	8.9	⎭
178	D	35	(a)	9,390	3.72	(e)	151	(e)	(e)	(d)
179	D	45	48	9,390	3.08	(e)	124	(e)	(e)	(d)
180	D	60	63	9,390	2.48	(e)	97	(e)	(e)	(d)
181	D	83	85	9,390	2.06	(e)	83	(e)	(e)	(d)
182	D	98	99	9,390	1.97	(e)	77	(e)	(e)	(d)
183	D	124	125	9,390	1.79	(e)	63	(e)	(e)	(d)
184	D	132	134	9,390	1.73	(e)	60	(e)	(e)	(d)
185	E	95	(a)	28,320	5.12	244	180	11.9	22.6	⎫ r = 19.61 in.;
186	E	95	(a)	21,550	4.02	197	147	11.2	19.9	⎬ w = 12.21 in.
187	E	95	(a)	15,540	3.03	154	(e)	10.6	17.2	
188	E	95	(a)	9,170	2.00	99	(e)	9.1	13.8	⎭

[a]Value not measured.

[b]Between 9,000 and 10,000 pounds.

[c]Only approximate values of pressures listed.

[d]Flat spot developed on tire for most of these runs.

[e]Value not determined.

TABLE X.- TIRE FOOTPRINT DATA - Concluded

(b) Tire B

Run	Test series	p_o, $\frac{lb}{sq\ in.}$	p, $\frac{lb}{sq\ in.}$	F_z, lb	δ_o, in.	A_g, in.^{2}	A_n, in.^{2}	b, in.	$2h$, in.	Remarks
189	A	37	(a)	(b)	3.12	178	136	10.7	18.2	(c)
190	A	37	(a)	(b)	3.23	176	134	10.6	18.0	(c)
191	A	57	(a)	(b)	2.56	134	101	9.5	15.9	(c)
192	A	77	(a)	(b)	(a)	109	83	9.5	14.3	(c)
193	A	96	(a)	(b)	1.88	94	71	8.7	13.6	(c)
194	A	34	38	(b)	3.12	173	131	10.7	18.0	(d)
195	A	36	37	(b)	3.43	182	138	10.9	18.5	(d)
196	A	55	58	(b)	2.34	134	100	10.1	15.9	(d)
197	A	59	63	(b)	2.51	139	106	10.3	16.1	(d)
198	A	74	76	(b)	2.21	109	83	9.5	14.6	(d)
199	A	83	85	(b)	2.08	108	83	9.4	14.5	(d)
200	A	93	97	(b)	1.81	91	69	8.4	13.6	(d)
201	A	98	100	(b)	1.93	92	71	8.5	13.8	(d)
202	A	108	113	(b)	1.66	81	61	7.8	13.2	(d)
203	A	(a)	130	(b)	1.59	72	55	7.3	12.6	(d)
204	B	75	81	15,000	3.23	172	130	10.7	18.3	
205	B	94	96	15,000	2.96	151	114	10.5	17.0	
206	B	115	119	15,000	2.54	130	98	10.1	15.9	
207	B	135	138	15,000	2.25	119	90	9.8	15.3	
208	D	35	38	9,390	3.70	(e)	151	(e)	(e)	(d)
209	D	45	48	9,390	3.19	(e)	129	(e)	(e)	(d)
210	D	60	61	9,390	2.72	(e)	103	(e)	(e)	(d)
211	D	81	84	9,390	2.30	(e)	85	(e)	(e)	(d)
212	D	98	99	9,390	2.15	(e)	77	(e)	(e)	(d)
213	D	124	125	9,390	1.89	(e)	64	(e)	(e)	(d)
214	D	133	134	9,390	1.86	(e)	62	(e)	(e)	(d)
215	E	85	(a)	28,190	5.68	255	186	12.0	23.1	r = 19.62 in.;
216	E	85	(a)	21,100	4.37	207	152	11.3	20.2	w = 12.17 in.
217	E	95	(a)	14,720	3.00	144	(e)	10.3	16.5	
218	E	95	(a)	8,780	2.04	93	(e)	8.5	13.5	

[a]Value not measured.

[b]Between 9,000 and 10,000 pounds.

[c]Only approximate values of pressures listed.

[d]Flat spot developed on tire for most of these runs.

[e]Value not determined.

1, 2, 3, 4: Strain-gage dynamometers for measuring side force and self-alining torque.
5, 6: Strain-gage dynamometers for measuring drag force.
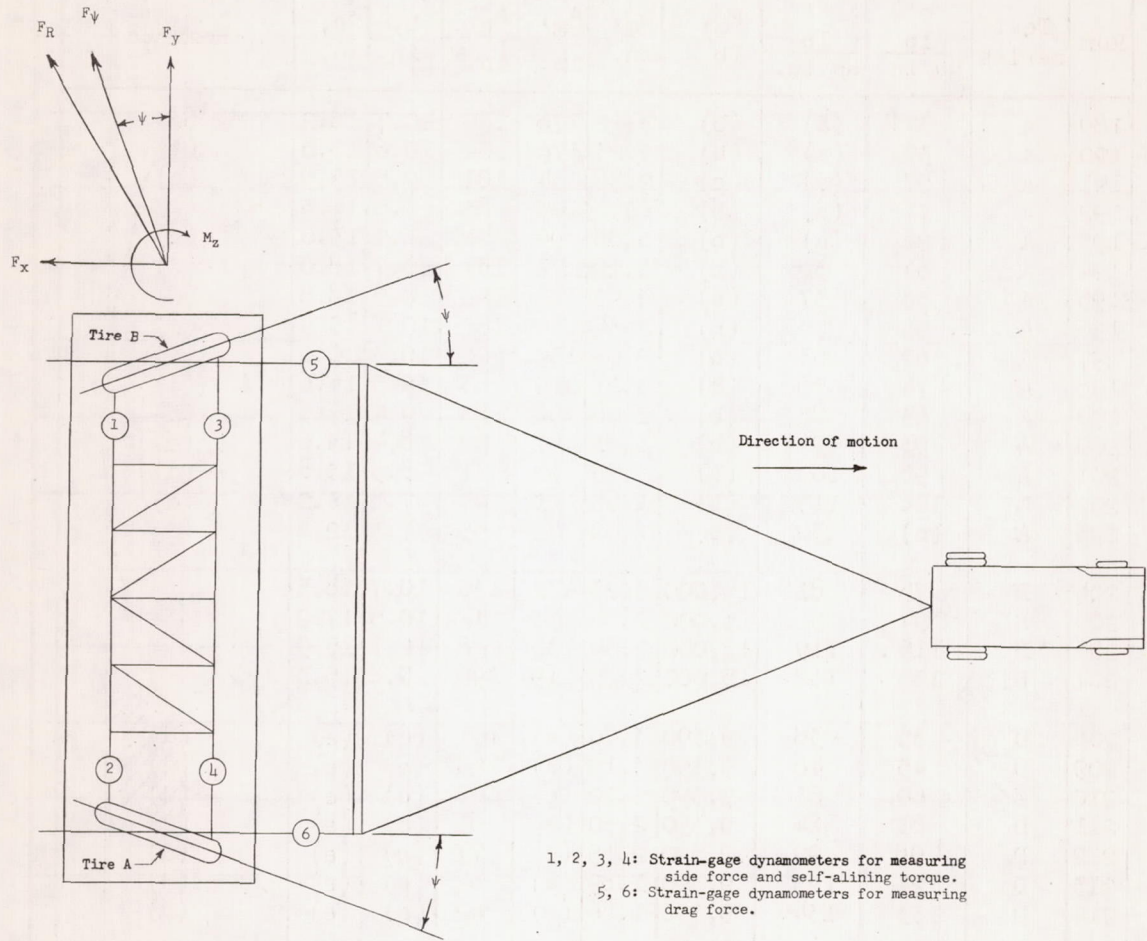
Figure 1.- Sketch of test vehicle.
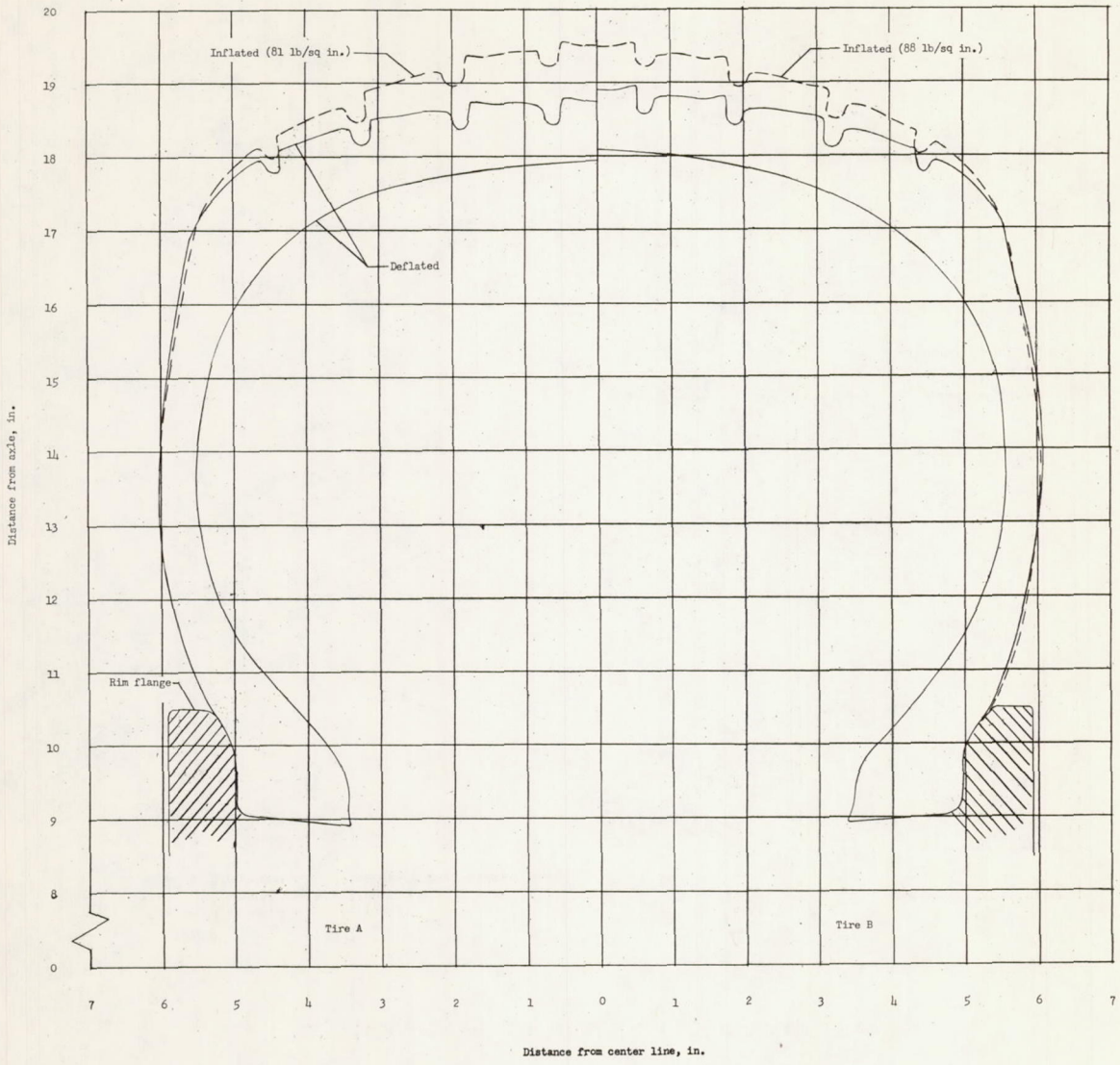
Figure 2.- Tire profiles.
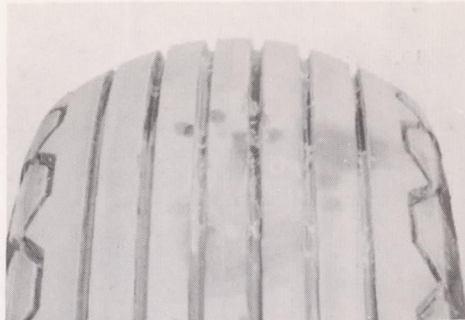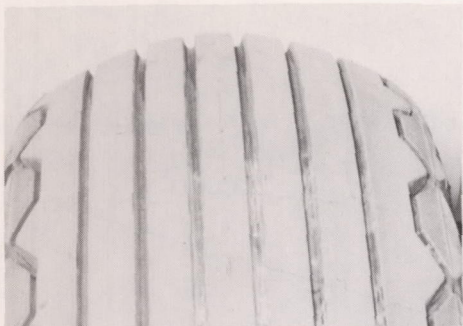
(a) At beginning of test.
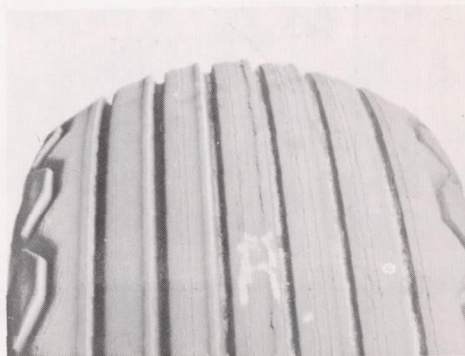
(b) At conclusion of test series B.
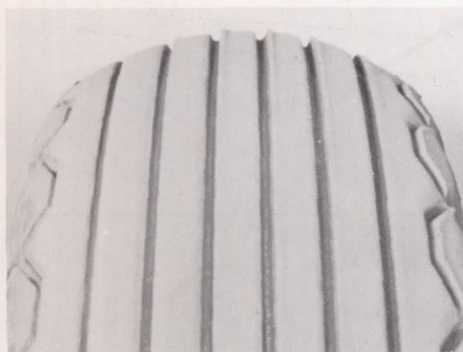
(c) At conclusion of test series E.   L-57-2726

Tire A   Tire B

Figure 3.- Tire wear.
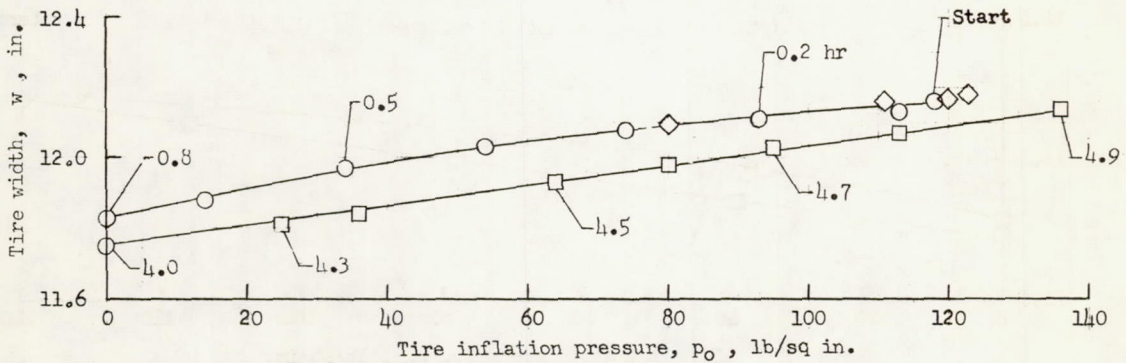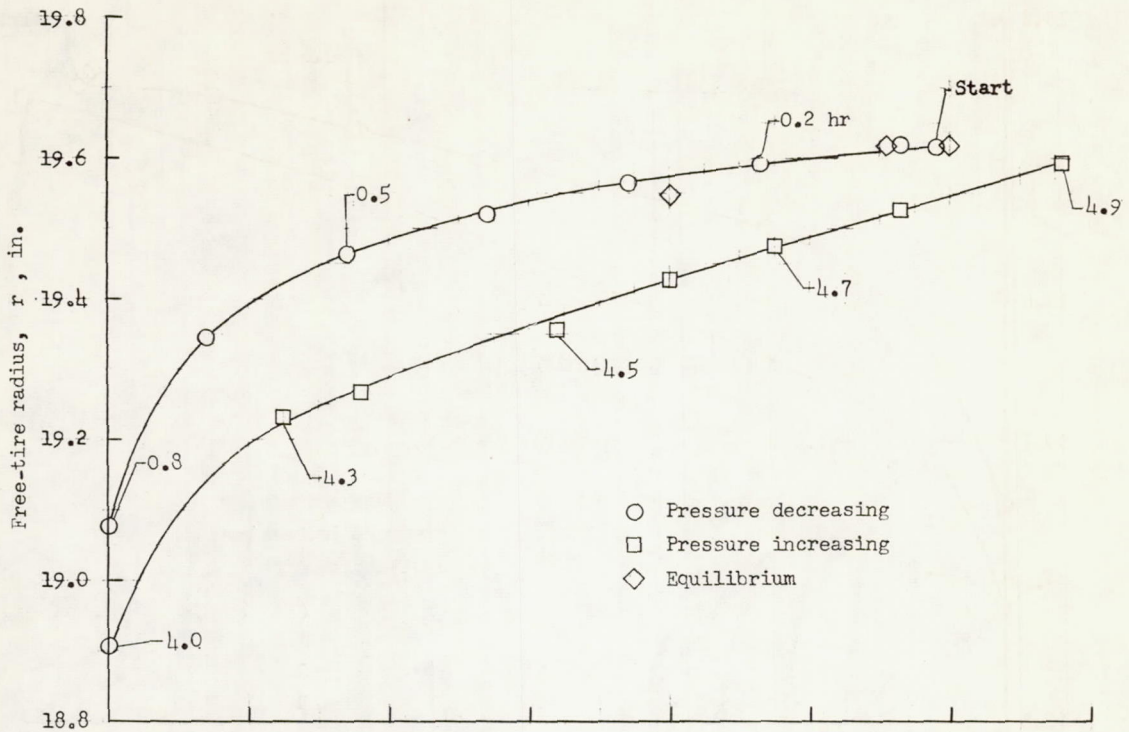
(a) Tire A.

Figure 4.- Free radius-pressure and width-pressure hysteresis loops.
Test series A and B.
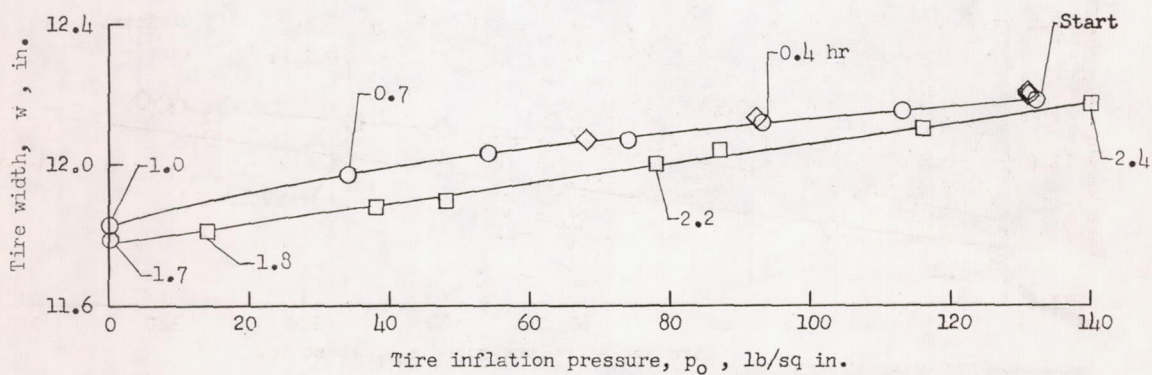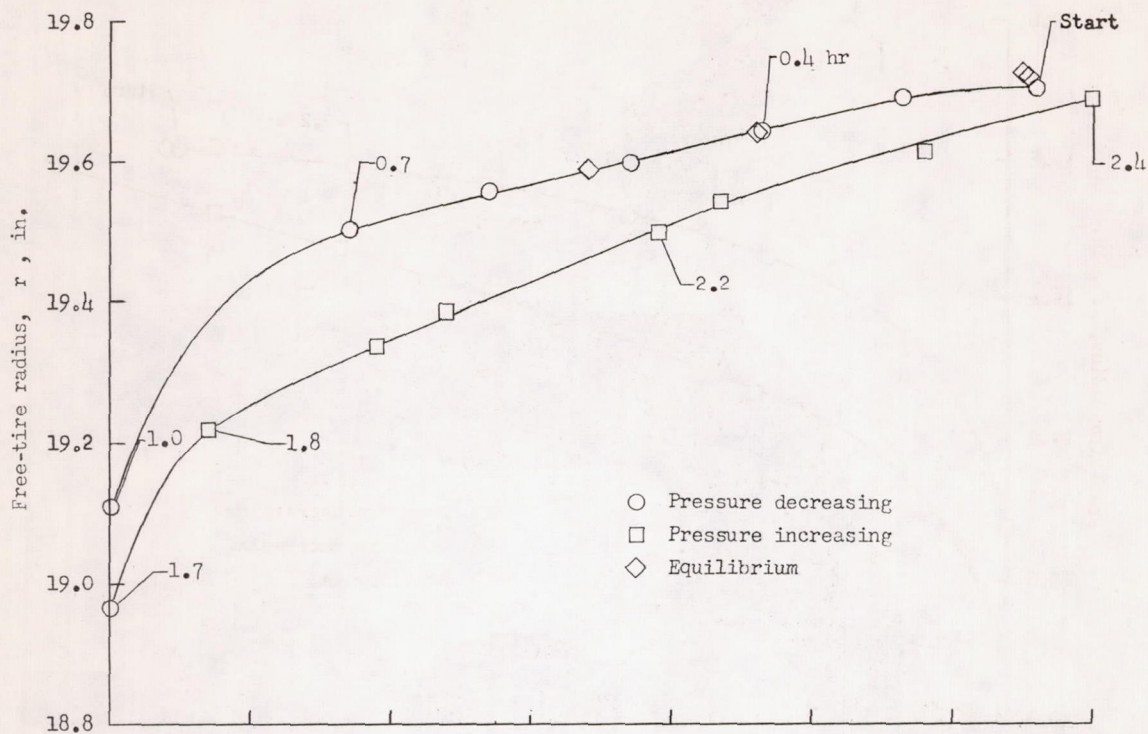
(b) Tire B.

Figure 4.- Concluded.
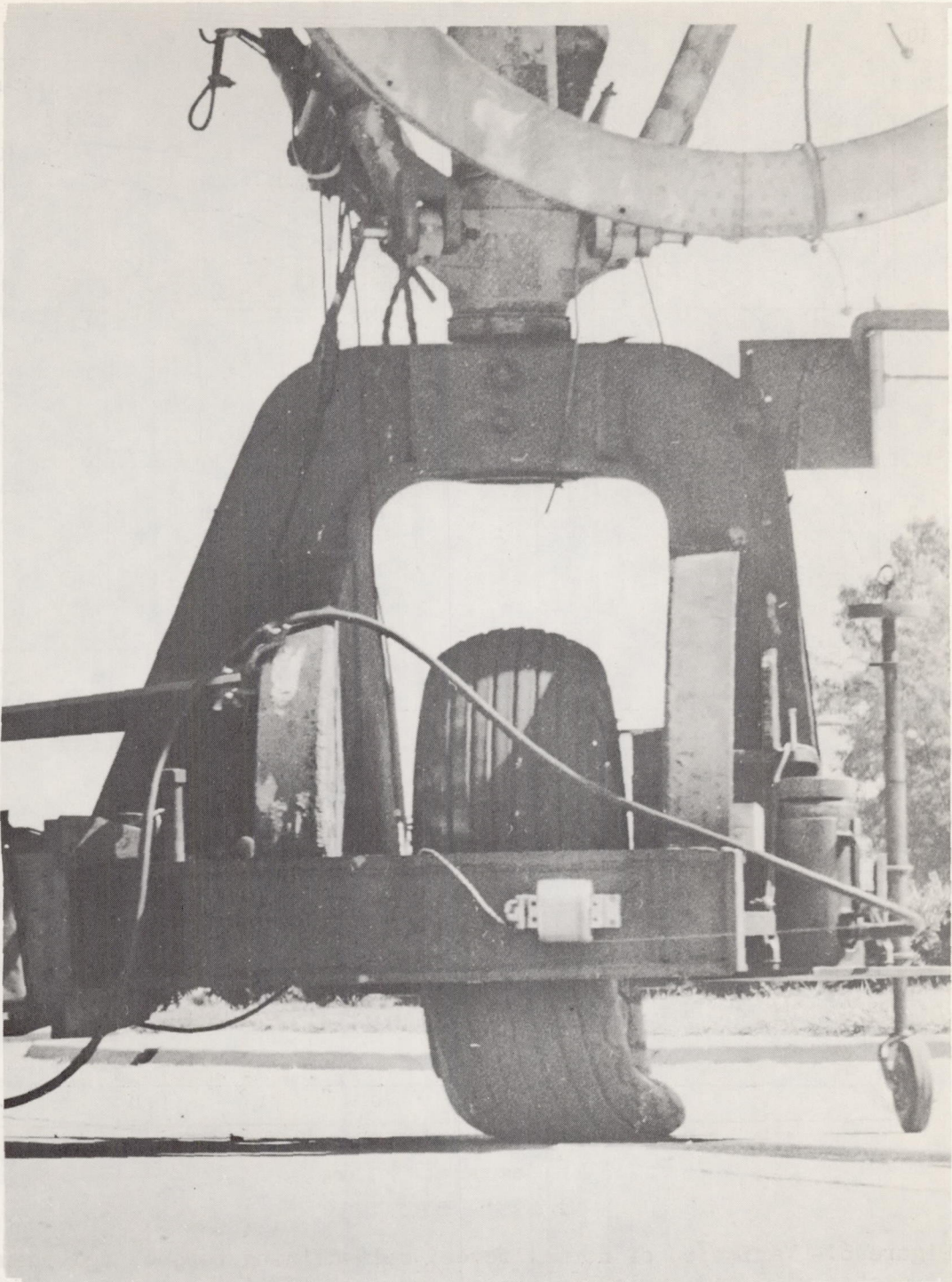
Figure 5.- Tire B under yawed rolling. $\psi = 17.5°$; run 54.
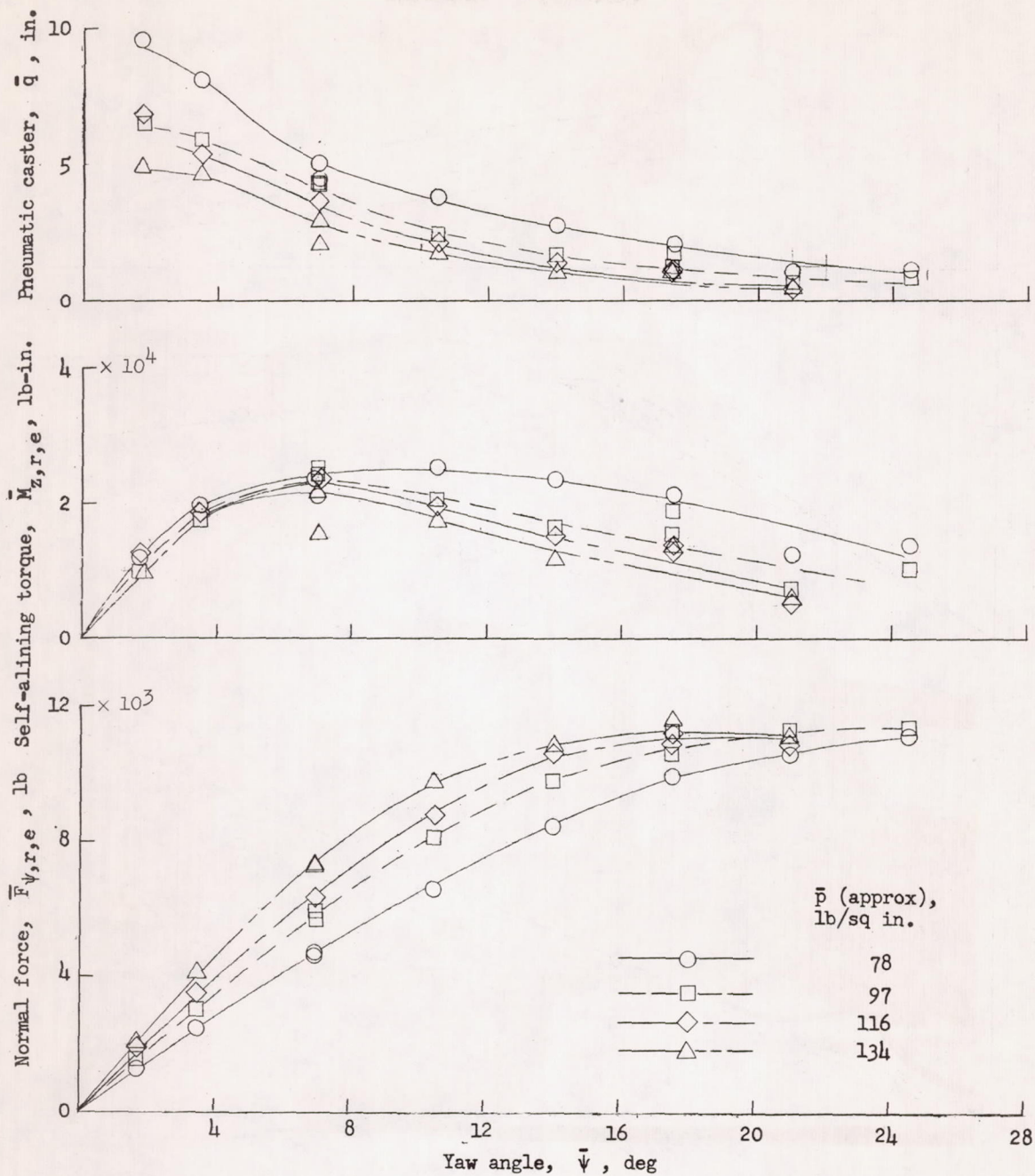
Figure 6.- Variation of normal force, self-alining torque, and pneumatic caster with yaw angle for the different inflation pressures investigated at $\overline{F}_z$ = 15,000 pounds. Test series B.
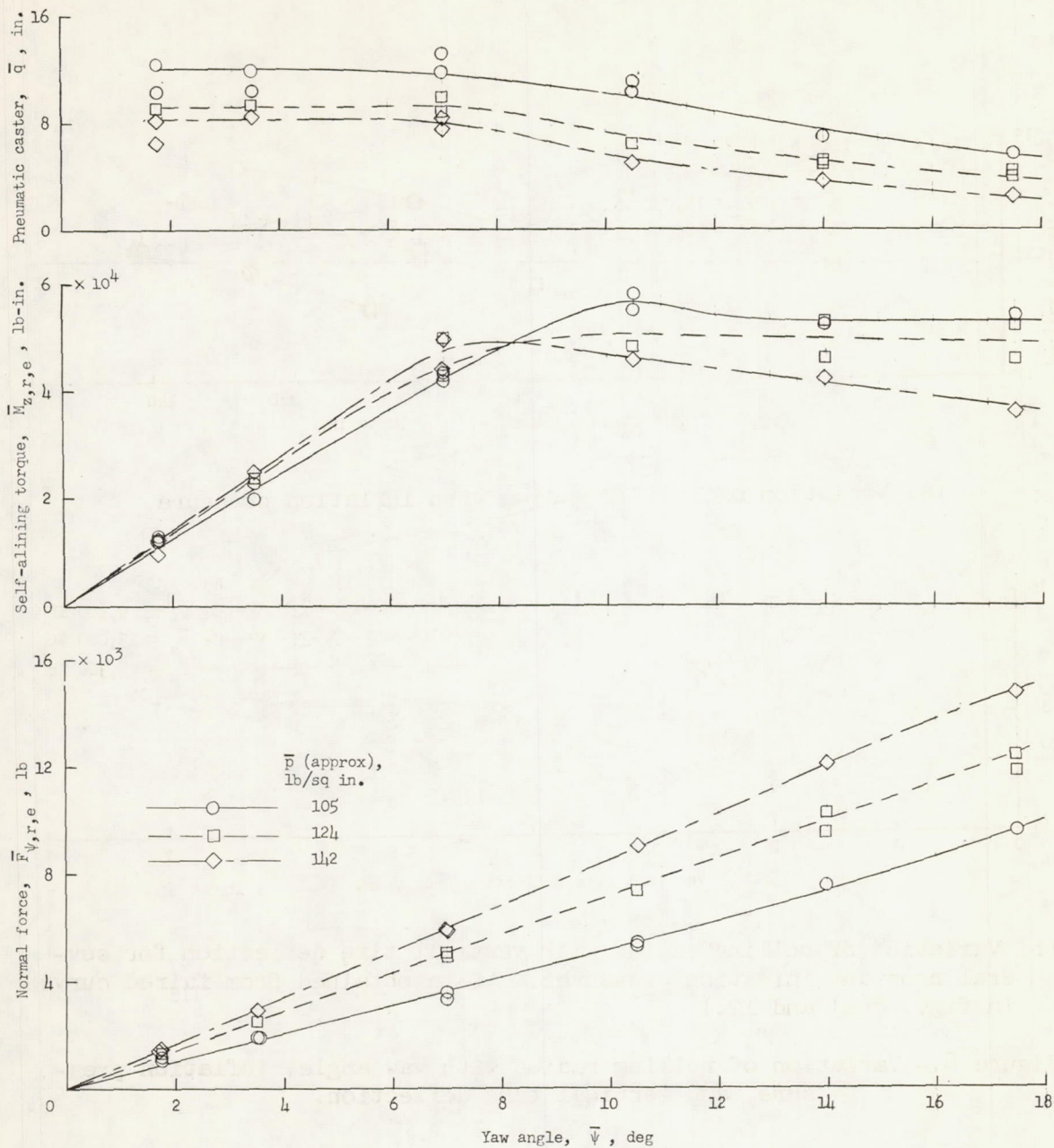
Figure 7.- Variation of normal force, self-alining torque, and pneumatic caster with yaw angle for the different inflation pressures investigated at $\overline{F}_z = 28,300$ pounds. Test series E.
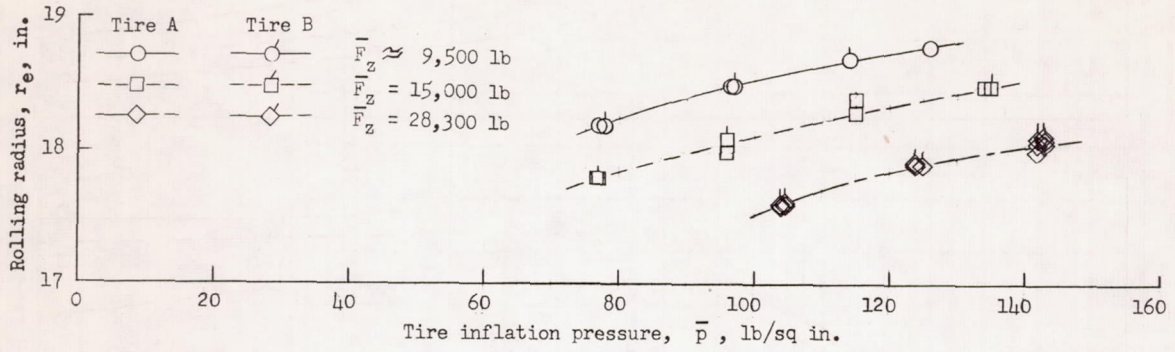
(a) Variation of rolling radius with inflation pressure.
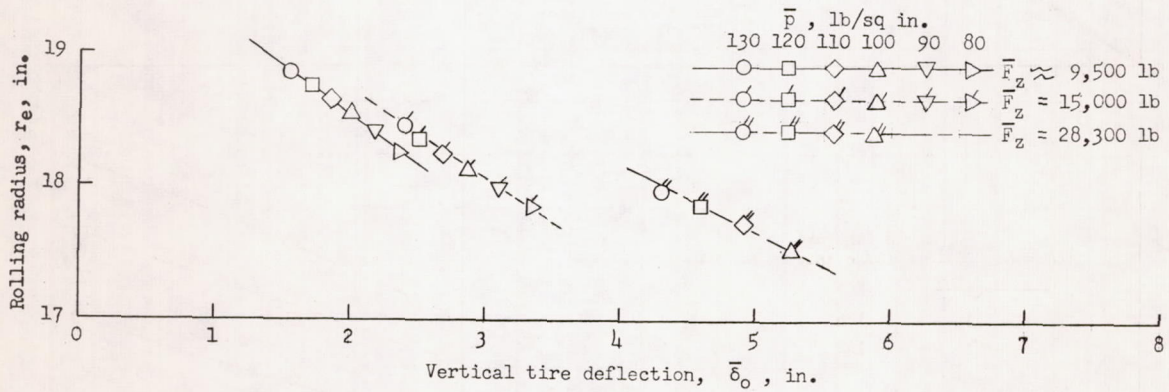
(b) Variation of rolling radius with vertical tire deflection for several constant inflation pressures. (Data obtained from faired curves in figs. 8(a) and 12.)

Figure 8.- Variation of rolling radius with yaw angle, inflation pressure, and vertical tire deflection.
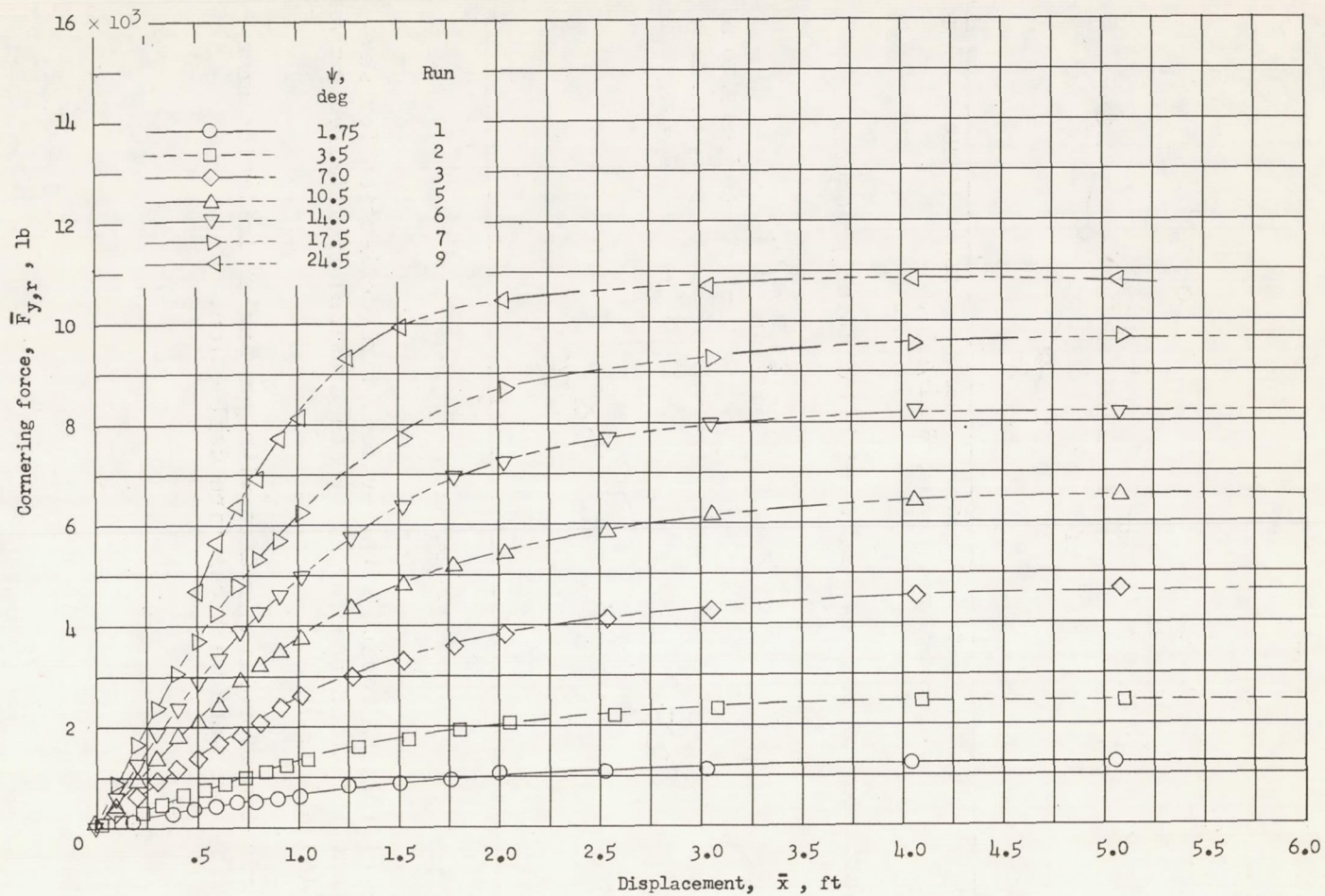
(a) Test series B; $\overline{F}_z$ = 15,000 pounds; $\overline{p} \approx 78$ pounds per square inch; $\overline{\delta}_o \approx 3.5$ inches.

Figure 9.- Buildup of cornering force with distance rolled for some typical runs at several pressures.
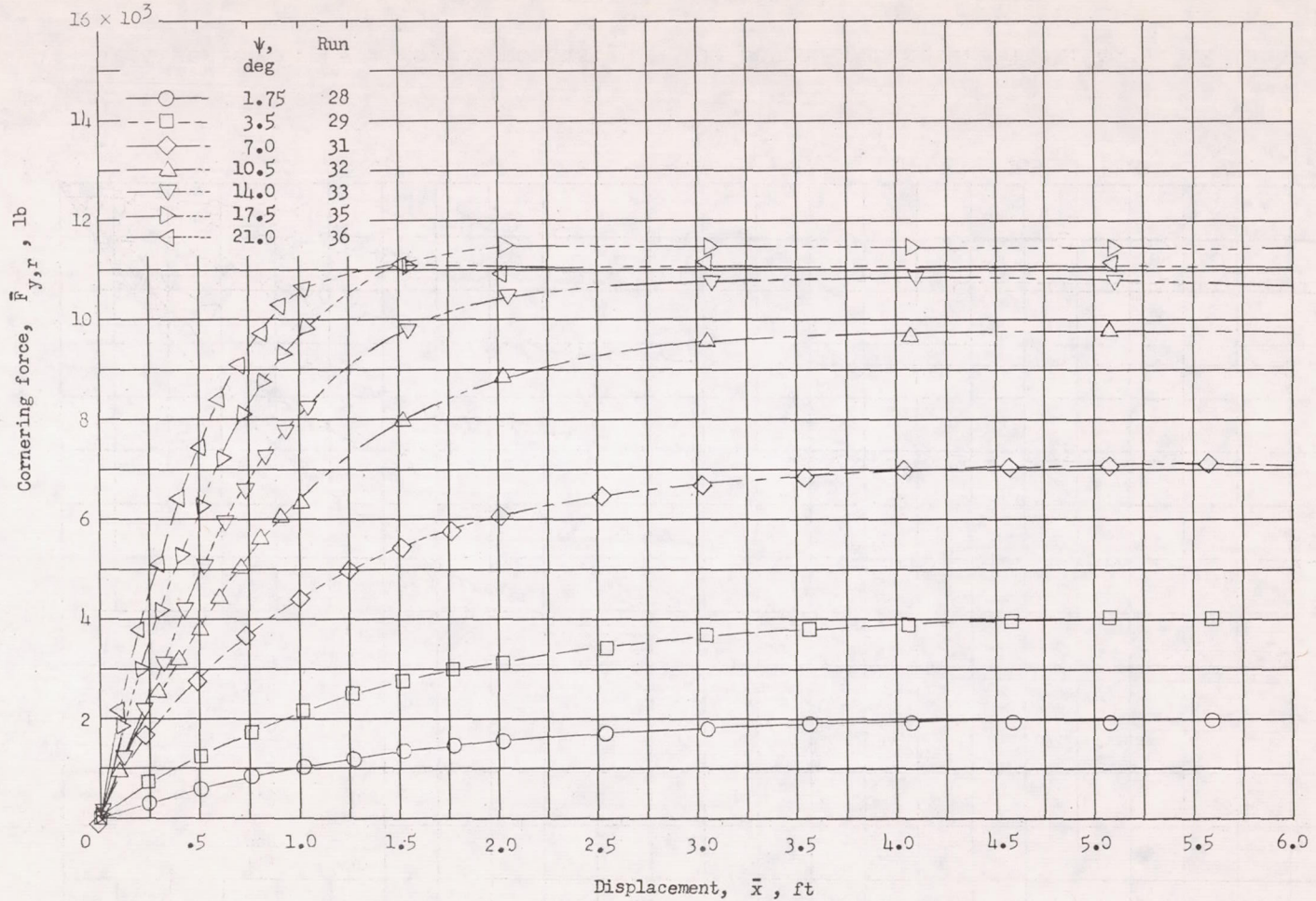
(b) Test series B; $\overline{F}_z = 15,000$ pounds; $\overline{p} \approx 134$ pounds per square inch; $\overline{\delta}_o \approx 2.4$ inches.

Figure 9.- Continued.
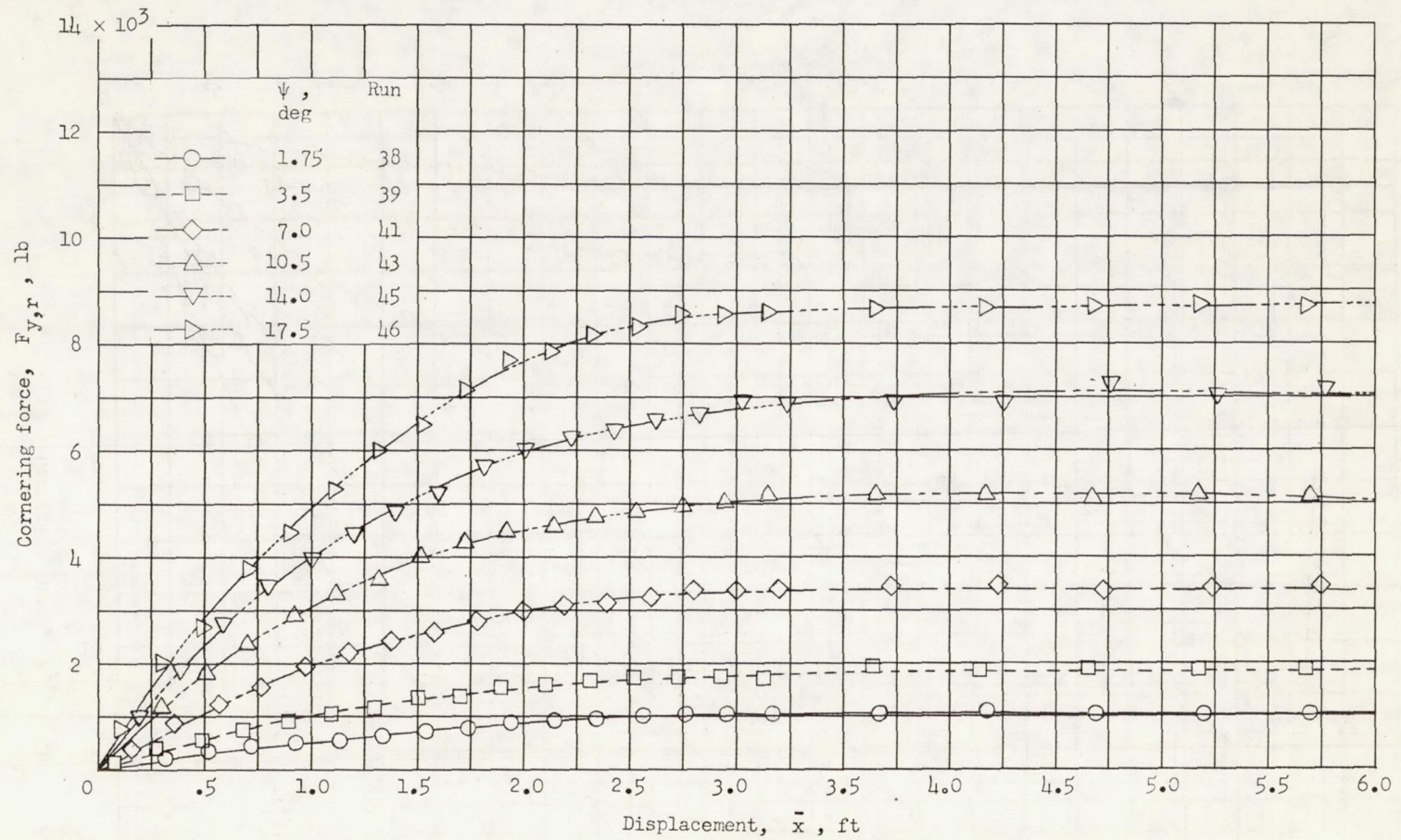
(c) Test series E; $\overline{F}_z = 28,300$ pounds; $\overline{p} \approx 105$ pounds per square inch; $\overline{\delta}_o \approx 5.2$ inches.

Figure 9.- Continued.
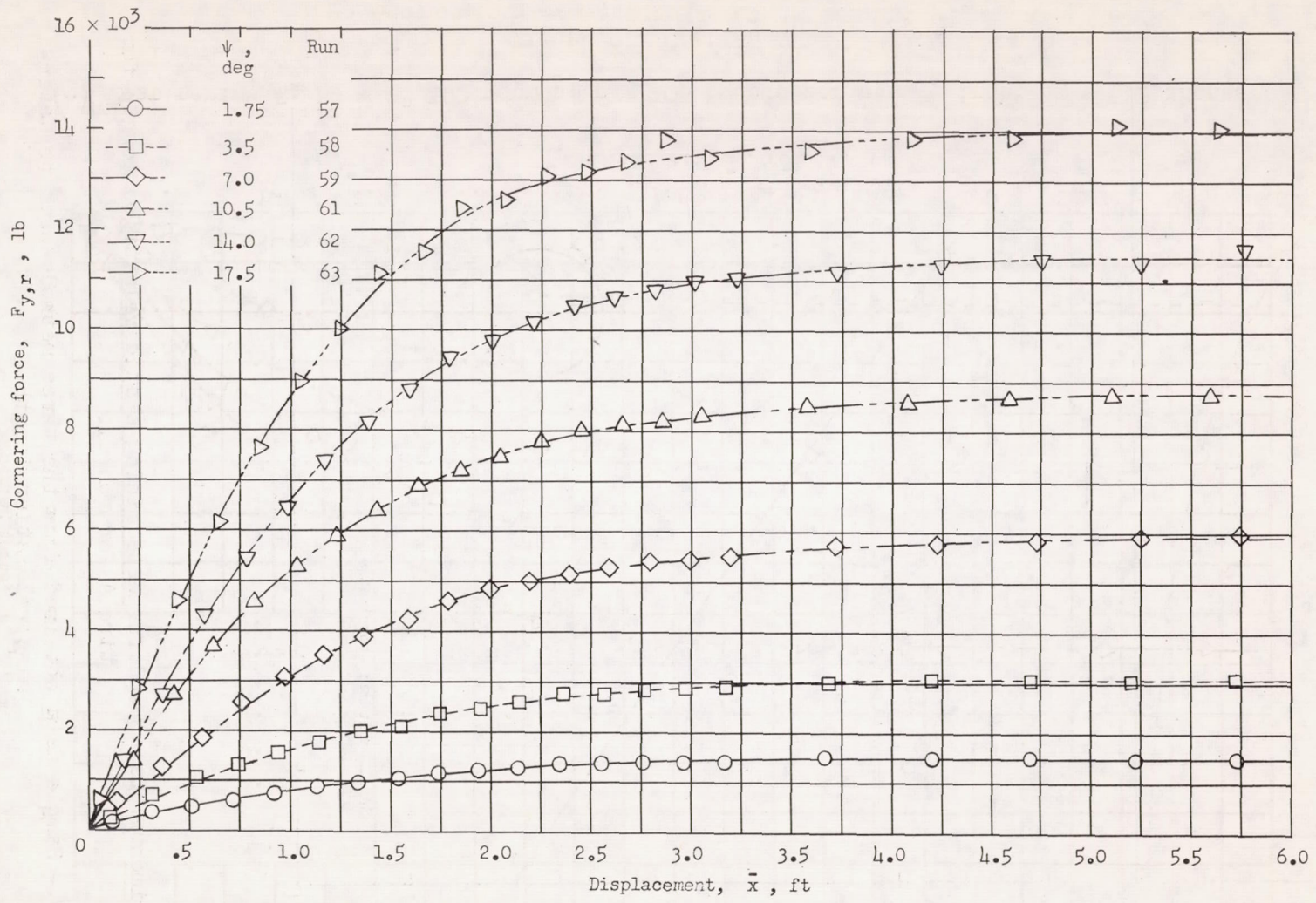
(d) Test series E; $\overline{F}_z$ = 28,300 pounds; $\overline{p} \approx$ 142 pounds per square inch; $\overline{\delta}_0 \approx$ 4.0 inches.

Figure 9.- Concluded.
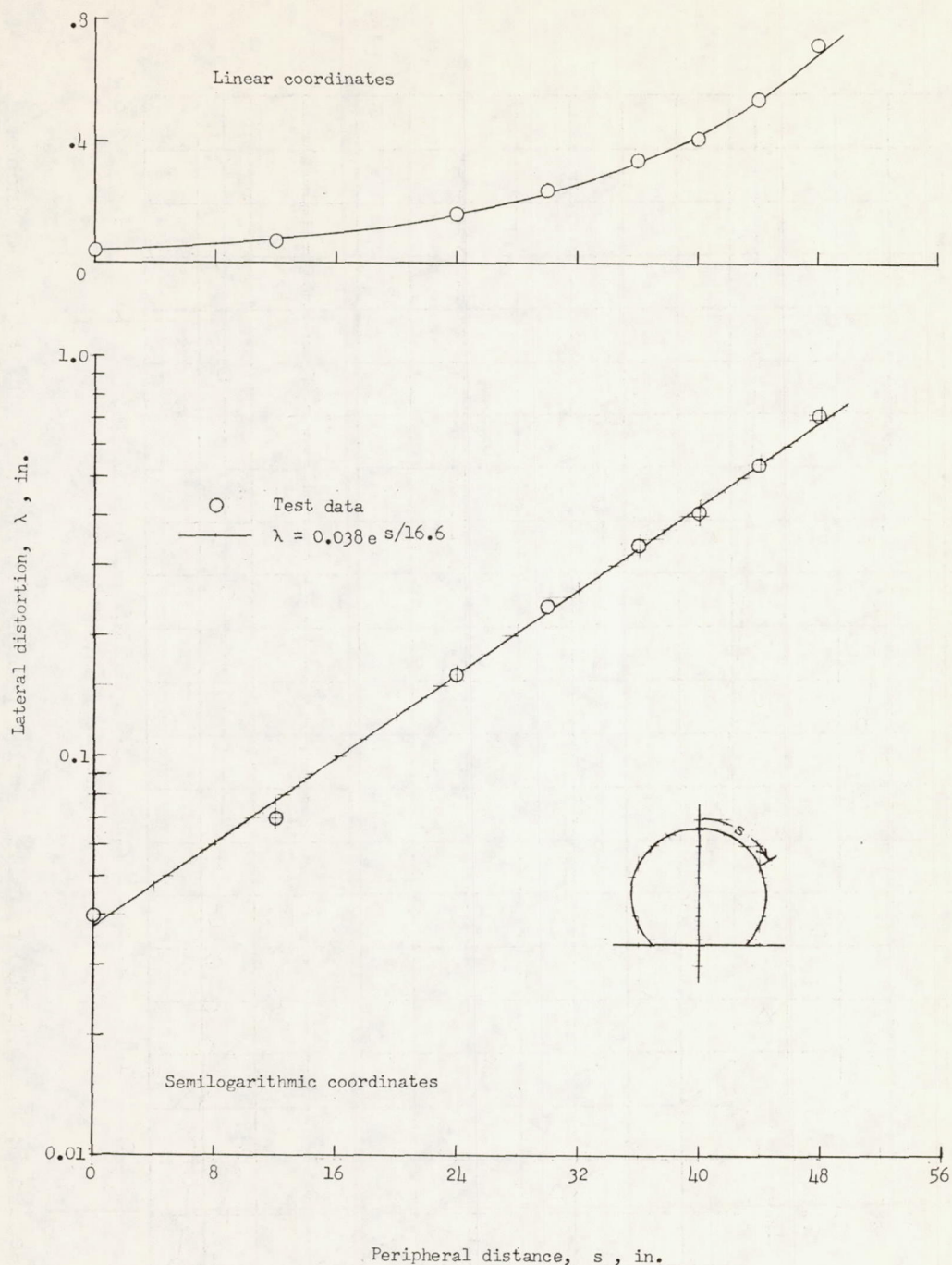
(a) Experimental data used for determining static relaxation length for tire A for run 81.

Figure 10.- Sample data obtained from the three methods used to determine relaxation length.

4×10^3

○ Test data

—— $\overline{F}_{y,r} = 9600\, e^{-\overline{x}/15.0}$

Linear coordinates

Cornering force, $\overline{F}_{y,r}$, lb

Semilogarithmic coordinates

Displacement, $\overline{x}$, in.
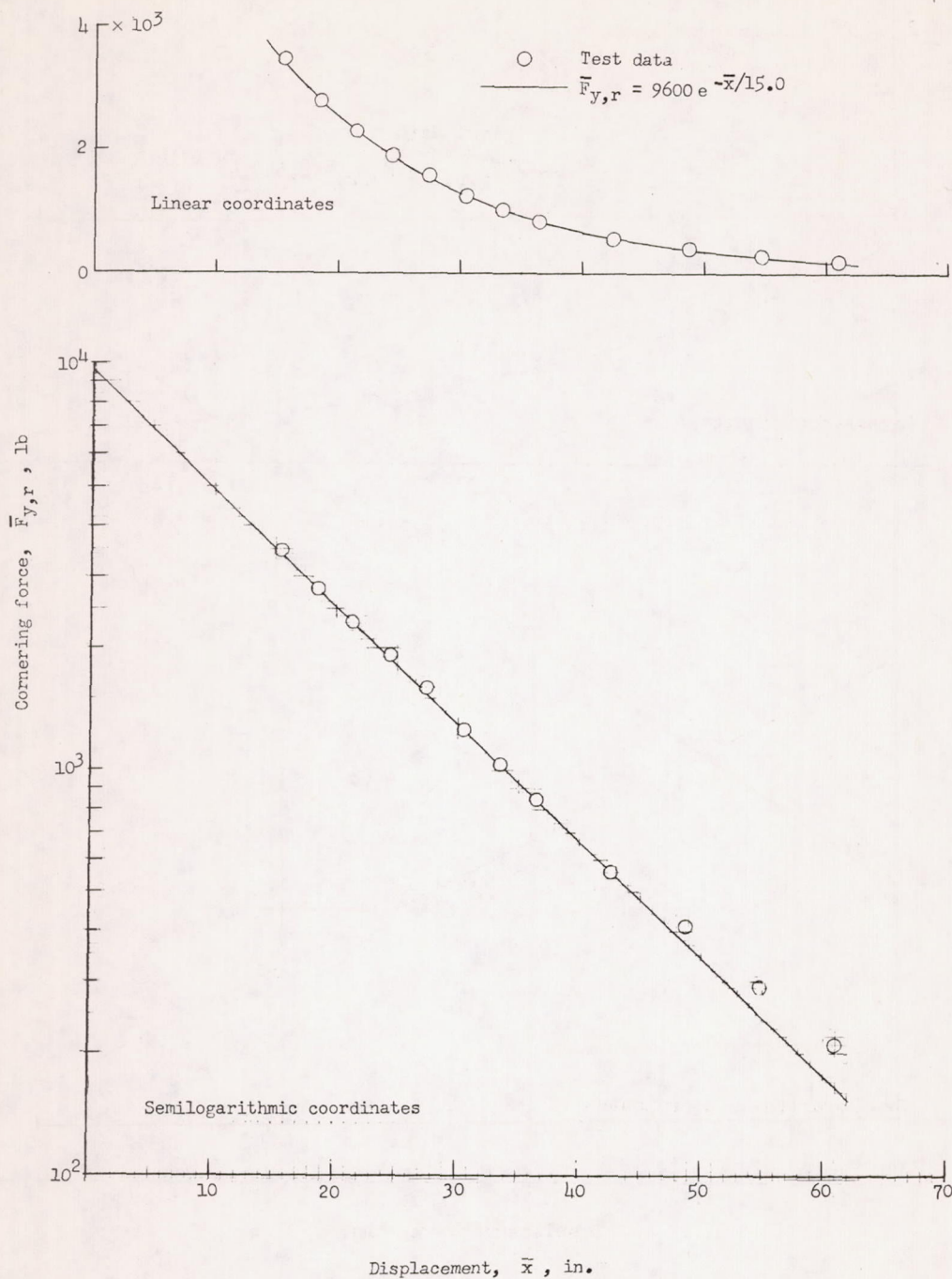
(b) Experimental data used for determining unyawed-rolling relaxation length for run 92.

Figure 10.- Continued.
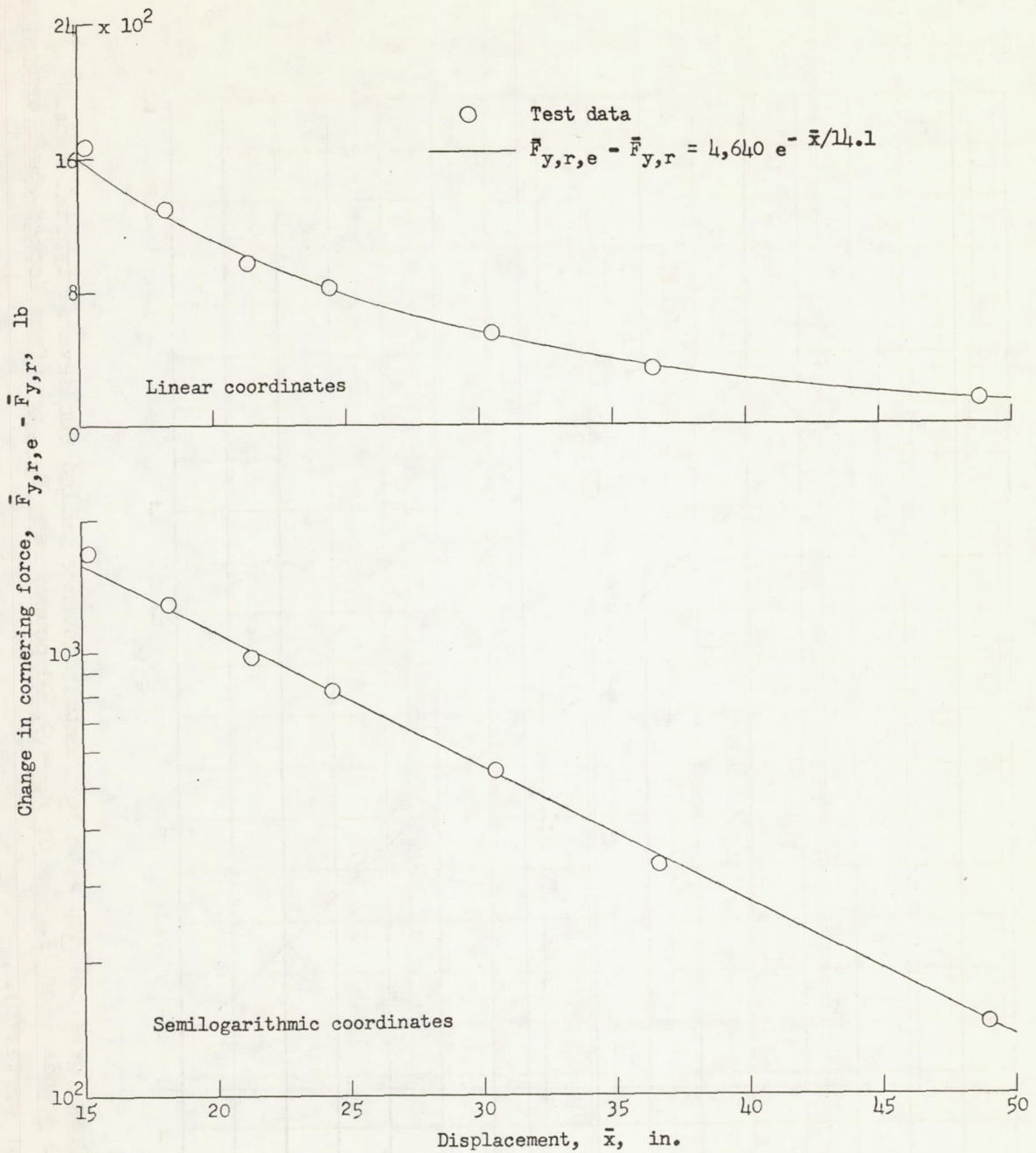
(c) Experimental data used for determining yawed-rolling relaxation length for run 4.

Figure 10.- Concluded.
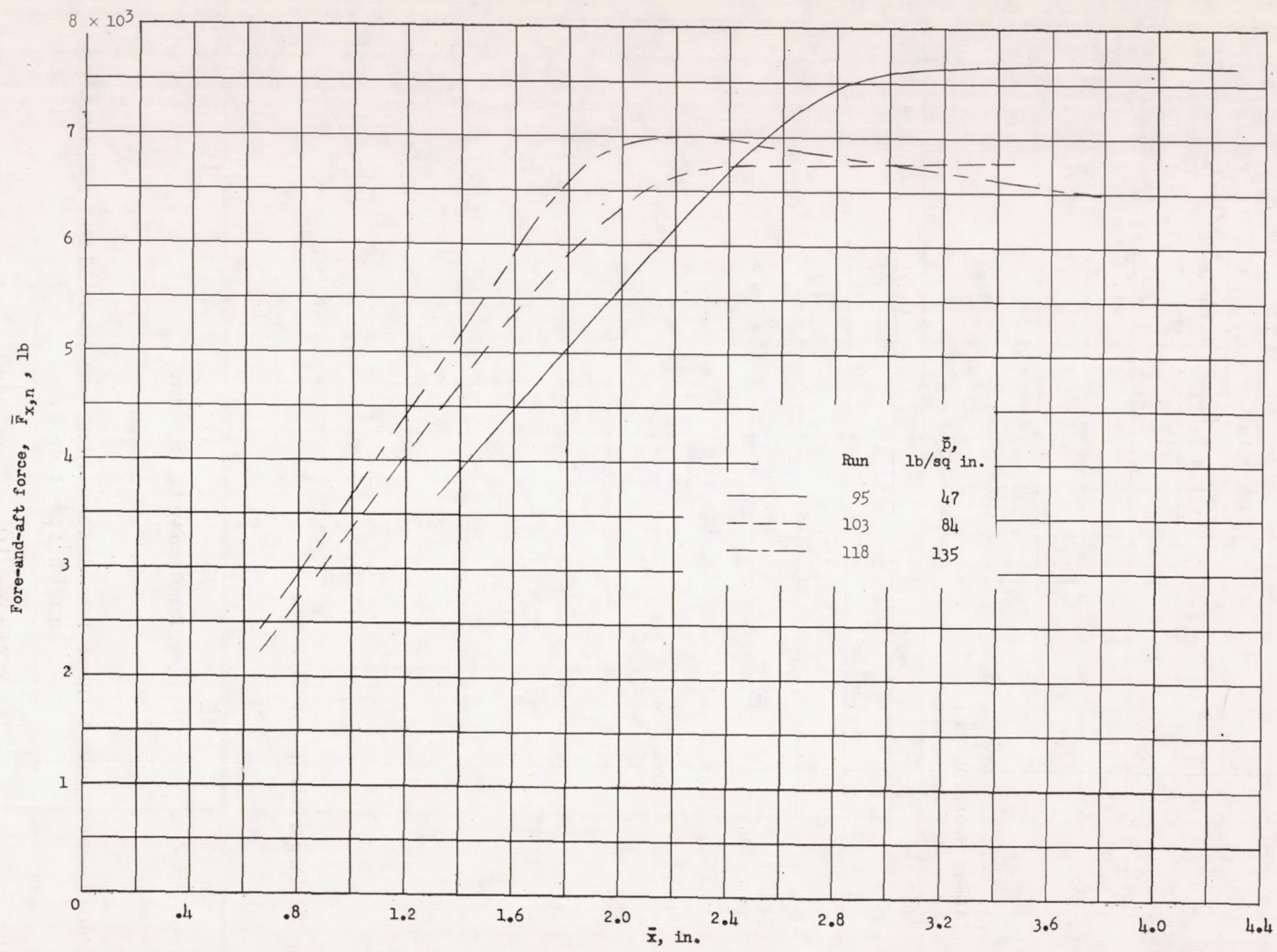
Figure 11.- Drag force buildup with horizontal distance pulled for several typical runs. $\overline{F}_z = 9,390$ pounds for $\overline{F}_{x,n} = 0$; $\overline{F}_x \approx 9,100$ pounds at $F_{x,n,m}$ (from locked-wheel drag tests; test series D).
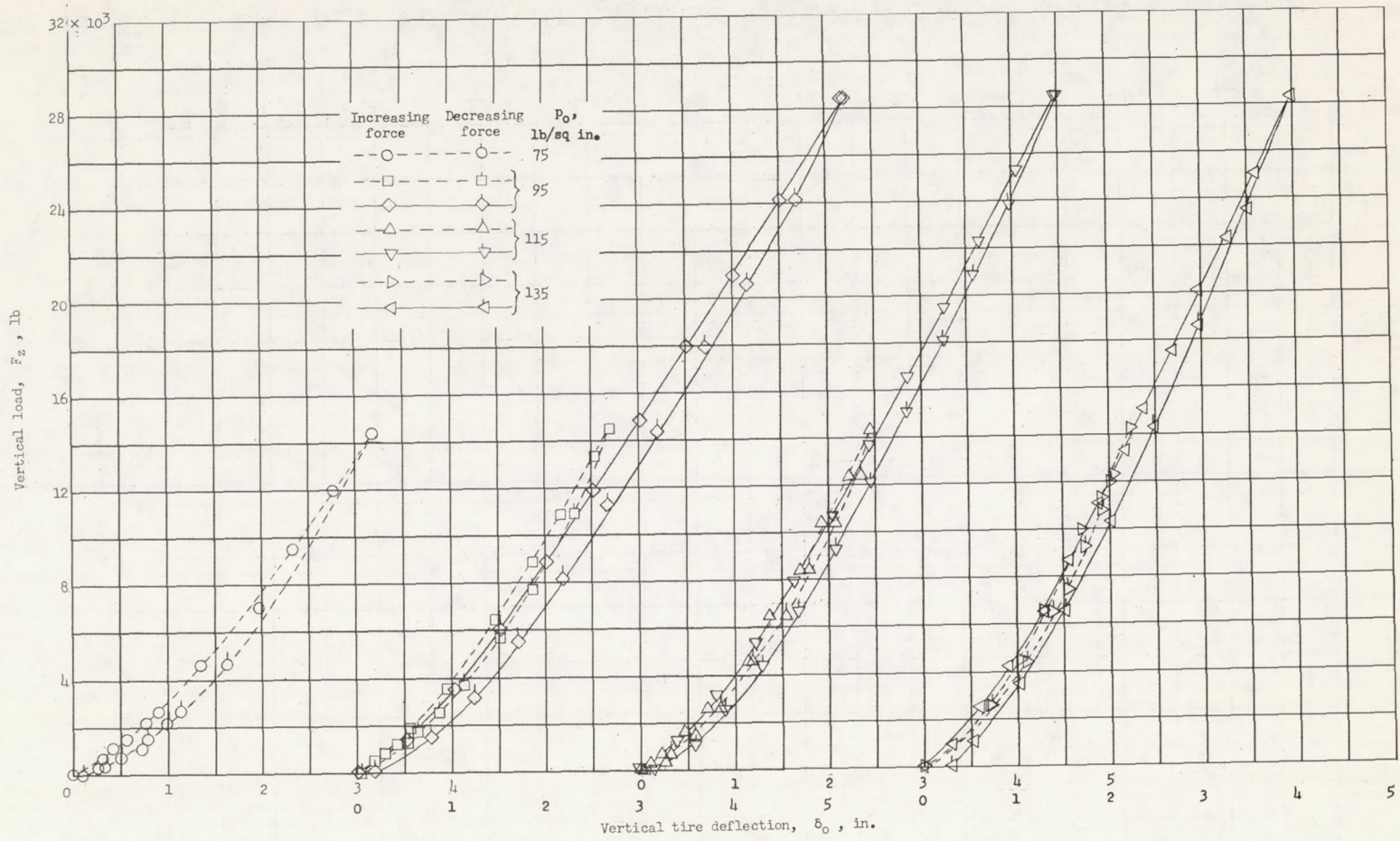
(a) Tire A.

Figure 12.- Variation of vertical load with vertical tire deflection at various initial inflation pressures.
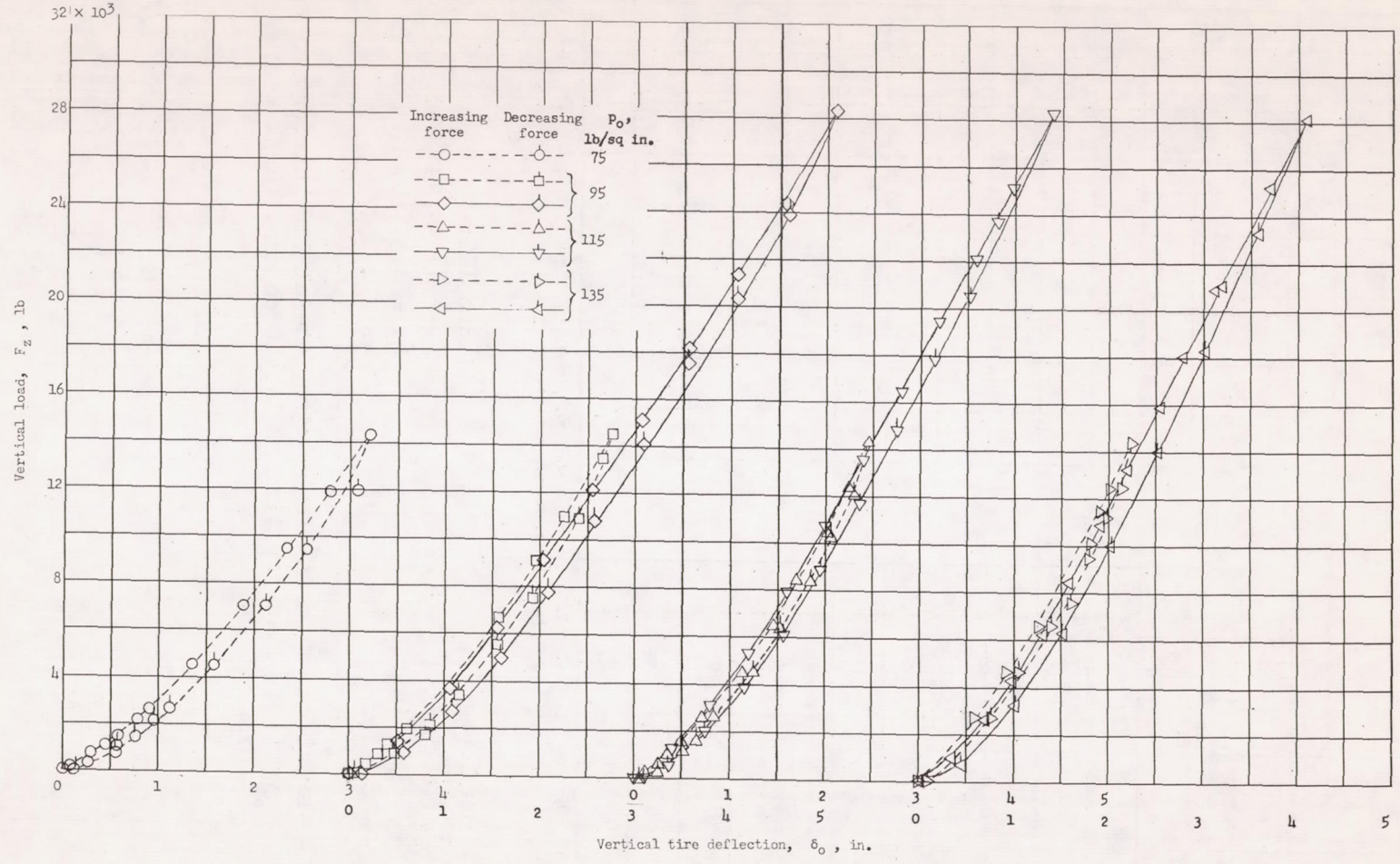
(b) Tire B.

Figure 12.- Concluded.
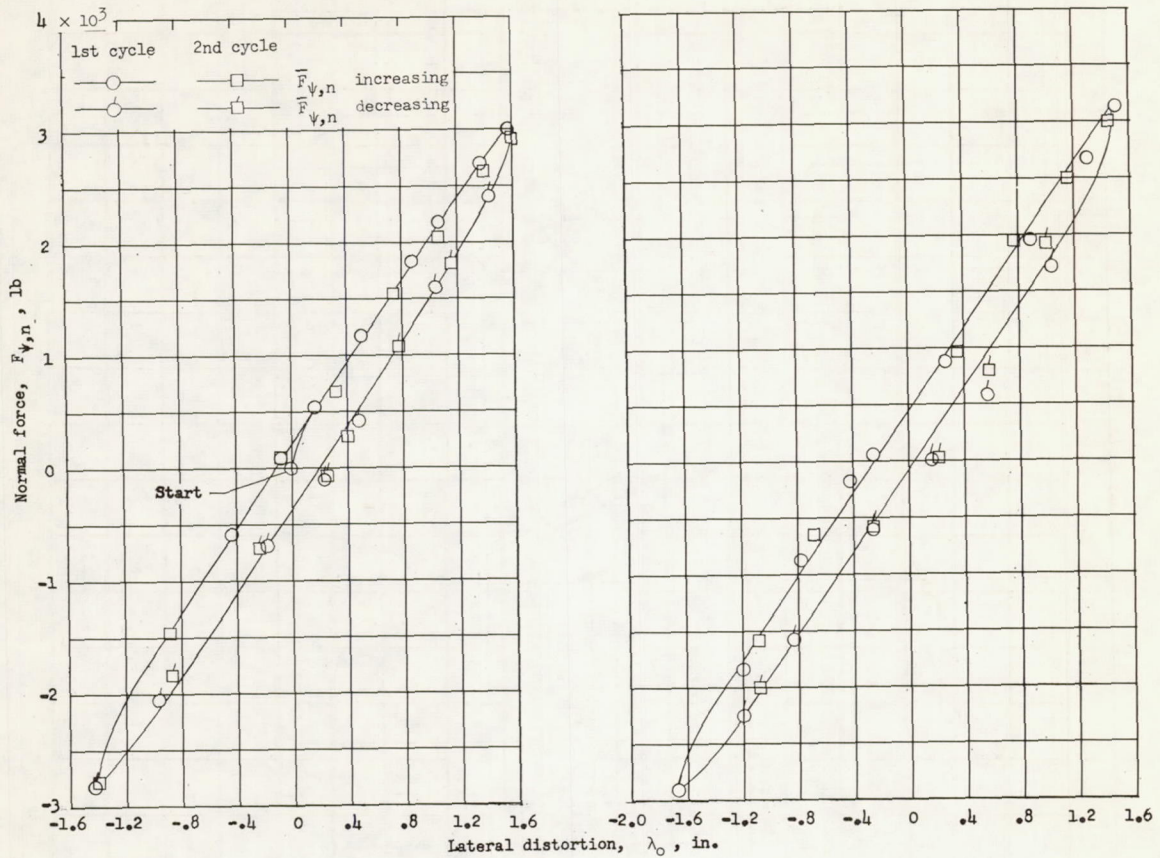
(a) Run 119;
   $\bar{p}_o = 75$ lb/sq in.;
   $\bar{\delta}_o = 3.3$ in.;
   43 sec/cycle.

(b) Run 120;
   $\bar{p}_o = 75$ lb/sq in.;
   $\bar{\delta}_o = 3.3$ in.;
   27 sec/cycle.

Figure 13.- Variation of normal force with lateral tire distortion for
   an average vertical load per tire of 14,400 pounds.   Test series B.
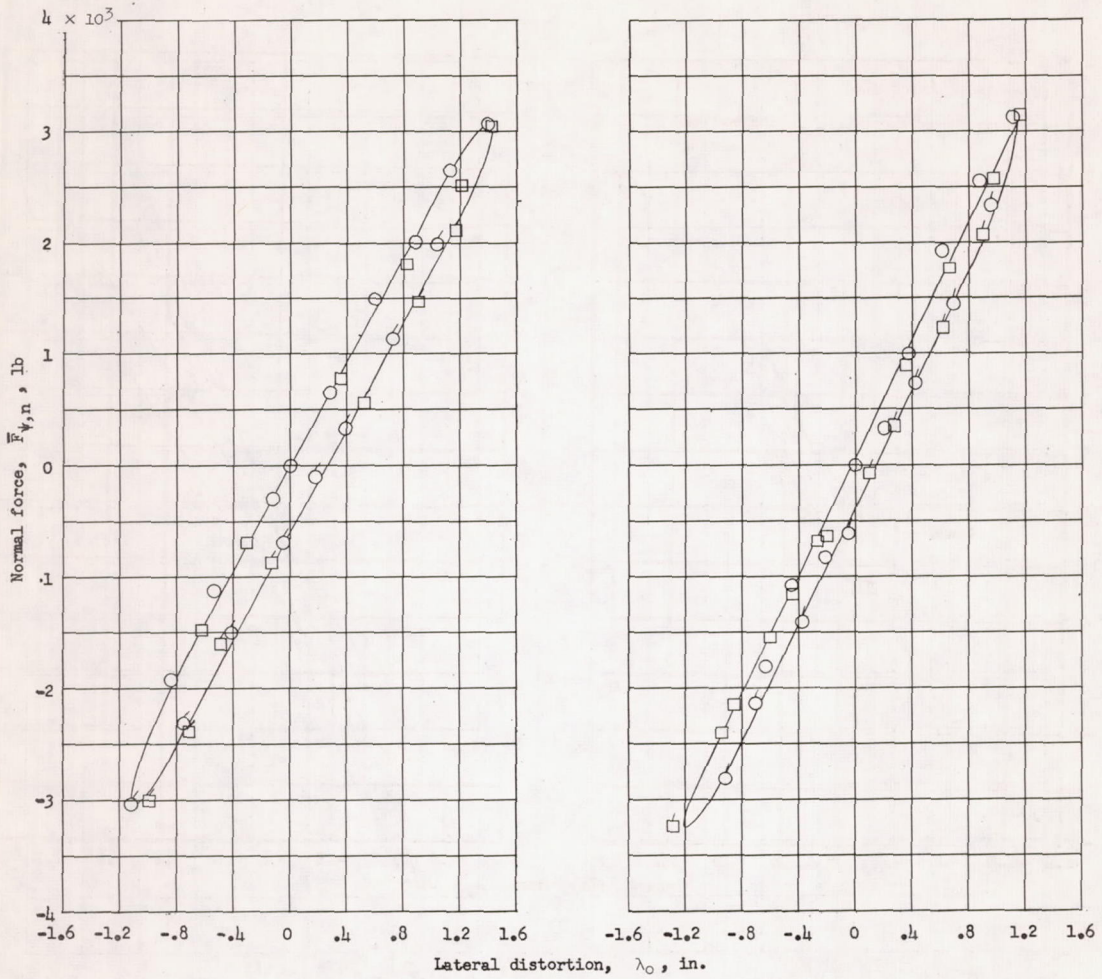
(c) Run 121;
$\bar{p}_0 = 95$ lb/sq in.;
$\bar{\delta}_0 = 2.8$ in.;
26 sec/cycle.

(d) Run 122;
$\bar{p}_0 = 115$ lb/sq in.;
$\bar{\delta}_0 = 2.6$ in.;
26 sec/cycle.

Figure 13.- Continued.
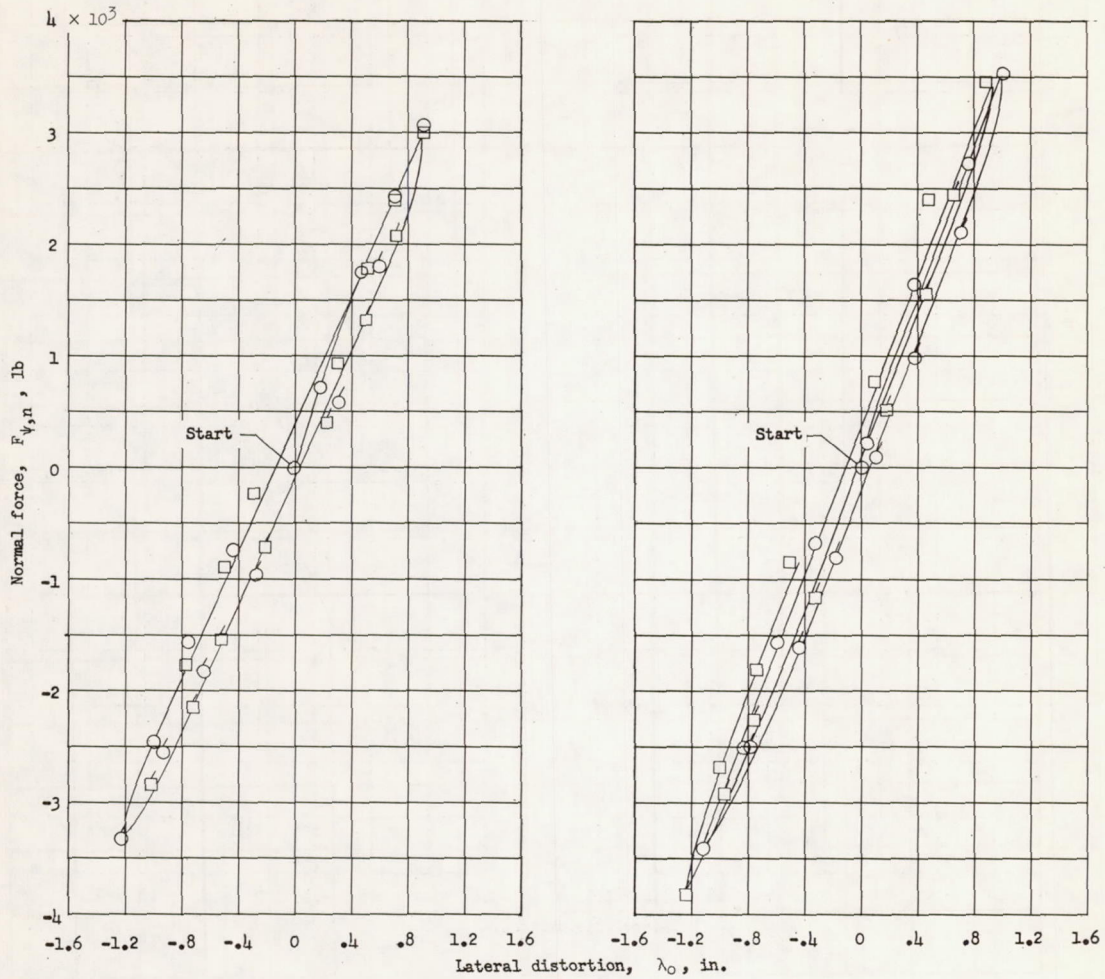
(e) Run 123;
   $\bar{p}_o$ = 135 lb/sq in.;
   $\bar{\delta}_o$ = 2.3 in.;
   21 sec/cycle.

(f) Run 124;
   $\bar{p}_o$ = 135 lb/sq in.;
   $\bar{\delta}_o$ = 2.3 in.;
   21 sec/cycle.

Figure 13.- Concluded.
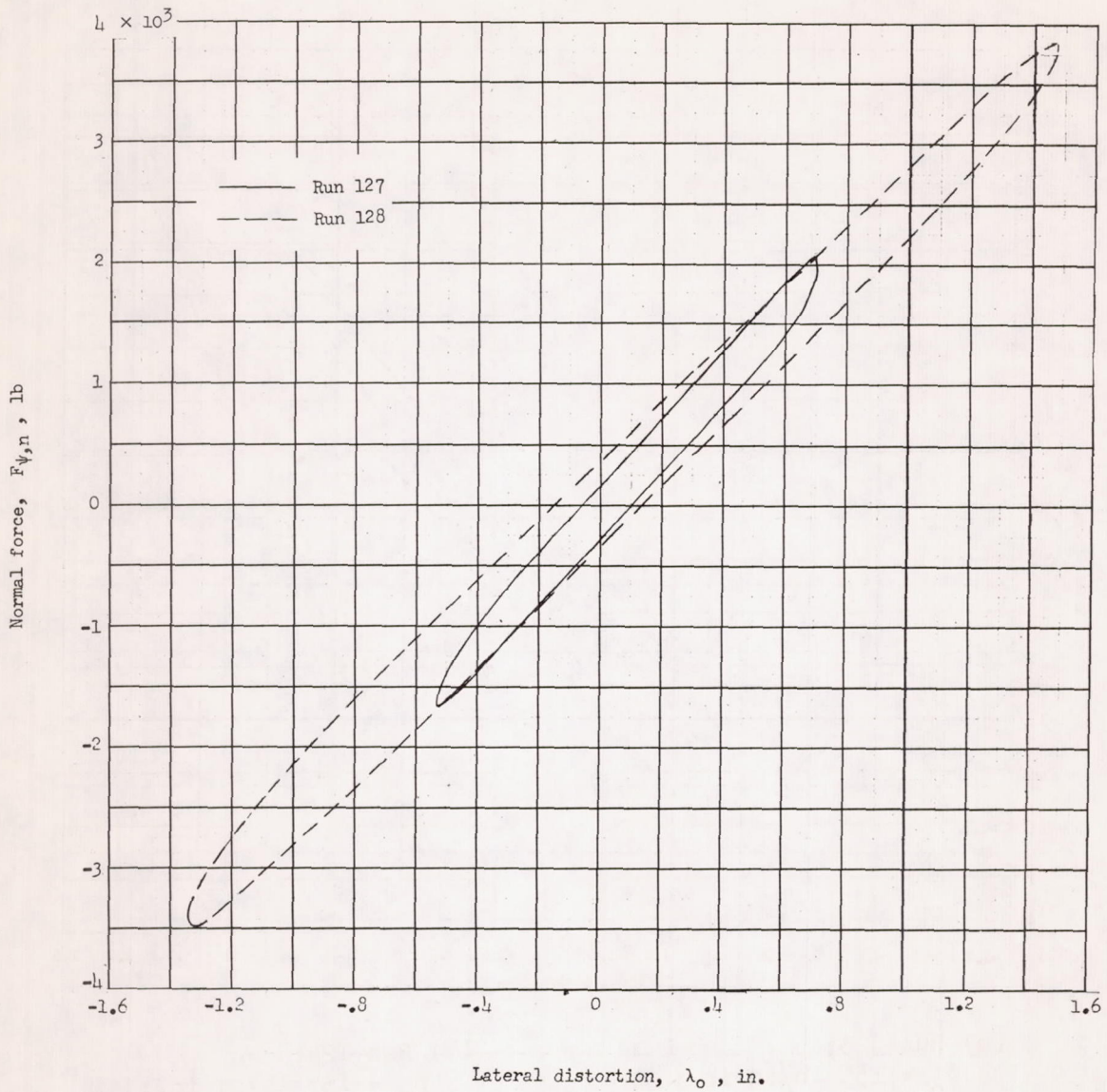
(a) $\bar{p}_o = 115$ pounds per square inch; $\bar{\delta}_o \approx 4.3$ inches.

Figure 14.- Variation of normal force with lateral tire distortion for a vertical load per tire of 28,300 pounds. Test series E.
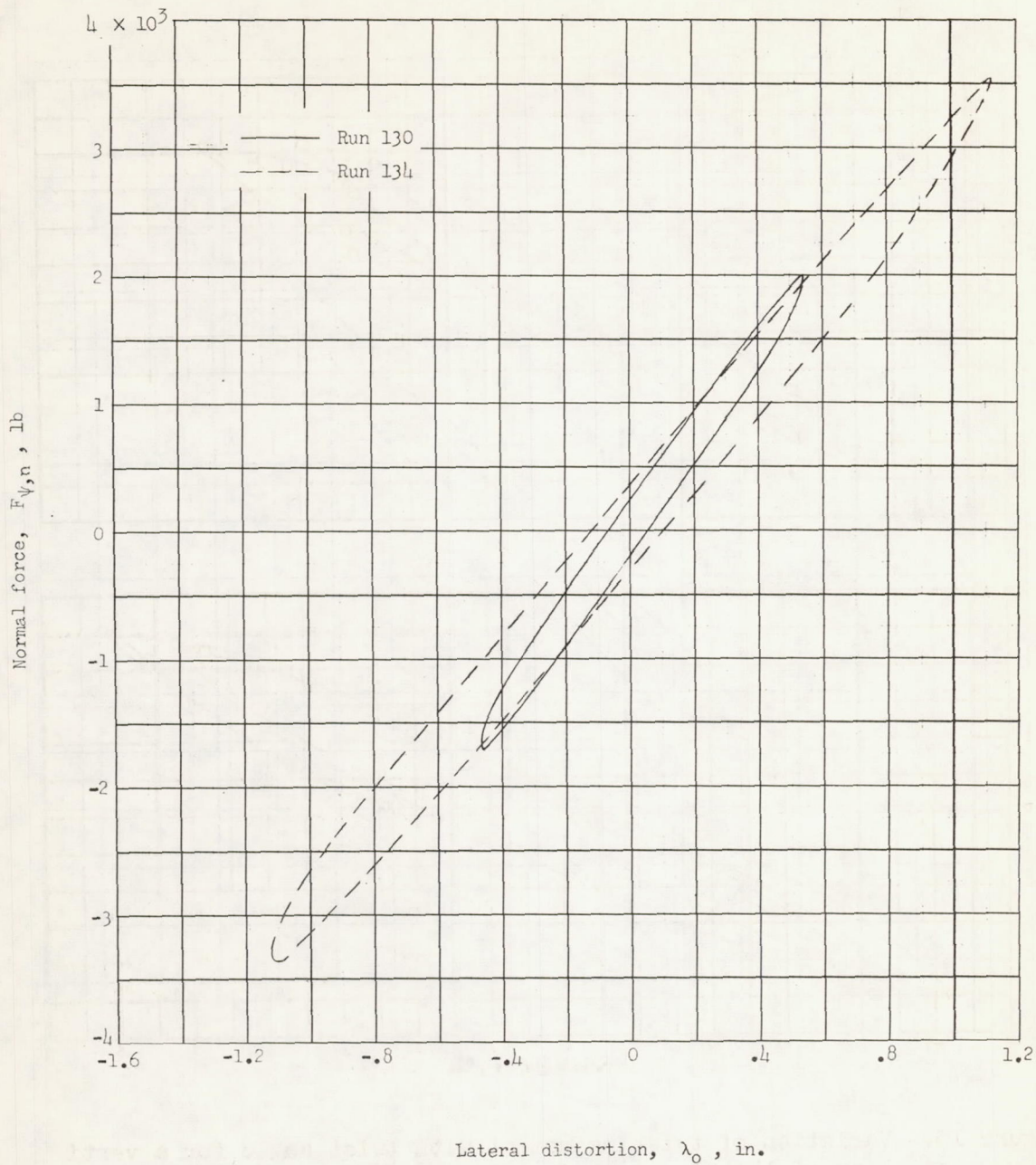
(b) $\bar{p}_O = 135$ pounds per square inch; $\bar{\delta}_O = 3.8$ inches.

Figure 14.- Concluded.
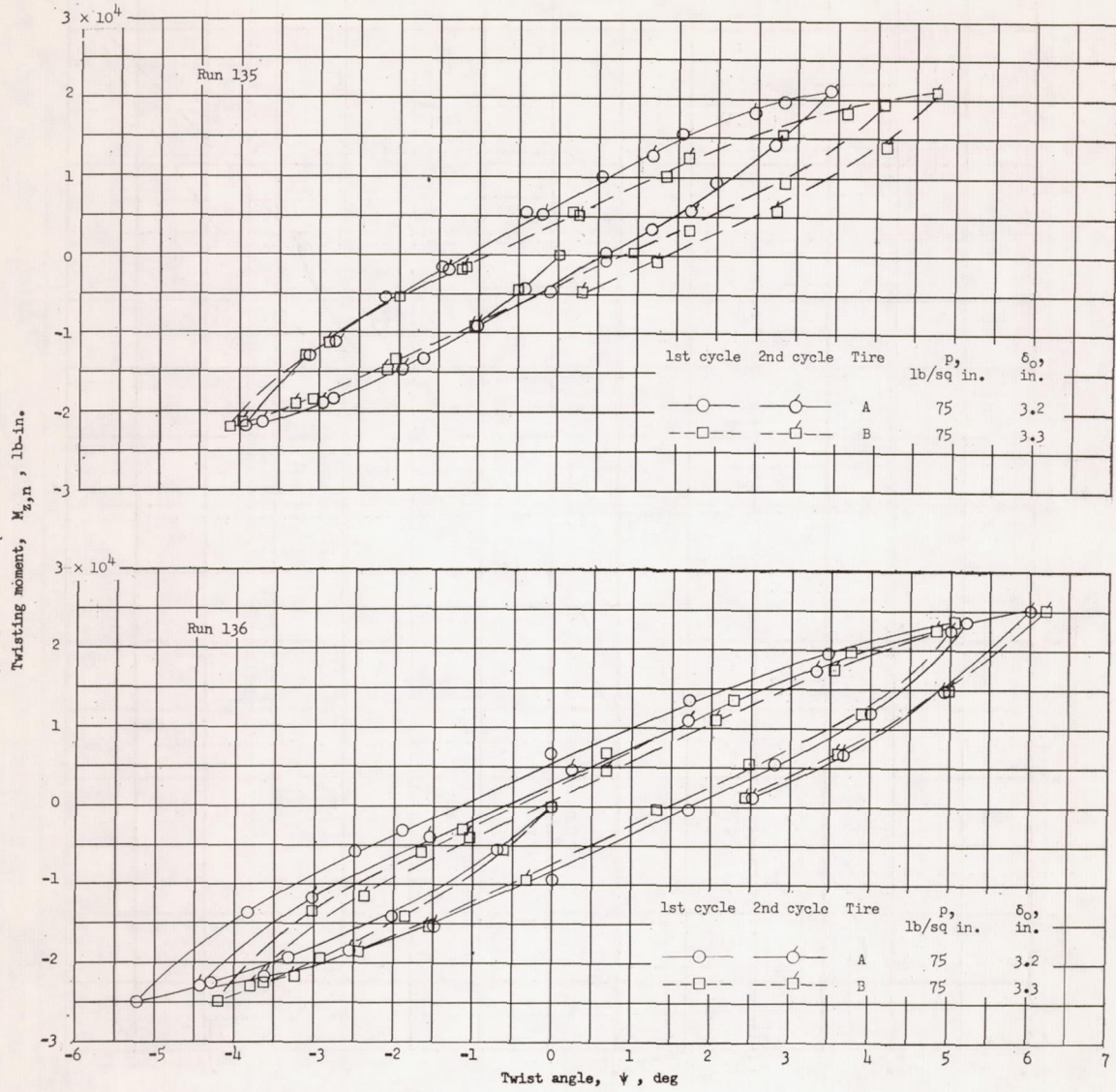
Figure 15.- Variation of twisting moment with twist angle for a vertical load of 14,400 pounds on each tire. Test series B.
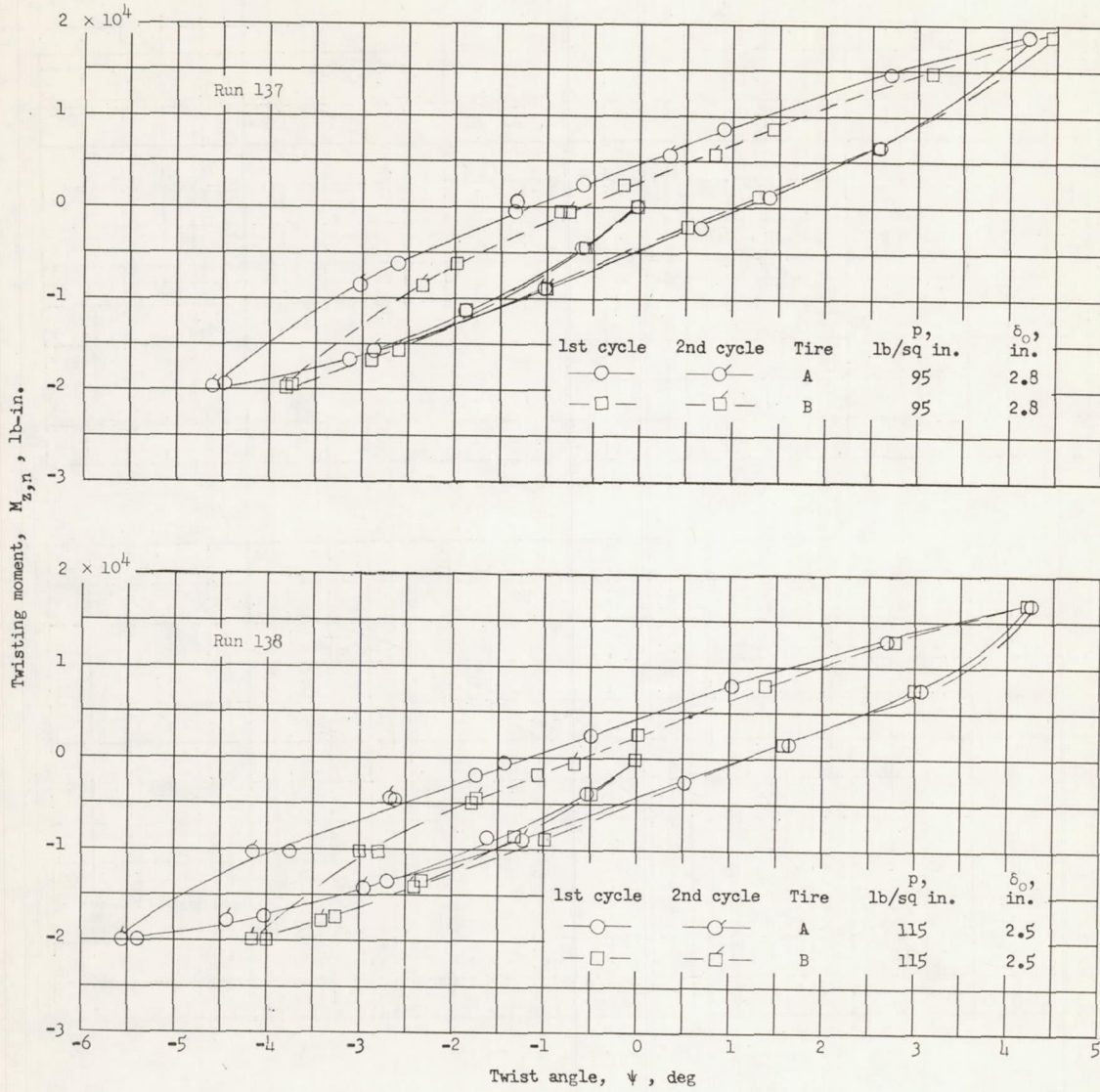
Figure 15.- Continued.
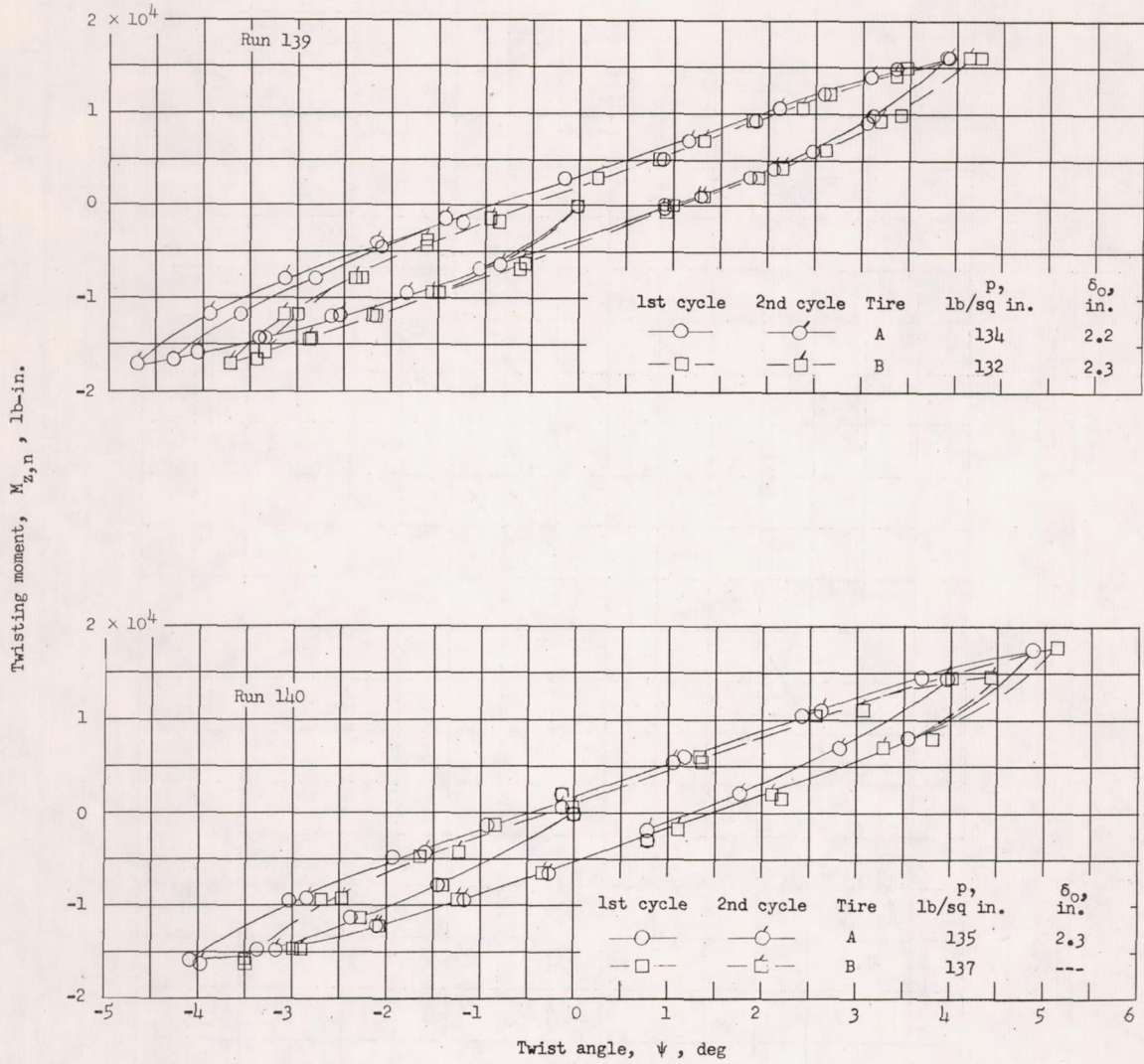
Figure 15.-. Concluded.
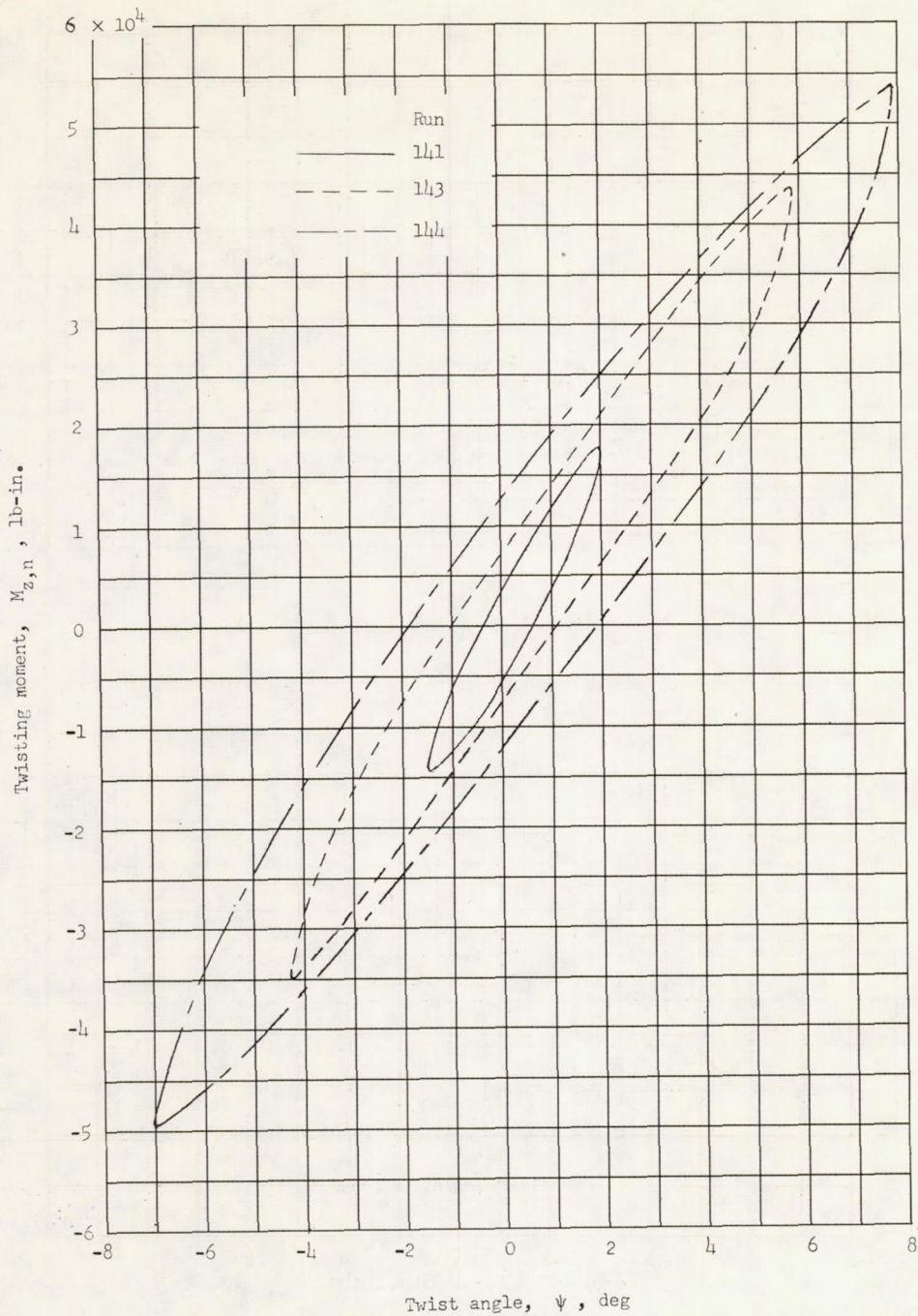
(a) Tire A; p ≈ 105 pounds per square inch; δ_o ≈ 5.0 inches.

Figure 16.- Variation of twisting moment with twist angle for a vertical
load of approximately 28,300 pounds on each tire.   Test series E.
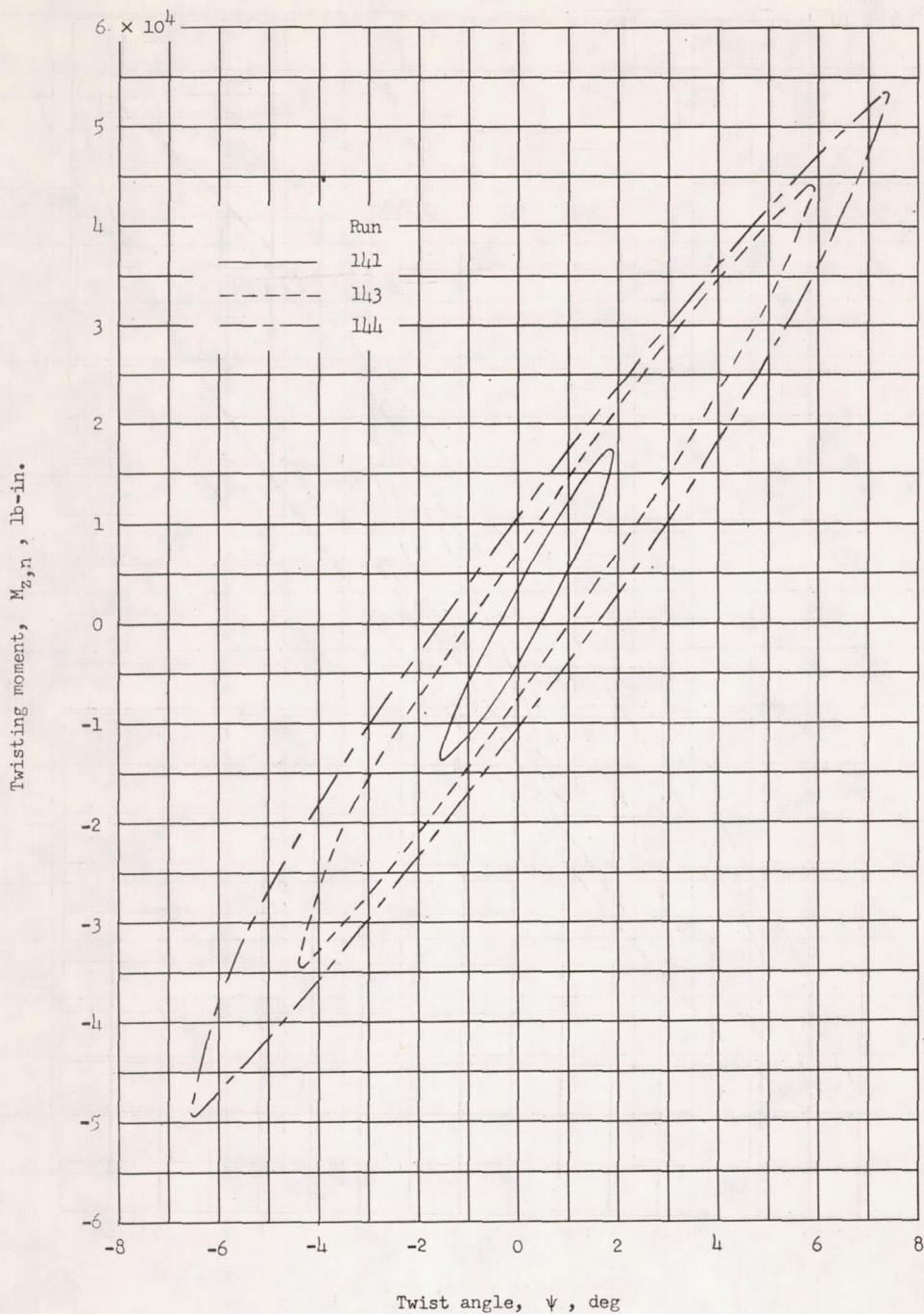
(b) Tire B; p ≈ 105 pounds per square inch; δ_o ≈ 5.0 inches.

Figure 16.- Continued.
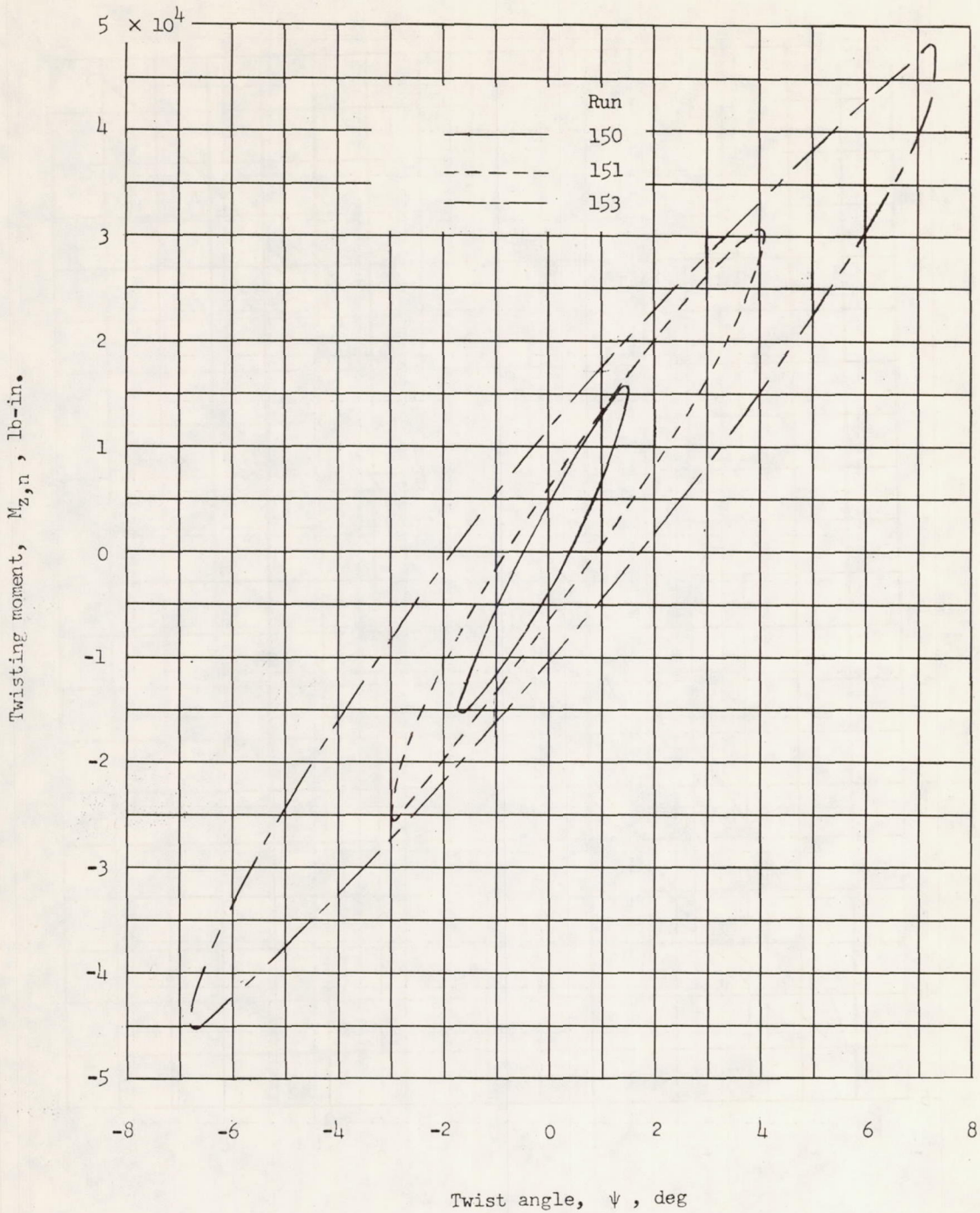
(c) Tire A; p = 142 pounds per square inch; $\delta_0 \approx 3.9$ inches.

Figure 16.- Continued.
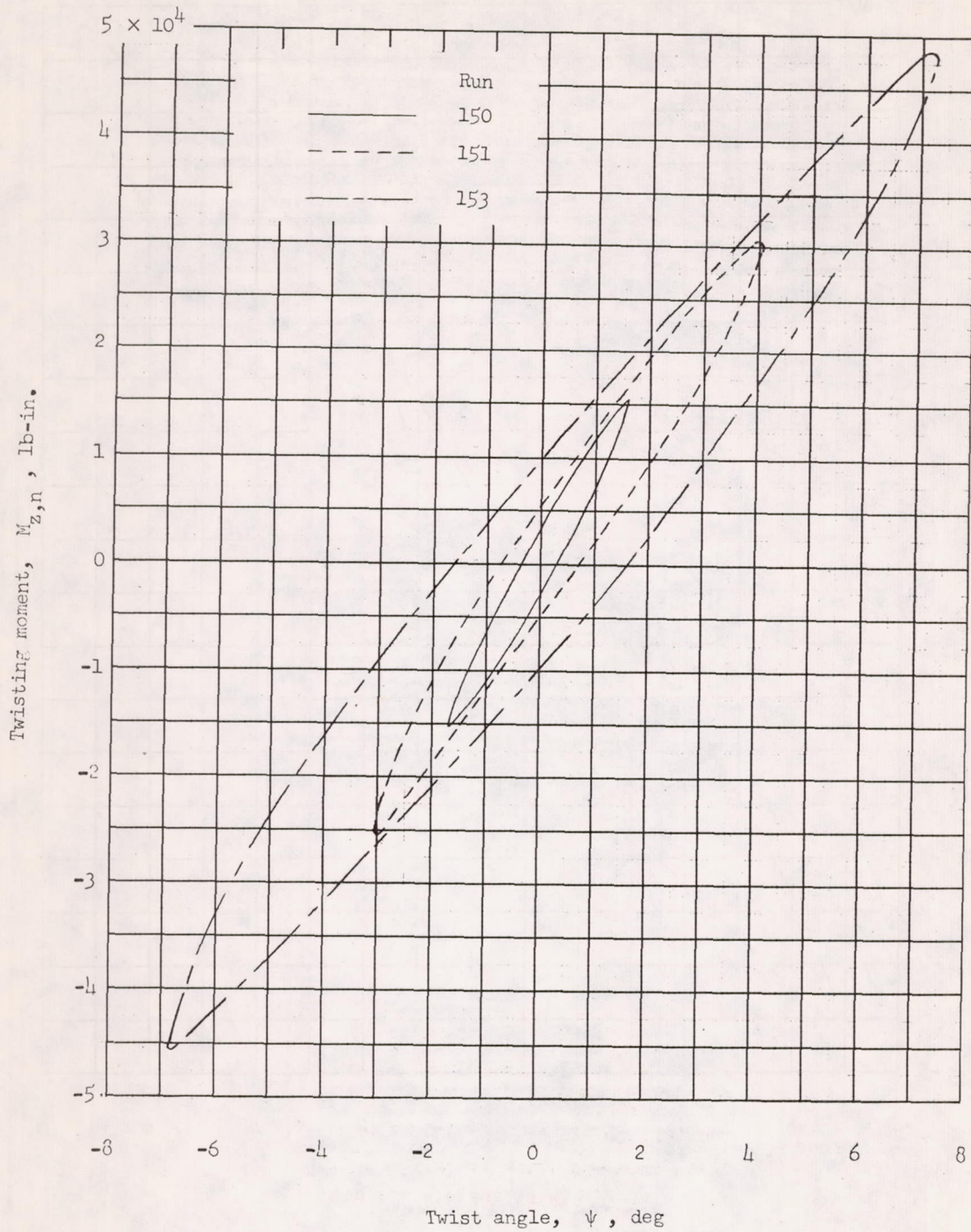
(d) Tire B; $p \approx 141$ pounds per square inch; $\delta_o \approx 3.9$ inches.

Figure 16.- Concluded.
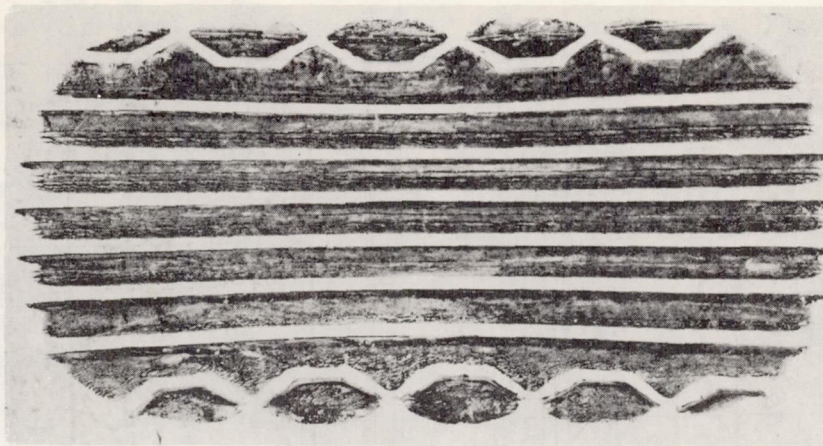
(a) Run 215; δ_O = 5.68 inches; p_O = 85 pounds per square inch;
F_Z = 28,190 pounds.
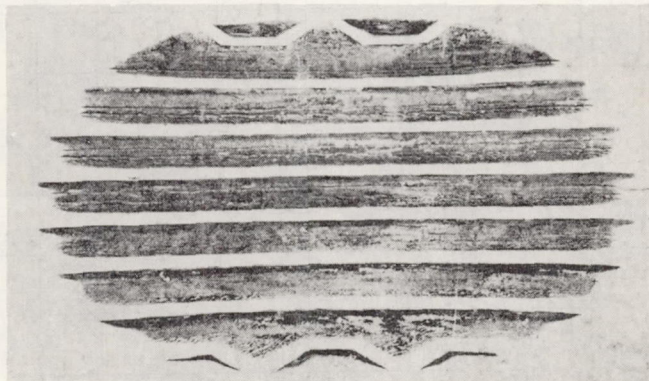
(b) Run 217; δ_O = 3.00 inches; p_O = 95 pounds per square inch;
F_Z = 14,720 pounds.
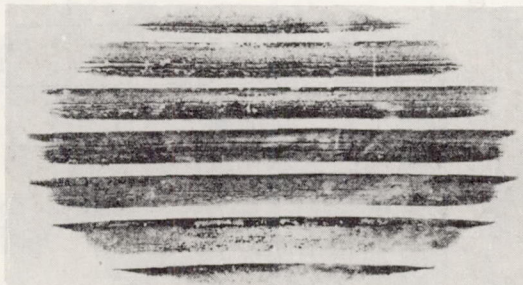
(c) Run 218; δ_O = 2.04 inches; p_O = 95 pounds per square inch;
F_Z = 8,780 pounds.

Figure 17.- Typical tire footprints for tire B.   L-97061
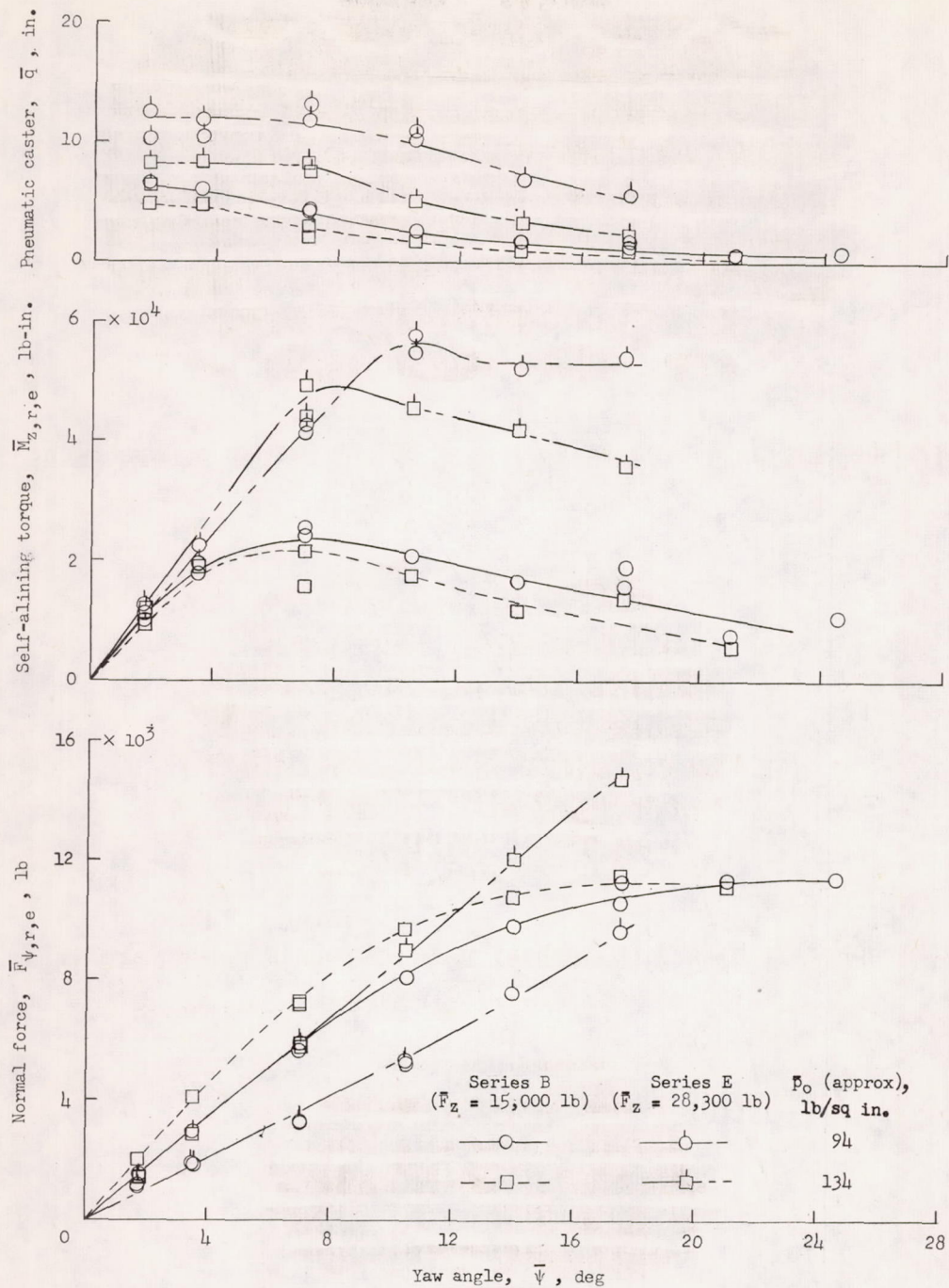
Figure 18.- Comparison of variation of normal force, self-alining torque, and pneumatic caster with yaw angle at two pressures for $\overline{F}_z$ = 15,000 pounds (test series B) and $\overline{F}_z$ = 28,300 pounds (test series E).
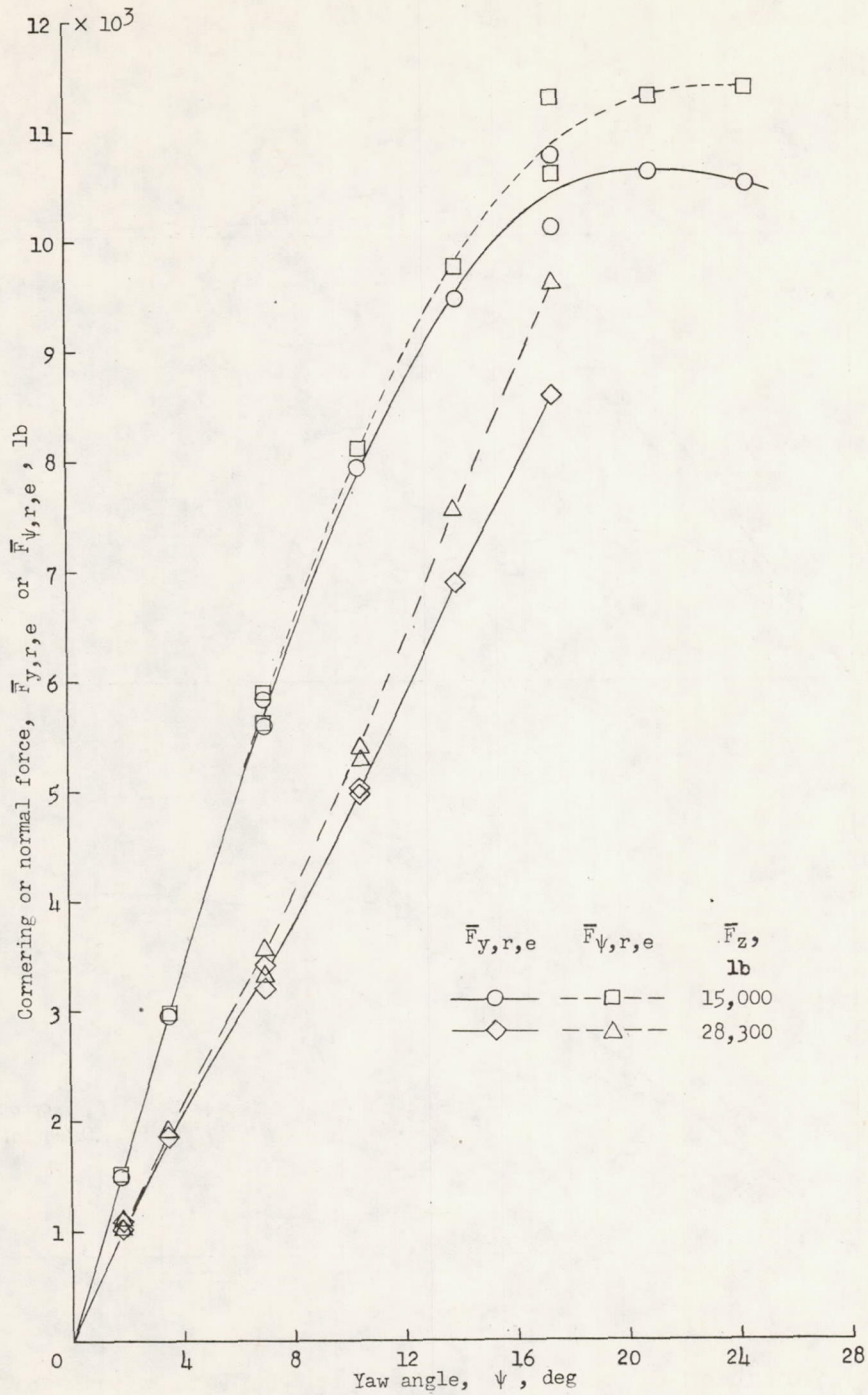
Figure 19.- Comparison of cornering-force and normal-force variations with yaw angle at $\bar{p}_O \approx 94$ pounds per square inch for two vertical loadings.
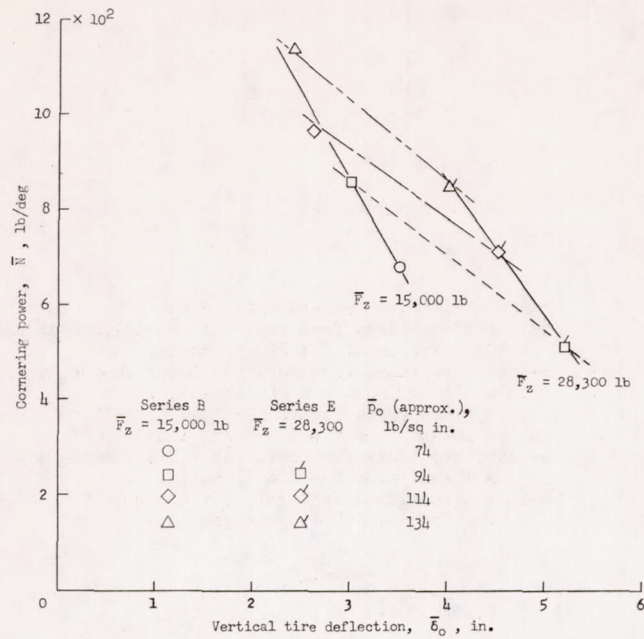
(a) Variation of cornering power with vertical tire deflection.
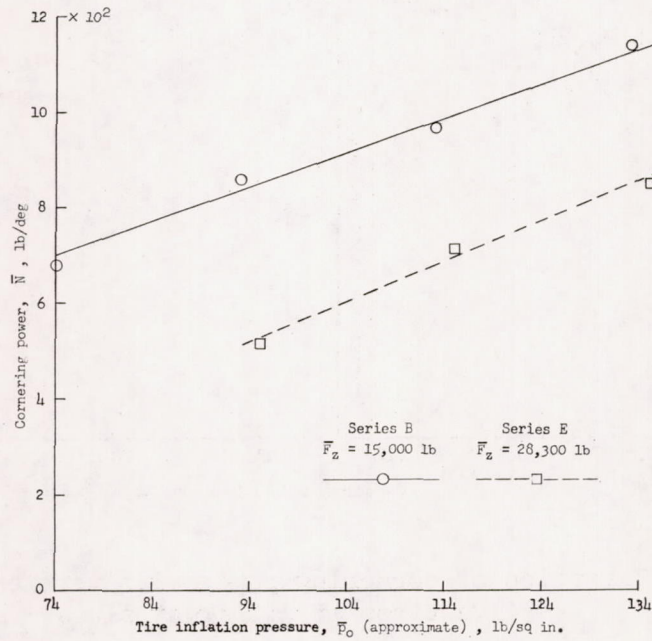
(b) Variation of cornering power with inflation pressure.

Figure 20.- Variation of cornering power with vertical tire deflection
and inflation pressure.
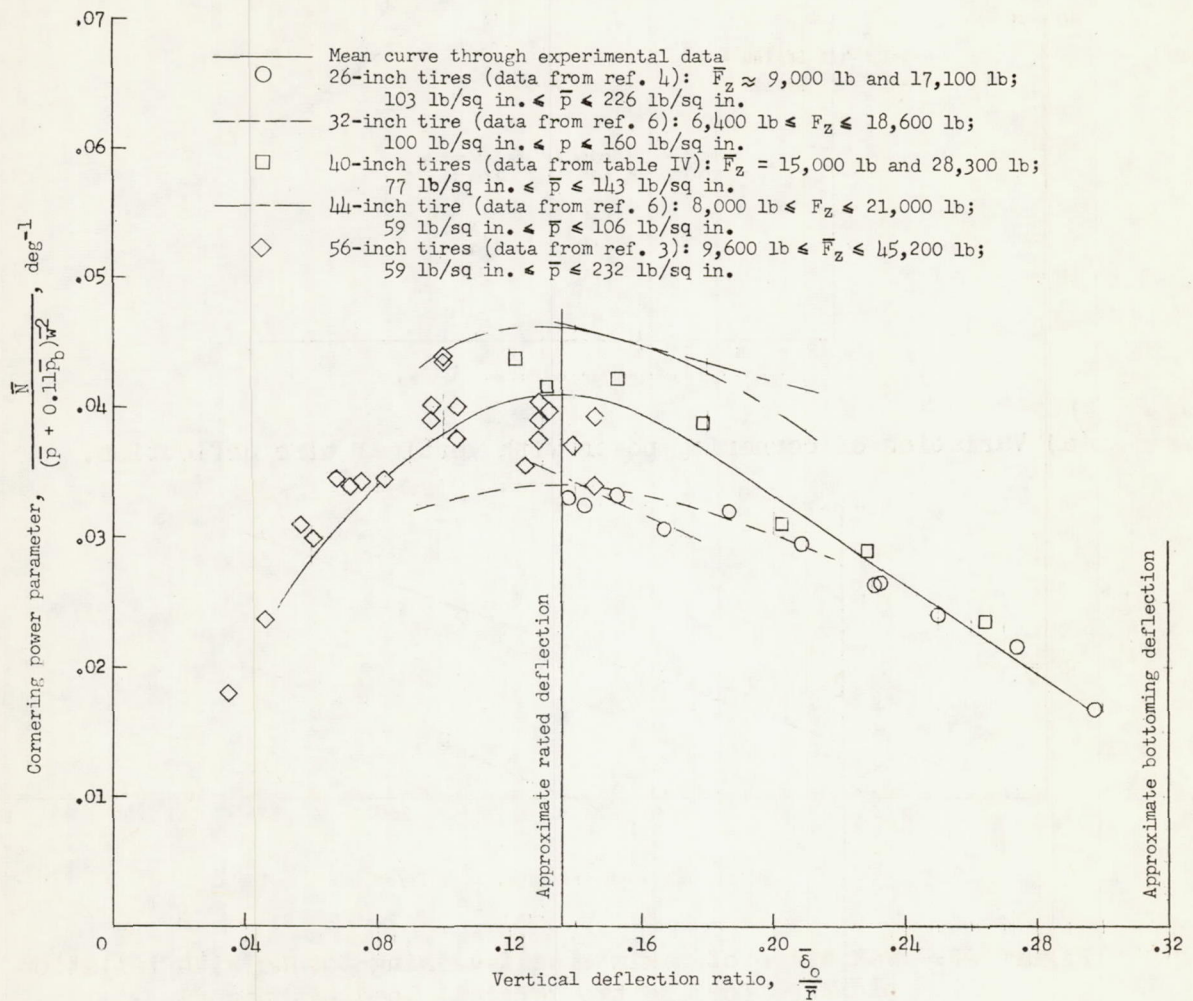
Figure 21.- Variation of cornering power with vertical deflection for five tires of different sizes.
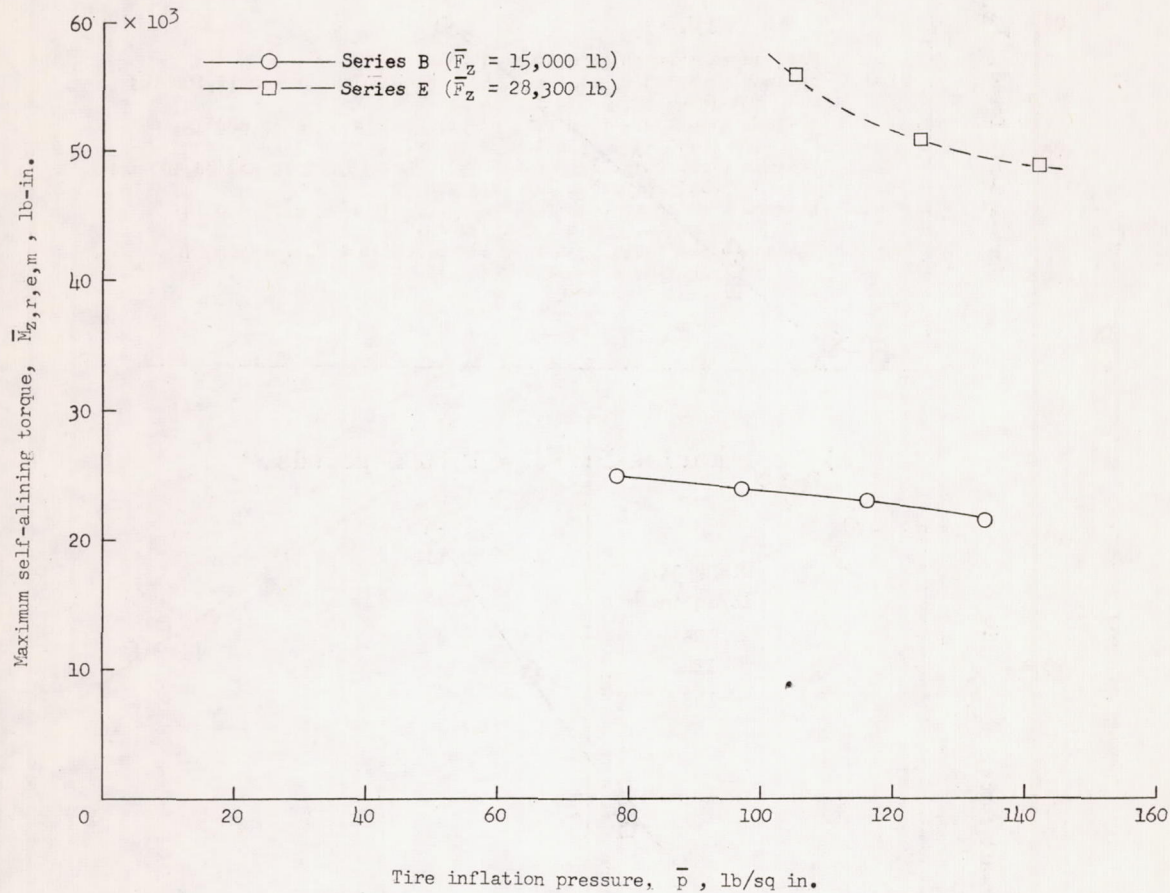
Figure 22.- Variation of maximum self-alining torque with inflation pressure for the two vertical loadings tested.
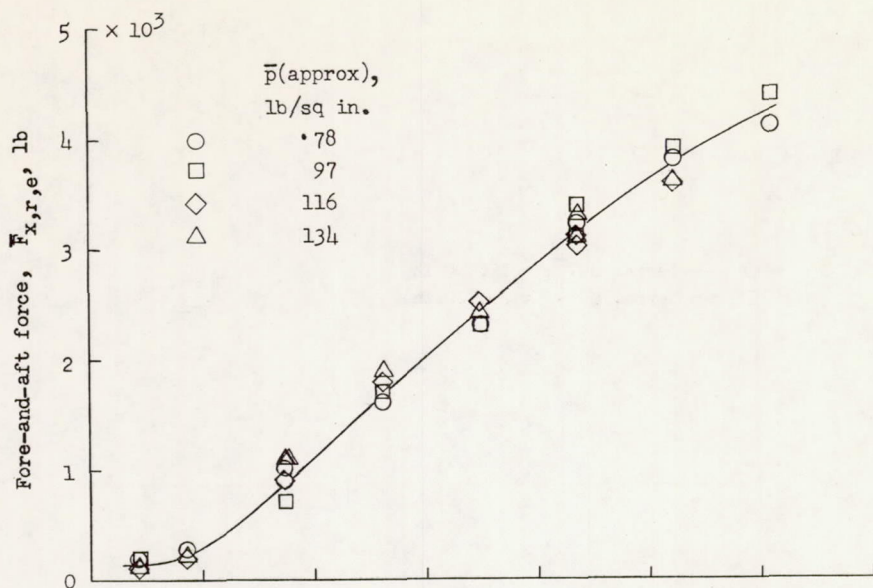
(a) Test series B; $\overline{F}_z$ = 15,000 pounds.
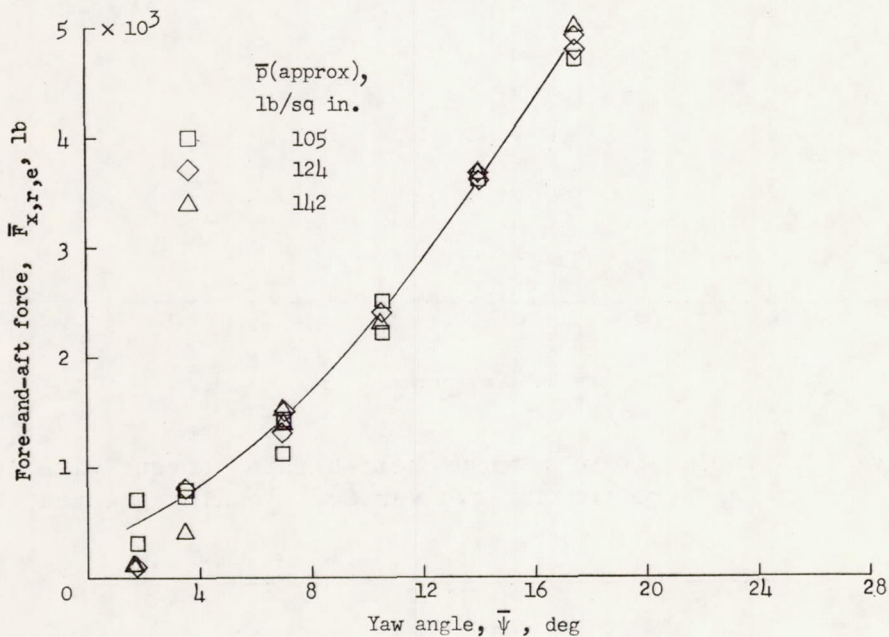
(b) Test series E; $\overline{F}_z$ = 28,300 pounds.

Figure 23.- Variation of drag force with yaw angle for the vertical-load and pressure ranges tested.
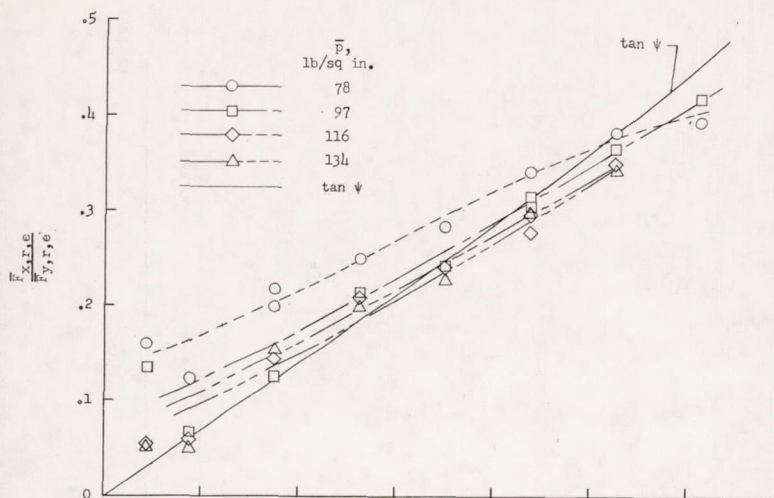
(a) Test series B; $\overline{F}_Z = 15,000$ pounds.
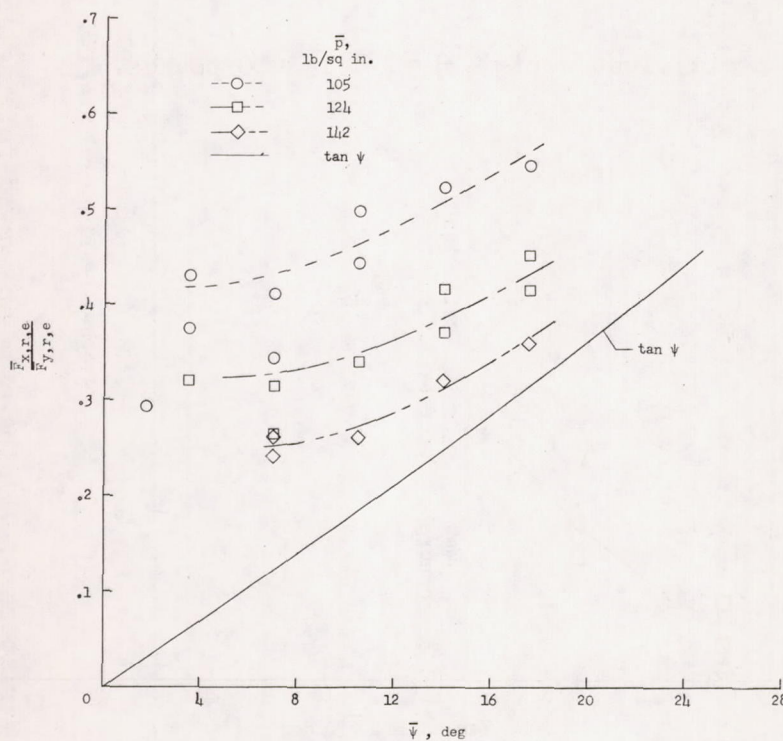
(b) Test series E; $\overline{F}_Z = 28,300$ pounds.

Figure 24.- Variation of the ratio of drag force to cornering force with yaw angle.
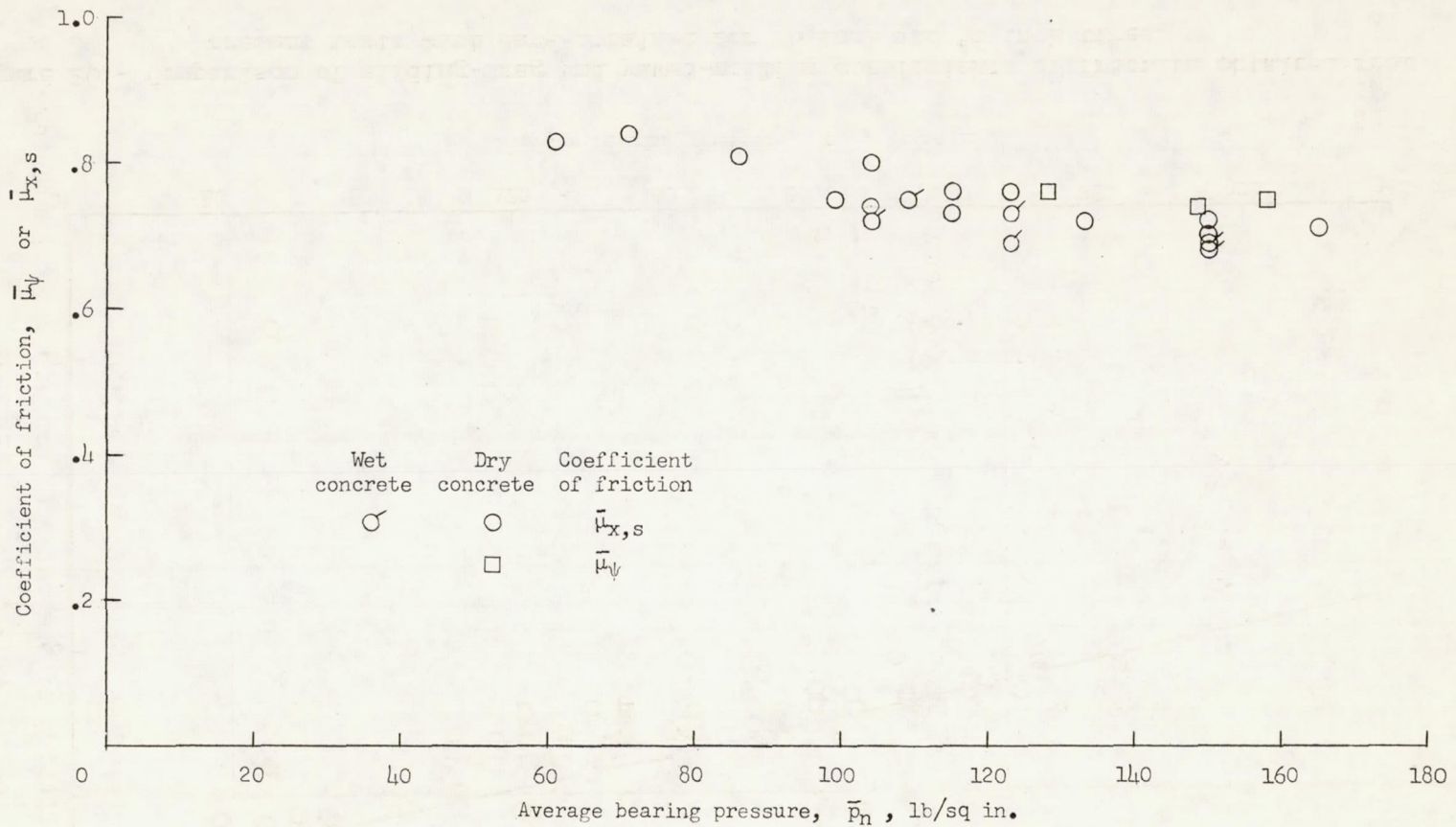
Figure 25.- Variation of sliding-drag and yawed-rolling coefficients of friction with average bearing pressure.
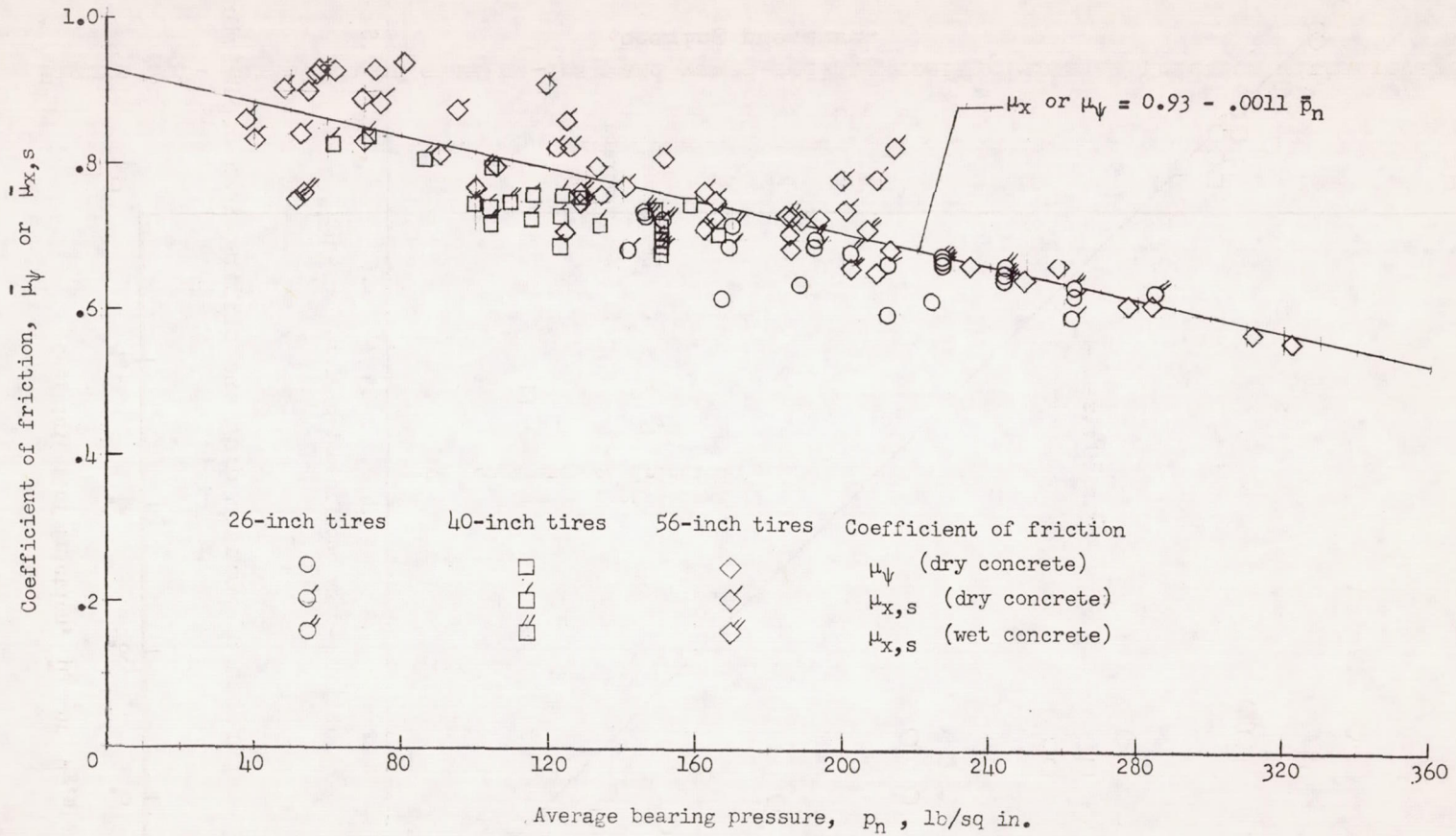
Figure 26.- Comparison of sliding-drag and yawed-rolling coefficients of friction obtained from present tests with data obtained for 26-inch and 56-inch tires.
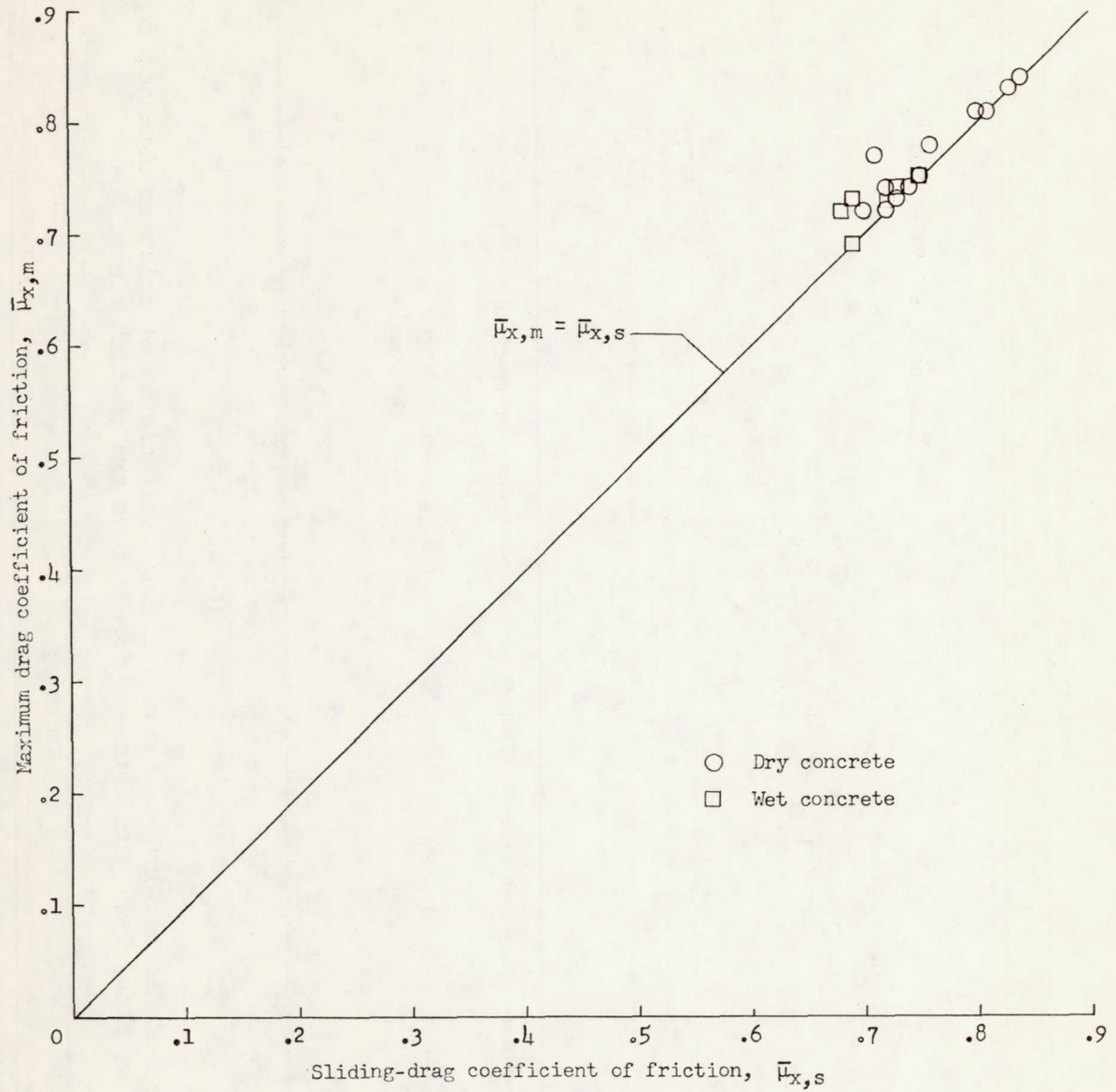
Figure 27.- Comparison of maximum drag and sliding-drag coefficients of friction.
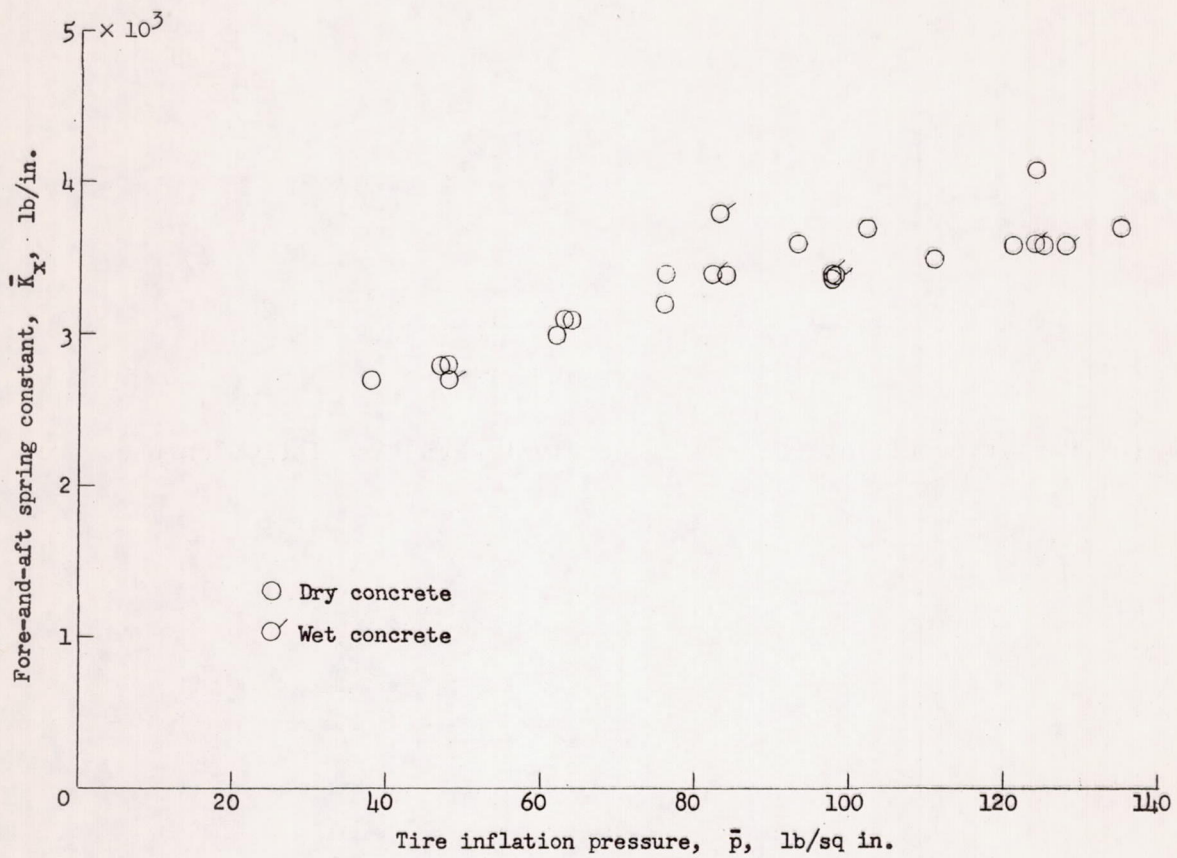
Figure 28.- Variation of fore-and-aft spring constant with tire infla-
tion pressure. Test series D; $F_z \approx 9{,}100$ lb.
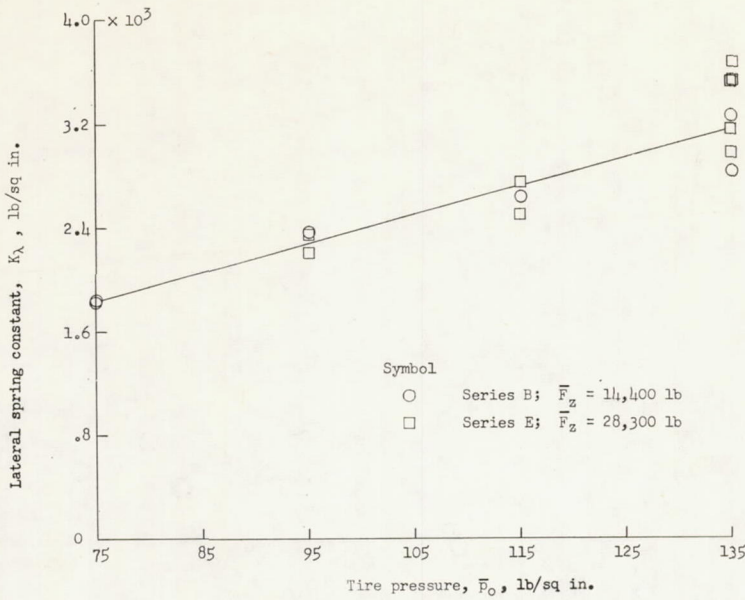
(a) Variation of lateral spring constant with tire inflation pressure.
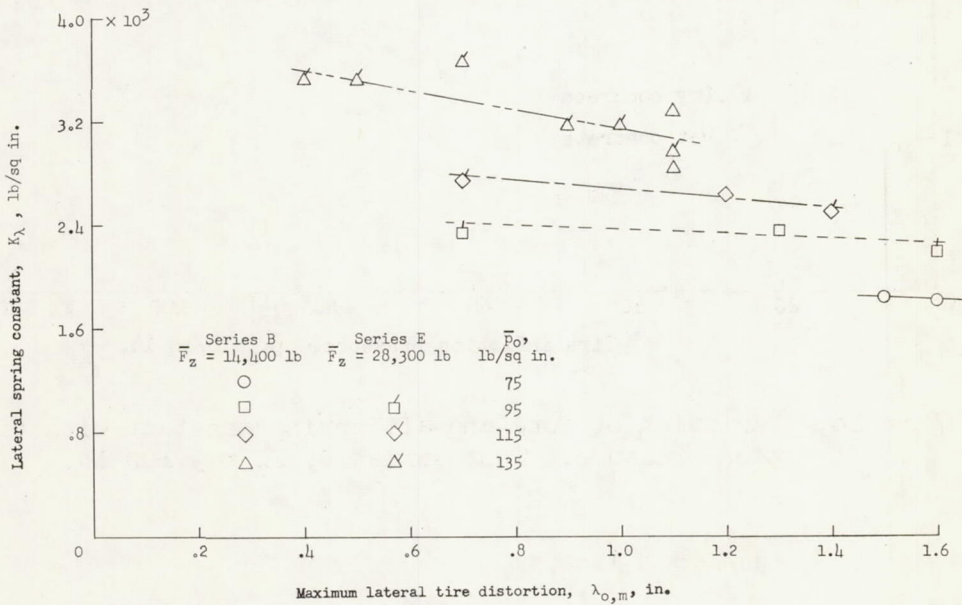
(b) Variation of lateral spring constant with amplitude of lateral
tire distortion.

Figure 29.- Variation of lateral spring constant with tire inflation
pressure and amplitude of lateral tire distortion.
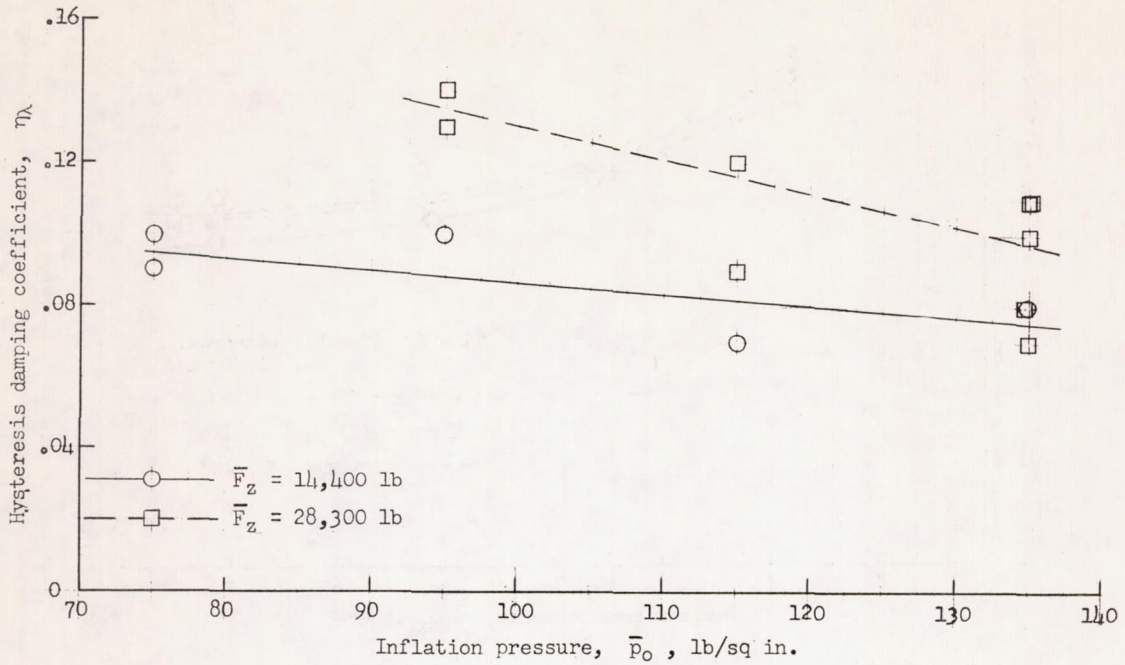
Figure 30.- Variation of hysteresis damping coefficient for lateral distortion with inflation pressure for two vertical loadings.
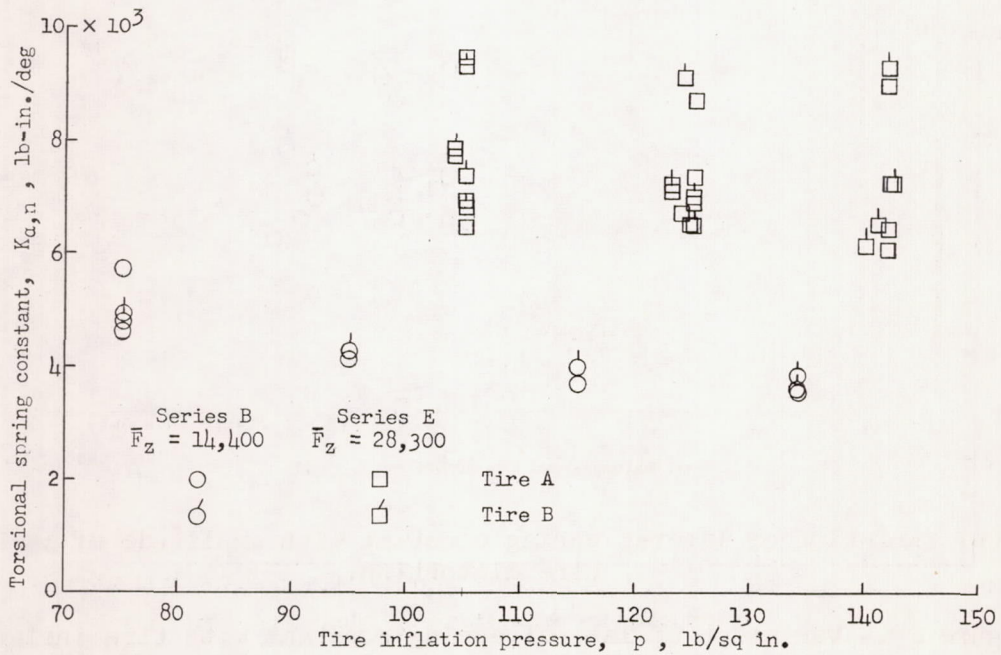
Figure 31.- Variation of torsional spring constant with tire inflation pressure for the two vertical loadings tested.
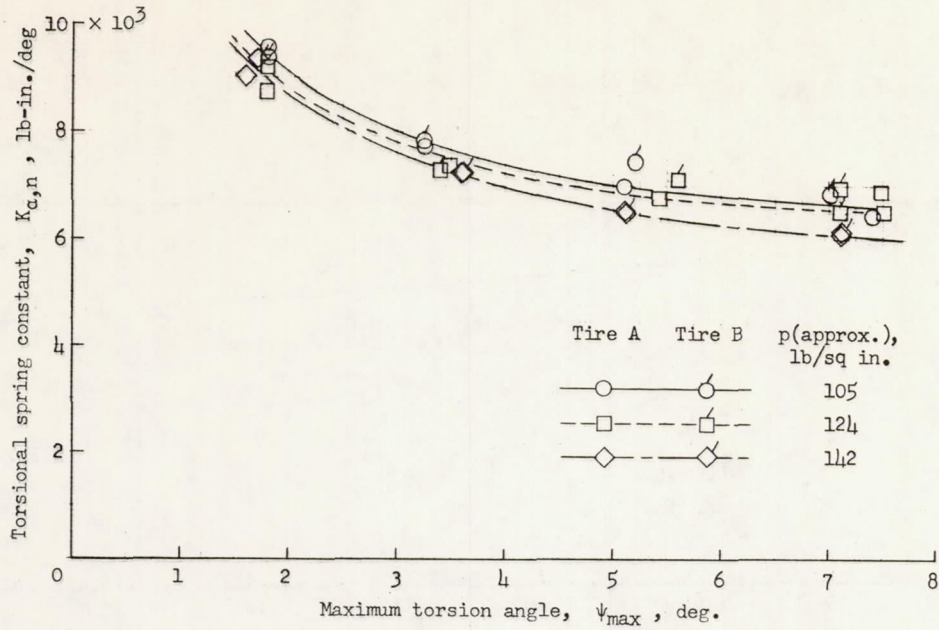
Figure 32.- Variation of static torsional spring constant with amplitude of hysteresis loop for several tire inflation pressures at the heavy vertical loading ($\overline{F}_z = 28,300$ lb).
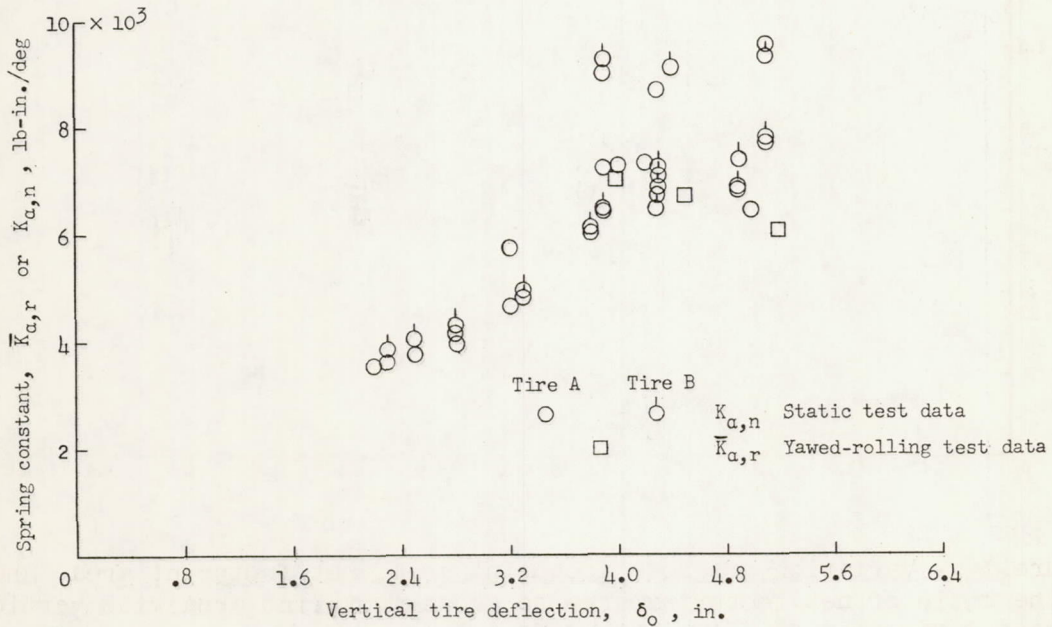
Figure 33.- Comparison of torsional spring constants from static and yawed-rolling tests. Test series B and E.
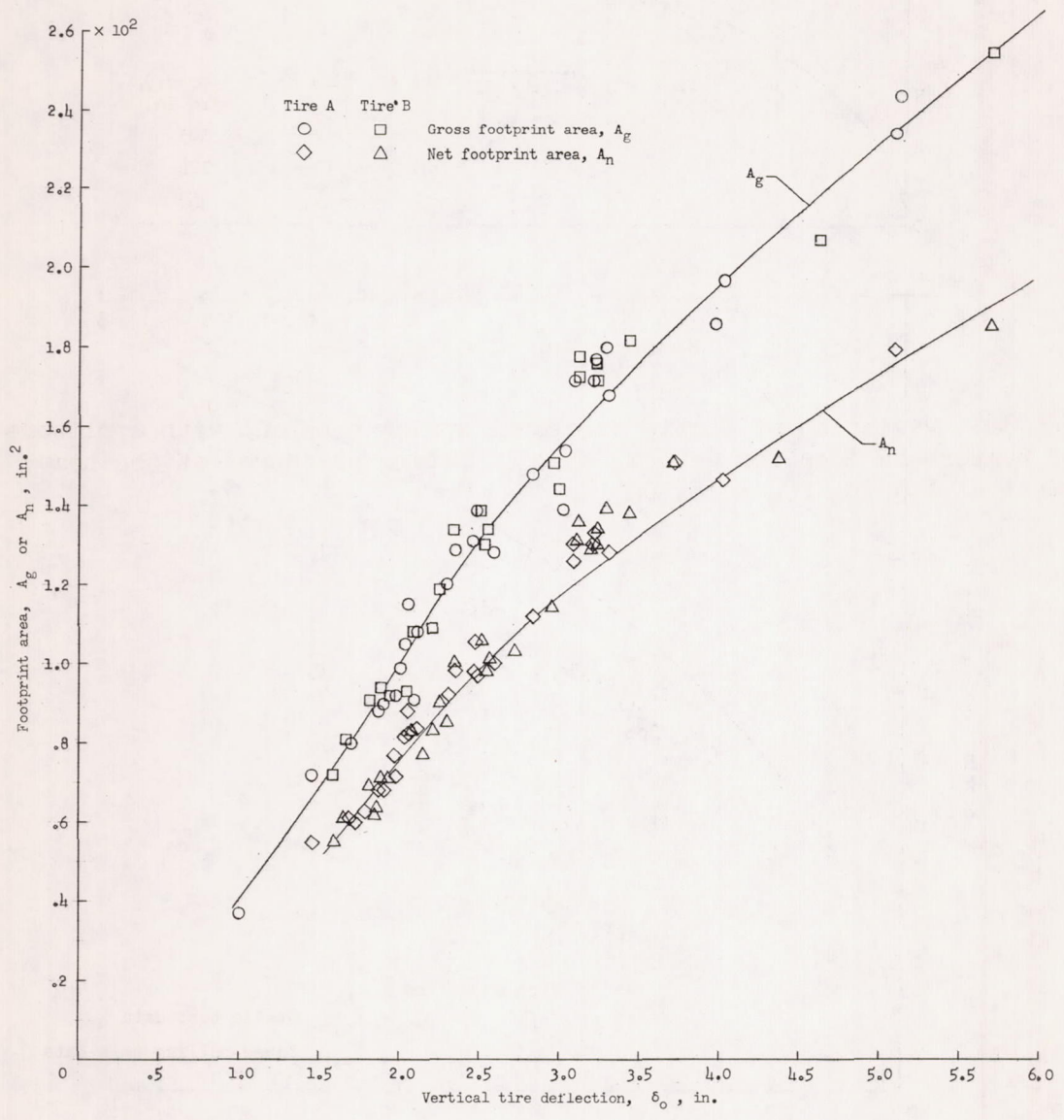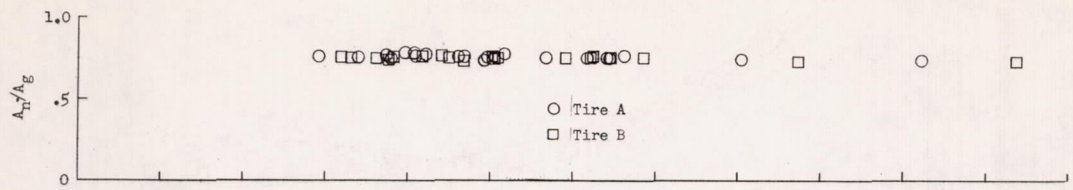
Figure 34.- Variation of gross footprint area, net footprint area, and the ratio of net footprint area to gross footprint area with vertical tire deflection for tires A and B.
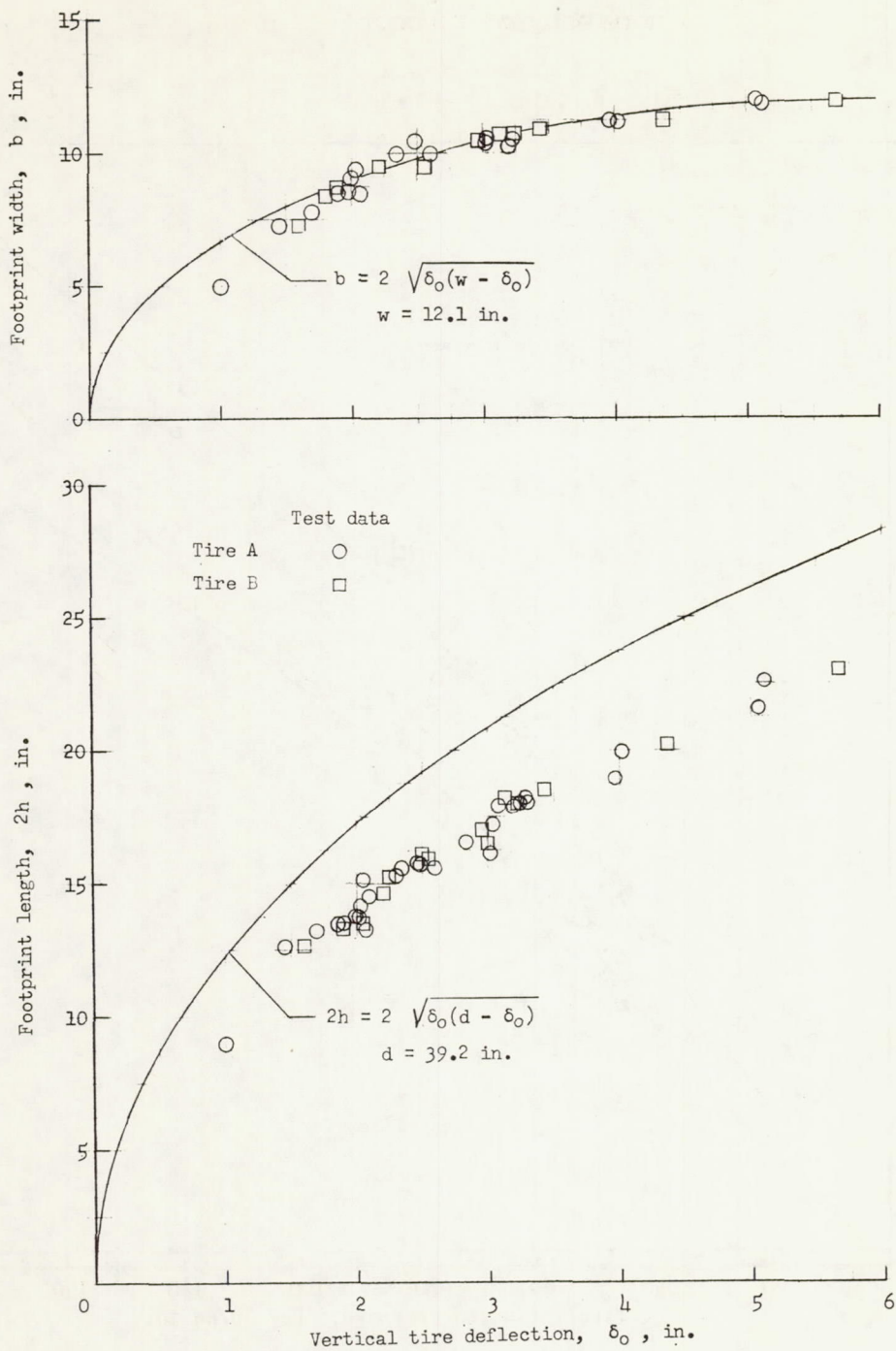
Figure 35.- Variation of footprint length and width with vertical deflection. Solid lines represent chord lengths of circles having diameters equal to the diameter and width at rated inflation pressure.
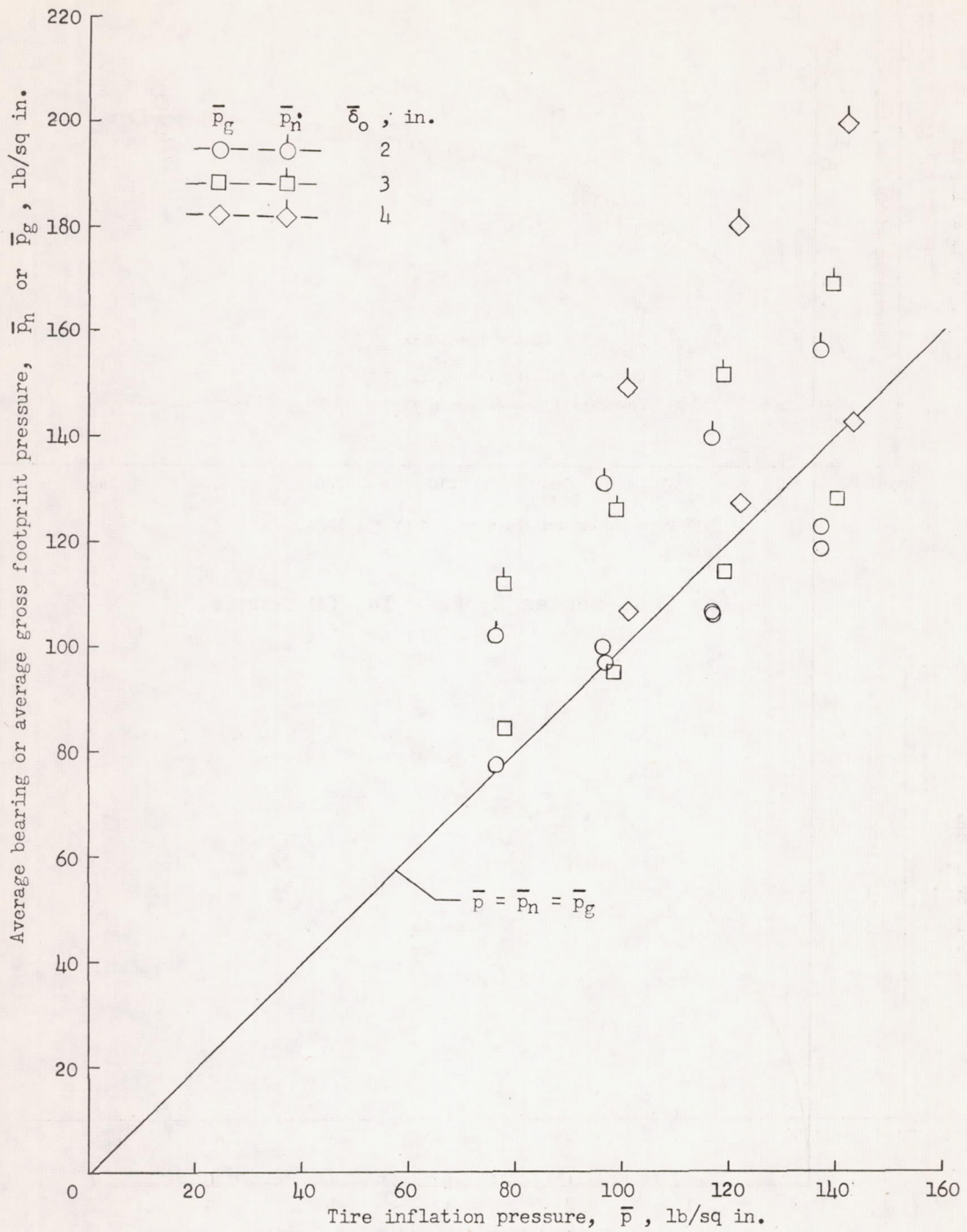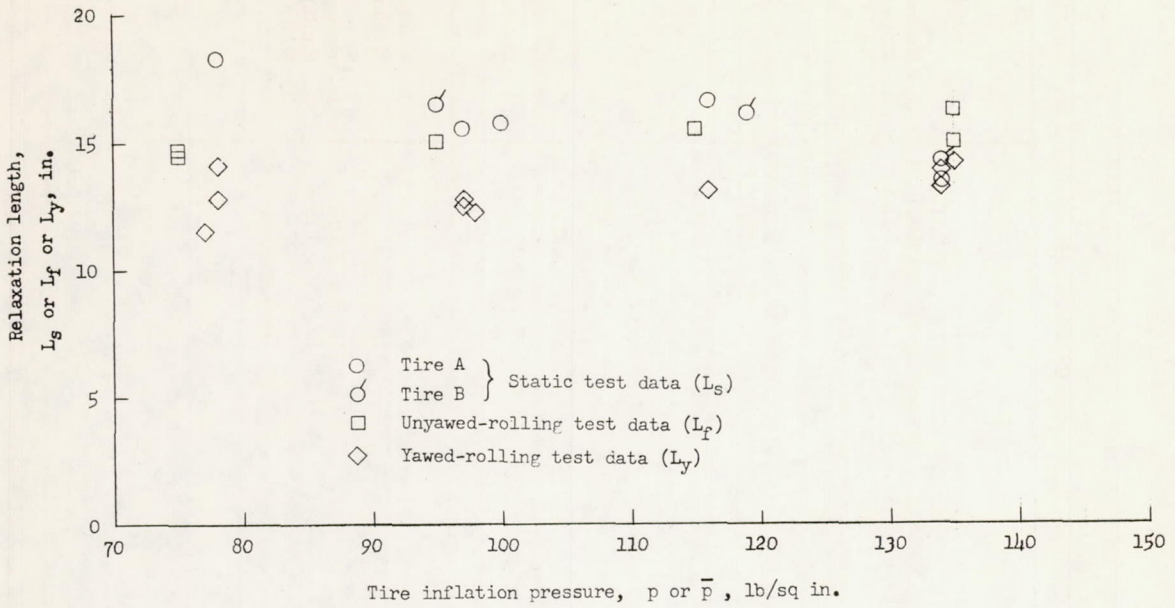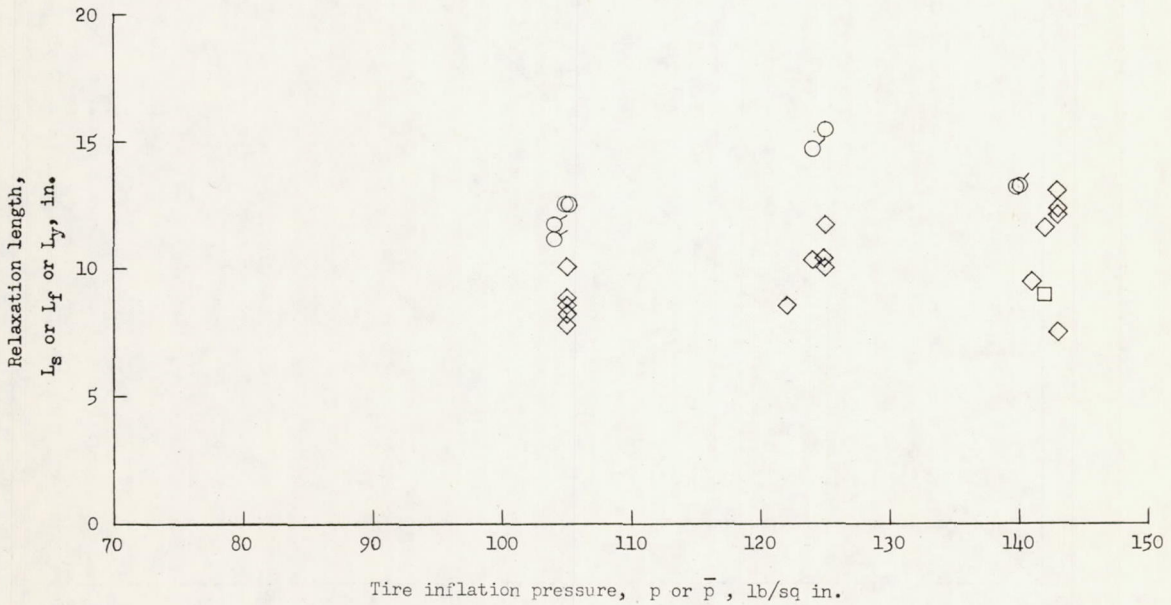
Figure 36.- Variation of average bearing pressure and average gross footprint pressure with tire inflation pressure for several constant vertical tire deflections.

(a) Test series B; $F_Z \approx 14{,}700$ pounds.

(b) Test series E; $F_Z \approx 28{,}300$ pounds.

Figure 37.- Variation of relaxation lengths with tire inflation pressure
for test series B and E.